Bioanalytical investigations of natural products and their derivatives:

Mode of resistance, pharmacological properties and off-target characterization of cystobactamids

Dissertation

zur Erlangung des Grades

des **Doktors der Naturwissenschaften**

der Naturwissenschaftlich-Technischen Fakultät

der Universität des Saarlandes

von

Timo Risch

Saarbrücken 2024

Tag des Kolloquiums:	23.04.2025
Dekan:	Prof. Dr.-Ing. Dirk Bähre
Berichterstatter:	Prof. Dr. Rolf Müller Prof. Dr. Alexandra K. Kiemer
Vorsitz:	Prof. Dr. Markus R. Meyer
Akad. Mitarbeiter:	Priv.-Doz. Dr. Martin Frotscher

Die vorliegende Arbeit wurde von Februar 2021 bis Dezember 2024 unter Anleitung von Herrn Prof. Dr. Rolf Müller am Helmholtz-Institut für Pharmazeutische Forschung Saarland (HIPS) angefertigt.

Abstract

The silent pandemic of antimicrobial resistances (AMR) is escalating worldwide. To preserve antimicrobial therapy, new strategies including innovative compound classes are crucial. Cystobactamids, derived from Myxobacteria, exhibit broad-spectrum activity against Gram-positive as well as Gram-negative multidrug-resistant bacteria, rendering them as promising candidates for antibiotic development. The potential success of new antibiotics is critically influenced by the inevitable development of resistances and the drug's safety profile. This thesis addresses both aspects comprehensively.

The mode of resistance of *Escherichia coli* to cystobactamids was investigated, revealing a so far unknown YgiV-mediated resistance mechanism, which also affects the regulation of bacterial virulence factors. Furthermore, prokaryotic and eukaryotic off-targets have been assessed using newly synthesized tool compounds, identifying the efflux pump AcrB and the HDL-receptor SCARB1 as primary off-target proteins in bacteria and human cells, respectively. Additionally, the *in vitro* and *in vivo* toxicity of cystobactamids was evaluated in eukaryotic models, demonstrating a favorable safety profile with notably protective properties against oxidative cell stress. In addition, pharmacokinetic and metabolic studies lead to a metabolic stabilization strategy that potentially enhances cystobactamid exposure-duration and thereby improves their efficiency as anti-infective agents.

Zusammenfassung

Die stille Pandemie der antimikrobiellen Resistenzen (AMR) eskaliert weltweit. Um antimikrobielle Therapien zu erhalten, sind neue Strategien, einschließlich innovativer Wirkstoffklassen, entscheidend. Cystobactamide, isoliert aus Myxobakterien, zeigen ein breites Wirkspektrum gegen Gram-positive und Gram-negative multiresistente Bakterien und gelten daher als vielversprechende Kandidaten für die Antibiotikaentwicklung. Der Erfolg neuer Antibiotika wird maßgeblich von der unvermeidlichen Entwicklung von Resistenzen und dem Sicherheitsprofil der Arznei beeinflusst. Diese Arbeit untersucht beide Aspekte umfassend.

Der Resistenzmechanismus von *Escherichia coli* gegenüber Cystobactamiden wurde analysiert und ein bisher unbekannter, YgiV-vermittelter Mechanismus entdeckt, der auch die Regulation bakterieller Virulenzfaktoren beeinflusst. Außerdem wurden prokaryotische und eukaryotische Off-Target-Proteine mithilfe funktionalisierter Verbindungen untersucht. So wurden die Effluxpumpe AcrB in Bakterien und der HDL-Rezeptor SCARB1 in menschlichen Zellen als primäre Off-Targets identifiziert. Die Toxizität des Cystobactamide wurde *in vitro* und *in vivo* in eukaryotischen Modellen untersucht, was ein exzellentes Sicherheitsprofil sowie Schutz vor oxidativem Zellstress zeigte. Die Ergebnisse pharmakokinetischer und metabolischer Studien führten zur Entwicklung einer Strategie, welche die Expositionsdauer der Cystobactamide verlängern und ihre Effizienz als Antiinfektiva verbessern könnte.

Veröffentlichungen der Dissertation

Im Folgenden sind Teile dieser Arbeit gelistet, welche im Rahmen der Promotion angefertigt wurden und, nach Genehmigung der Naturwissenschaftlichen-Technischen Fakultät vertreten durch den Mentor, veröffentlicht wurden oder derzeit in Vorbereitung zur Veröffentlichung sind:

1. **Timo Risch**, Dominik Kolling, Dietrich Mostert, Tim Seedorf, Dominik Heimann, Daniel Kohnhäuser, Felix Deschner, Franziska Fries, Danny Solga, Jil-Sophie Hilgers, Jan Dastbaz, Stefano Mancini, Anna K. H. Hirsch, Mark Brönstrup, Andreas Kirschning, Stephan A. Sieber, Jennifer Herrmann, and Rolf Müller (2024). **YgiV promoter mutations cause resistance to cystobactamids and reduced virulence factor expression in *Escherichia coli***. *npj Antimicrobials and Resistance*. 10.1038/s44259-024-00050-7

2. **Timo Risch**, Benedikt Hellwinkel, Dietrich Mostert, Andreas M. Kany, Danny Solga, Tim Seedorf, Dominik Heimann, Jessica Hoppstädter, Daniel Kohnhäuser, Jil-Sophie Hilgers, Franziska Fries, Felix Deschner, Mark Brönstrup, Andreas Kirschning, Stephan A. Sieber, Thomas Pietschmann, Alexandra K. Kiemer, Jennifer Herrmann, and Rolf Müller (2024). **Cystobactamid off-target profiling reveals favorable safety, superoxide reduction, and SCARB1 inhibition in eukaryotes**. *npj Drug Discovery – Manuscript in revision*

Weitere Veröffentlichungen, zu denen im Rahmen der Promotionsarbeit ein wissenschaftlicher Beitrag geleistet wurde, welche aber keinen Teil dieser Thesis darstellen:

3. Till Reinhardt, Nina Bach, Alex Rothemann, Adrian Jauch, Yassmine El Harraoui, Sigrid Müller-Deubert, Martin Köllen, **Timo Risch**, Rolf Müller, Franziska Traube, Denitsa Docheva, Stefan Zahler, Jan Riemer, Stephan A. Sieber (2024). **Chemical proteomics reveal human off-targets of fluoroquinolone induced mitochondrial toxicity.** *Angewandte Chemie – Manuscript in revision*

4. Felix Deschner, Dietrich Mostert, Jan-Martin Daniel, Alexander Voltz, Dana C. Schneider, Navid Khangholi, Jürgen Bartel, Laís Pessanha de Carvalho, Madita Brauer, Tatiana Gorelik, **Timo Risch**, F.P. Jake Haeckl, Laura Herraiz-Benitez, Anastasia Andreas, Andreas M. Kany, Gwenaëlle Jézéquel, Walter Hofer, Mathias Müsken, Jana Held, Markus Bischoff, Ralf Seemann, Heike Brötz-Oesterhelt, Tanja Schneider, Stephan Sieber, Rolf Müller, and Jennifer Herrmann (2024). **The natural product class of chlorotonils exerts a novel mechanism of action and addresses multiple antibacterial targets**. *Cell Chemical Biology – Manuscript in revision*

5. Vida Mashayekhi, Annika Schomisch, Sari Rasheed, Ernesto Aparicio-Puerta, **Timo Risch**, Daniela Yildiz, Marcus Koch, Simon Both, Nicole Ludwig, Thierry M. Legroux, Andreas Keller, Rolf Müller, Gregor Fuhrmann, Jessica Hoppstädter & Alexandra K. Kiemer (2024). **The RNA binding protein IGF2BP2/IMP2 alters the cargo of cancer cell-derived extracellular**

vesicles supporting tumor-associated macrophages. *Cell Communication and Signaling.* https://doi.org/10.1186/s12964-024-01701-y

6. Sebastian Adam, Franziska Fries, Alexander von Tesmar, Sari Rasheed, Selina Deckarm, Carla F. Sousa, Roman Reberšek, **Timo Risch**, Stefano Mancini, Jennifer Herrmann, Jesko Koehnke, Olga V. Kalinina, and Rolf Müller (2024). **The Peptide Antibiotic Corramycin Adopts a β-Hairpin-like Structure and Is Inactivated by the Kinase ComG.** *Journal of the American Chemical Society.* https://doi.org/10.1021/jacs.3c13208

7. Felix Deschner, **Timo Risch**, Claas Baier, Dirk Schlüter, Jennifer Herrmann, & Rolf Müller (2023). **Nitroxoline resistance is associated with significant fitness loss and diminishes in vivo virulence of *Escherichia coli***. *Microbiology Spectrum*. https://doi.org/https://doi.org/10.1128/spectrum.03079-23

8. Philip Schippers, Sari Rasheed, Yu Mi Park, **Timo Risch**, Lea Wagmann, Selina Hemmer, Sascha K. Manier, Rolf Müller, Jennifer Herrmann & Markus R. Meyer (2023). **Evaluation of extraction methods for untargeted metabolomic studies for future applications in zebrafish larvae infection models.** *Scientific Reports.* https://doi.org/10.1038/s41598-023-34593-y

Contents

1. Introduction

1.1 HISTORY OF ANTIMICROBIAL HUMAN THERAPY

In our current developed world, we take effective antimicrobial therapy as given. We rely on antimicrobial therapy in various situations, such as treating common colds (whether necessary or not), preventing secondary infections, supporting co-treatment during immunosuppression or cancer therapy, and minimizing the risk of infections during surgeries. We, as the modern human kind, do not even think about living in a world, where a simple, uncomplicated infection could lead to untreatable conditions with inevitable death. However, this was the case in the pre-antibiotic era, where no antibacterial chemotherapy was available.

One key principle of antimicrobial therapy being applied for centuries is the use of natural compound producing organisms to combat infections. The oldest document of the treatment of infections by the use of competing microorganisms is the Eber´s papyrus from 1550 BC. There, the use of moldy bread and medicinal soil was described to treat open wounds and prevent infections. This practice was spread from Egypt to China, Serbia, and Greece.[1]

However, limited understanding of how and why these treatments cause an antimicrobial effect restricted the effectiveness and continued development of such therapies. One of the pioneers in understanding the human body as a chemical system was Theophrastus von Hohenheim (1493-1541), better known as Paracelsus. He contributed many aspects during the medical revolution in emphasizing the importance of combining knowledge with observations. Paracelsus is known as the “father of toxicology” as he pioneered the dose response concept. His famous principle “Sola dosis facit venenum”, only the dose makes the poison, remains one of the most important dogmas in pharmacology and toxicology. Although his conclusions were

limited by the knowledge and technology at the time, his ideas of characterizing the human body as a complex chemical system shaped the future of medicinal research.[2] The principle of antimicrobial chemotherapy can be traced back to Paul Ehrlich´s experiments to stain bacterial cells with specific dyes. His research led to the development of the first synthetic antimicrobial compound salvarsan. Salvarsan is an arsenic-based pro-drug developed to treat *Treponema pallidum* as cause of syphilis.[3] His “magic bullet” approach remains one of the key principles for the development of selective therapies with limited side effects. The bacteriologist Gerhard Domagk, who developed the sulfonamide prodrug prontosil (Noble Prize in 1939), successfully continued his work. The development of prontosil was inspired by Ehrlich´s work of selective dyes targeting bacterial cells and led to the class of sulfonamide antibiotics as first broad spectrum active antimicrobial compounds in clinical use.[4] Sulfonamides are still in use today; however, their use has been widely substituted by the discovery and use of the natural product penicillin and later developments in the field.

In 1929, Alexander Fleming was observing an inhibition zone around a contamination on a Petri dish, surrounded by weakly growing bacteria. This contamination was identified as the fungus *Penicillium*. Flemming postulated, that this antimicrobial effect originates from a natural compound produced by this fungus and called it penicillin. Furthermore, he recognized the value of this compound for the therapy of infectious diseases caused by penicillin sensitive pathogens.[5] Penicillin’s potential for human therapy remained unexploited until Howard Florey and Ernst Chain successfully produced and isolated penicillin for the treatment of various infections in man in 1941. Fleming, Florey and Chain received the Nobel Prize in Physiology and Medicine in 1945 “for the discovery of penicillin and its curative effect in various infectious diseases”.

The golden age of antibiotics (1940s to 1960s) was characterized primarily by the discovery of such antimicrobial natural products originating from microorganisms like fungi and bacteria.[6] Selman Waksman pioneered the work on systematically profiling antibiotic substances derived from microbes. He postulated that microbial secondary metabolites, which are natural products not essential for cell survival but advantageous for environmental competition, have the function to destroy competing microbes. Thereby, he discovered a rich source of bioactive secondary metabolites from the bacterial genus *Streptomyces*, including streptomycin and neomycin. Importantly, streptomycin was the first agent active against the widespread tuberculosis (Noble Prize in 1952).[7] Waksman´s work initiated the golden age of antibiotic discovery, which in turn revolutionized modern medicine. Antibiotics not only made the safe treatment of severe infections possible, for the first time in human history, but also paved the way for advanced medicinal approaches, including novel options for cancer therapy, immunotherapy, and complex surgeries. By substantially reducing the overall mortality from bacterial infections, antibiotics contributed to an increase in the average human lifespan by 23 years.[7,8]

The pharmaceutical research and industry recognized the potential for economic success of antibiotic development, and from the 1940s to the 1960s, various antibiotics were developed to target nearly all infectious diseases cause by bacterial pathogens. However, by the 1970s, with the decreased urge for the development of novel antimicrobial compounds, pharmaceutical companies, regulators, and society lost interest in antibiotic development, paving the way for bacteria to adapt.[1]

It was also Fleming who forecasted in his noble lecture that “the time may come when penicillin can be bought by anyone in the shops. Then there is the danger that the ignorant man may easily underdose himself and by exposing his microbes to non-

lethal quantities of the drug make them resistant".[9] He was proven right by history (**Figure I.1**).

The development of antimicrobial resistance (AMR) is one of today's major global health threats that emerged due to the widespread and inappropriate use of antibiotics.[10] AMR occurs when bacteria adapt to the exposure of antimicrobial agents, resulting in less effective or completely ineffective drugs. Resistance development is accelerated by overuse in clinical and out-patient settings, misuse in agricultural practices, underdosing, and non-compliance by patients.[1,6,11,12] The consequences of AMR include higher treatment costs, prolonged hospital stays, and increased mortality rates associated with bacterial infections.[10,13] From an economic perspective, the development of novel antibiotic agents that can overcome existing resistance presents substantial hurdles for the pharmaceutical industry. The cost of research and development (R&D) for new antibiotics is immense, including high-risk (and low-gain) investments with long times for clinical trials and subsequent regulatory approvals. The profit generated by antibiotics is generally lower than for drugs treating chronic diseases. Antibiotics are typically used for short-term treatment, unlike drugs for chronic diseases that provide long-term, stable revenues for pharmaceutical companies. Another discouragement is antibiotic stewardship programs designed to preserve the effectiveness of new antibiotics.[14,15] These programs promote the limited use of last-line antibiotics to slow the spread of resistance, which in turn limits sales and further reduces profit potential.[16] As a result, many pharmaceutical companies have abandoned antibiotic research and development in favor of more profitable markets, such as immunotherapy, oncology and cardiovascular disease treatments. With stagnation of antibiotic development the gap is widening between the increase in AMR and the availability of new effective treatment options.[10,17,18] Public health

experts plead for alternative business models, which are supposed to allow the profitable development of antibiotics from an economic perspective. These include public-private partnerships, subsidies by the governments, and incentives to encourage antibiotic innovation and ensure sustainable drug development pipelines.[19,20] Without these measures, the threat posed by the silent AMR pandemic could lead to a post-antibiotic era, where common infections become incurable, posing serious risks to global health and economic stability.[20]

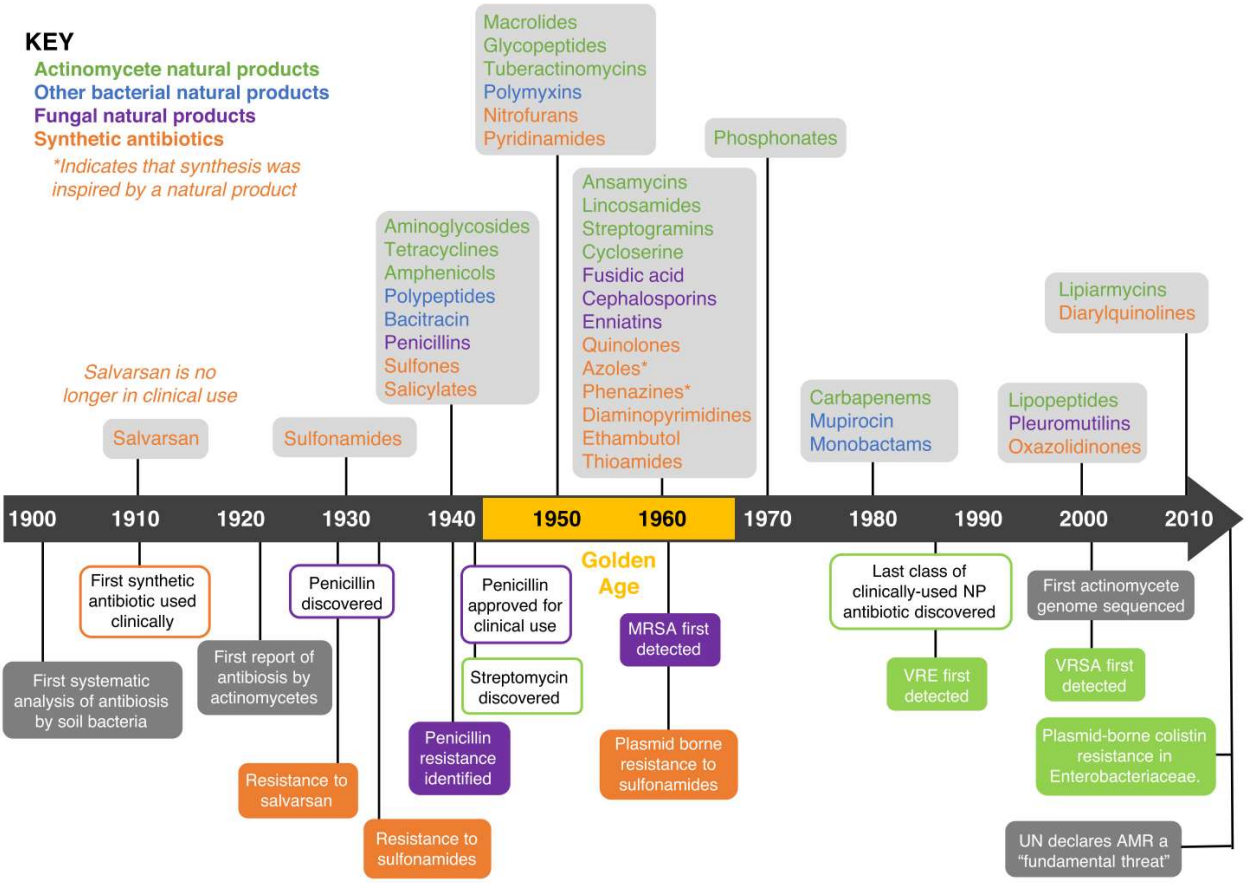

Figure I.1 Timeline of antibiotics discovery and key events in antimicrobial resistance development. This timeline highlights the decades in which new antibiotic classes were introduced in clinical settings, color-coded by origin: green for actinomycetes, blue for other bacteria, purple for fungi, and orange for synthetic compounds. Important milestones in antimicrobial resistance (AMR) are noted, including the emergence of methicillin-resistant *Staphylococcus aureus* (MRSA), vancomycin-resistant *enterococci* (VRE), vancomycin-resistant *S. aureus* (VRSA), and plasmid-mediated colistin resistance in *Enterobacteriaceae*. (Figure taken from *Hutchings et al., Current Opinion in Microbiology, 2019)*[1]

1.2 ANTIMICROBIAL CLASSES, MODES OF ACTION, AND RESISTANCE MECHANISMS

Antibiotics can be classified differently based on their origin, chemical structure, area of application or mode of action. In the following, major antibiotic classes will be summarized based on their antibacterial mechanism and cellular target structures. In addition, major mechanisms that bacteria develop to obtain resistance will be discussed.

1.2.1 Major antibiotic classes and their mode of action

The general aim of antibiotic chemotherapy is the disruption of bacterial cell homeostasis, protein function, and biochemical processes that are distinct from those in humans or animals, enabling specific and targeted therapeutic intervention without serious side effects. These targets include but are not limited to bacterial envelope integrity, protein biosynthesis, folic acid biosynthesis, and replication and transcription mechanisms.[1,21] (**Figure I.2a**)

Antibiotics targeting the bacterial cell envelope, such as β-lactam antibiotics, disrupt bacterial cell integrity by inhibiting DD-transpeptidases (penicillin-binding proteins), enzymes responsible for crosslinking the peptide side chains during the final stages of peptidoglycan biosynthesis. This inhibition leads to the weakening of the cell wall, ultimately resulting in disruption of the bacterial cell homeostasis.[22] Additionally, polymyxin antibiotics directly compromise bacterial cell envelope integrity by interacting with the outer membrane phospholipids and lipopolysaccharides. The hydrophobic tail of polymyxin disrupts the membrane structure through a detergent-like mechanism, causing membrane destabilization and cell death.[23]

Antibiotics that inhibit protein biosynthesis act on bacterial ribosomal subunits, which differ vastly from the mammalian ribosomes, thus disrupting the translation process in

bacteria specifically.[24,25] These antibiotics can be sub-classified into two groups based on the ribosomal subunit they target: inhibitors of the 30S subunit, such as aminoglycosides and tetracycline, and inhibitors of the 50S subunit, such as macrolides and lincosamides. 50S subunit inhibitors primarily interfere with peptidyl transferase activity, thereby halting peptide elongation during translation. In contrast, aminoglycosides as 30S subunit inhibitors disrupt the proofreading function of the ribosome, leading to the synthesis of truncated or misfolded proteins with incorrect amino acid sequences. Tetracyclines also bind to the 30S subunit, directly preventing the attachment of aminoacyl-tRNA and thereby inhibiting peptide chain elongation.[26]

The bacterial folic acid biosynthesis pathway represents a selective target for antibiotics, as mammals, including humans, lack the ability to synthesize folate and instead rely on dietary intake. In bacteria, this pathway is essential for the synthesis of purine and pyrimidine bases, which are critical for nucleic acid metabolism and cell division. Inhibitors of this pathway, such as sulfonamides and trimethoprim, exploit this difference between bacteria and humans.[27] Sulfonamides act as structural analogs of *para*-aminobenzoic acid (PABA), a substrate for dihydropteroate synthase, thereby inhibiting the formation of dihydropteroate, a precursor of folic acid.[28,29] Trimethoprim, on the other hand, selectively inhibits dihydrofolate reductase, an enzyme involved in converting dihydrofolate to tetrahydrofolate, the active form required for purine and pyrimidine synthesis. The inhibition of these two steps results in a severe folate deficiency, disrupting bacterial growth and replication.[30]

Antibiotics that inhibit RNA synthesis, such as rifamycins, target bacterial RNA polymerase, an essential enzyme in the transcription process. RNA polymerase is responsible for synthesizing RNA from a DNA template, a crucial step in gene expression and bacterial growth.[31] Rifamycins, for example, bind to the β-subunit of

bacterial RNA polymerase, blocking the formation of the transcription initiation complex and preventing the elongation of the RNA transcript.[32] This inhibition effectively halts bacterial RNA synthesis, leading to a cessation of protein production and eventual bacterial cell death.[33,34] By specifically targeting bacterial RNA polymerase, these antibiotics are highly selective, as mammalian cells rely on a structurally different RNA polymerase complex, minimizing toxicity to the host.[33]

A further important class of antibiotics are the quinolone antibiotics. Quinolone antibiotics inhibit the bacterial topoisomerase II, specifically the bacterial gyrase.[35] DNA gyrase is a key bacterial enzyme that introduces negative supercoils into DNA, essential for processes such as replication, transcription, and repair. As a type II topoisomerase, gyrase functions by ATP-dependent capturing of a T(transferring)-segment of DNA. Subsequently, the gyrase is creating a temporary double-strand break in the G(gate)-segment of DNA, allowing the T-segment to pass through, and then religating the break in the G-segment.[36,37] This action reduces positive supercoiling, enabling DNA to remain compact and accessible. In replication, DNA gyrase relieves the positive supercoils generated ahead of the replication fork, facilitating smooth progression. It also plays a role in transcription by maintaining the relaxed DNA state needed for efficient gene expression and makes DNA more accessible for repair and recombination.[38] Since DNA gyrase is unique to bacteria and absent in human cells, it serves as an advantageous antibiotic target. Quinolone antibiotics (e.g., ciprofloxacin) inhibit DNA gyrase by stabilizing the enzyme-DNA complex and suppress the religation after cleavage, resulting in lethal DNA breaks in bacteria.[35]

1.2.2 Major antibacterial resistance mechanisms

As mentioned above, with inappropriate usage of antibiotics like underdosing, bacteria evolve various resistance mechanisms to adapt to the selective pressure caused by the antimicrobial treatment. Bacterial resistance to antibiotics arises through genetic mutations, horizontal gene transfer, and/or selection of pre-exisiting resistant phenotypes, leading to reduced efficacy of antimicrobial agents.[12]

One of the most widespread mechanisms of resistance involves the production of β-lactamases, enzymes that hydrolyze the β-lactam ring in β-lactam antibiotics, including penicillins and cephalosporins, rendering them ineffective.[22,39] The emergence of extended-spectrum β-lactamases (ESBLs), metallo-β-lactamases (MBLs) and carbapenemases has further expanded resistance to advanced β-lactams, including carbapenems, which are often used as last-line antibiotics.[40,41] To counteract this resistance, β-lactamase inhibitors, such as clavulanic acid, have been developed to restore β-lactam antibiotic activity in combination therapy.[40] Furthermore, novel β-lactam antibiotics with modified structures have been explored to circumvent β-lactamase-mediated resistance.[19,42]

Polymyxin resistance, particularly in Gram-negative bacteria, poses a growing challenge. Resistance mechanisms typically involve modifications of the bacterial outer membrane, particularly lipopolysaccharides. The addition of 4-amino-4-deoxy-L-arabinose or phosphoethanolamine addition to lipid A and the polysaccharide units decreases the negative charge of the outer membrane, thus reducing polymyxin affinity.[43–45] This modification is particularly concerning, as polymyxins remain one of the few classes of last-resort antibiotics active against multidrug-resistant (MDR) pathogens.[23]

Reduction of influx is another key resistance mechanism. By downregulating the expression of porin channels and receptor proteins facilitating antibiotic entry, bacteria hinder the uptake of antibiotics, rendering them less effective.[46,47]

Efflux pump overexpression is a prominent resistance mechanism, particularly well-studied in *E. coli*.[48] One example is the AcrAB-TolC system, a tripartite efflux pump that expels a broad range of chemically diverse antibiotics, including β-lactams, tetracyclines, and quinolones. The AcrAB-TolC system consists of AcrA (the intermembrane protein), AcrB (the transporter protein), and TolC (the outer membrane channel).[49,50] The active efflux of antibiotics from the cytosol and the periplasm lowers intracellular drug concentrations, thereby reducing drug efficacy. Overexpression of efflux pumps, such as AcrAB-TolC, is frequently associated with high-level resistance to multiple antibiotics, particularly in clinical isolates of Gram-negative bacteria.[49]

Target site mutations represent another significant mechanism of resistance, particularly for antibiotics that target the bacterial ribosome and DNA gyrase.[35,51] Mutations in ribosomal subunits result in protein structure modifications, which impair the binding of antibiotics such as aminoglycosides, macrolides, and tetracyclines.[26,52] Similarly, mutations in the DNA gyrase enzyme confer resistance to quinolones. In the *gyrA* gene, mutations in the quinolone-resistance-determining region (QRDR), e.g., leading to Ser83Leu substitution, impair drug binding. Mutations in *gyrB*, often located in ATP-binding regions of the encoded gyrase B subunit, have the ability to further reduce quinolone affinity.[35] One potential approach to overcome cross-resistance due to target site mutations is the development of next-generation antibiotics that act through novel mechanisms and/or target alternative bacterial structures.[19]

In summary, the development of antibiotic resistances is a multifactorial process involving a variety of mechanisms such as β-lactamase production, structural

modifications, reduced influx, efflux pump overexpression, and target site mutations (**Figure I.2b**). Addressing these resistances requires a comprehensive understanding of their molecular basis, continuous innovation in antibiotic design and the exploration of novel therapeutic strategies, as well as the development of combination therapies to minimize the development of resistances.[20]

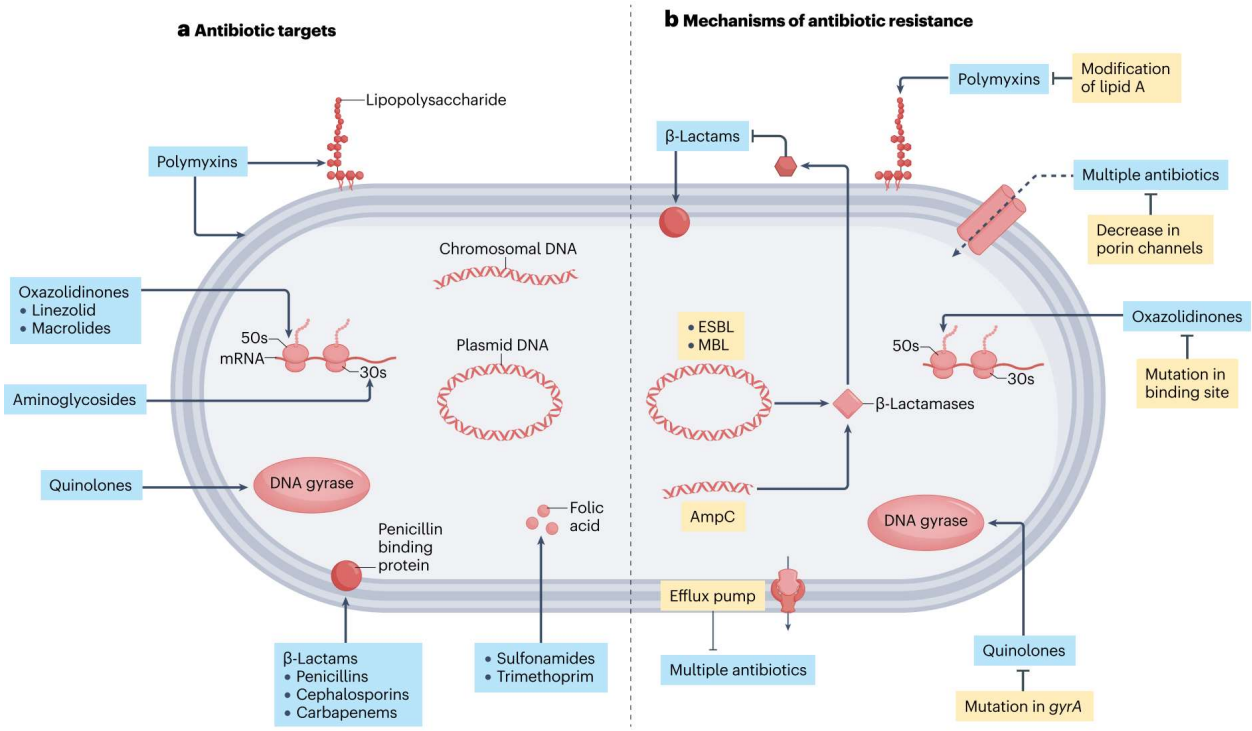

Figure I.2 Antibiotic targets and resistance mechanisms exemplified for *Escherichia coli*. Left panel **a** illustrates the targets of various antibiotics used to treat *E. coli* and other Gram-negative bacteria. Polymyxins act on the outer membrane phospholipids and lipopolysaccharides of Gram-negative bacteria, disrupting membrane integrity. Oxazolidinones block the large ribosomal subunit to inhibit protein synthesis, while aminoglycosides act on the small ribosomal subunit to achieve a similar effect. Quinolones inhibit DNA synthesis by targeting essential bacterial enzymes, and β-lactam antibiotics interfere with cell wall synthesis. Sulfonamides inhibit folic acid synthesis by targeting dihydropteroate synthase. Trimethoprim inhibits folate synthesis by binding to the dihydrofolate reductase. Right panel **b** depicts the resistance strategies adopted by *E. coli* and Gram-negative pathogens. These include the production of β-lactamases to inactivate β-lactam antibiotics, overexpression of efflux pumps to expel antibiotics, and suppression of porin channels to limit antibiotic entry. Additionally, modifications to lipid A prevent recognition by polymyxins, while mutations in DNA synthesis and protein synthesis pathways render oxazolidinones and quinolones ineffective. Abbreviations: ESBL, extended-spectrum β-lactamase; MBL, metallo-β-lactamase. (Figure taken from *Schwartz et al., Nature Reviews Nephrology, 2023)*[53]

1.3 DEVELOPMENT OF NOVEL ANTIMICROBIAL AGENTS

1.3.1 Phases of the drug development process

The development process of a drug and thereby also for novel antibiotics comprises primarily 5 phases. These phases can be categorized in discovery and development, preclinical research, clinical research, review and approval, and post-approval safety monitoring.[54]

The discovery and development phase is initiated by selecting a therapeutic area based on an unmet medical need and the potential for an economical benefit for the companies. Subsequently, various methods are employed for a so-called “Hit-identification”, marking the starting point of the structural optimization process. These techniques include the screening of naturally occurring substances, which offer a rich source of chemical diversity, random high-throughput screening of large chemical libraries, or *in silico* virtual screening using computational models and docking simulations with subsequent targeted synthesis and *in vitro* evaluation.[55–57]

Following identification, these “hits” mostly need optimization to enhance activity, optimize the pharmacokinetic profile, reduce toxicity and ensure feasibility for production scale up. This process is part of the “hit to lead” optimization. The “lead optimization” aims to meet all preclinical requirements, including *in vitro* and *in vivo* pharmacodynamics, pharmacokinetics and toxicological testing. Subsequently, the compound progresses into the “candidate” state.[58,55,59]

The candidate compound is then prepared for production scale up, which can be achieved synthetically, semi-synthetically and biotechnologically. Scale-up is critical to fulfill the demand of the active ingredient for formulation development for (pre-) clinical use, and to perform extensive safety pharmacology studies, including off-target

screening, genotoxicity, reproductive toxicology, carcinogenicity, such as organotoxicity, across various biological systems and dosing regimens.

These structural, chemical and biological data are used to support patent application on the compound (series), securing the intellectual property rights obtained during the development process, and importantly, to prepare for clinical phases in humans.[54,60]

Clinical trials proceed in three main phases. In the clinical phase I, the compound in its preliminary formulation is for the first time administered to human in the so called “first-in-man” studies. This usually involves 20-80 healthy, male, non-smoking or drinking volunteers between the age 18 and 55. The phase I studies evaluate the pharmacokinetic profile and safety of the novel compound in multiple dosing regimens, providing initial insights into optimal dosing for the treatment of patients with a decreased risk of adverse events. Some compounds may be discontinued at this stage because of insufficient pharmacokinetics or too severe adverse events observed after exposure.[54,61,62]

Phase II clinical trials assess the efficacy of the candidate including 100-500 patients, suffering from the targeted disease. Initially, the efficacy and safety in the target population is investigated, usually with a single maximal tolerated dose as “proof of concept” in a cohort of up to 100 patients (phase IIa). Phase IIb includes dose-ranging studies to identify the optimal dose for clinical safety and efficacy. Additionally, drug product formulation and production procedures are further developed. Most candidates fail during phase II studies because of a lack of efficacy or the occurrence of severe adverse side effect, which have not or could not been de-risked beforehand.[63]

Even if the phase II trials give positive results for a candidate, the progression into phase III is also dependent on the comparison to competitors on the market, remaining patent life and the technical and regulatory feasibility for success.[54]

Phase III of clinical development involves ~1000-5000 patients in typically randomized, blinded trials comparing the candidate to a placebo control or standard-of-care treatments. Phase III aims to further refine the formulation, dosing and assess the efficacy of a candidate compound compared to these controls, as well as the safety profile in a bigger cohort, to potentially identify rarely occurring side effects. Comparison with a so-called “gold standard” can aim to demonstrate non-inferiority, equivalence, or superiority.

In the review and approval phase, the sponsor submits the New Drug Application (NDA) or Marketing Authorization Application (MAA) to the regulatory agencies (United Sates Food and Drug Administration or European Medicinal Agency, respectively). Questions of the agencies will be referred back to the sponsor. For a regulatory approval, the candidate must have shown a favorable risk-benefit ratio during the clinical trials and the NDA or MAA must demonstrate measures to ensure pharmaceutical quality, efficacy, and safety.[54,62,64,65]

Post-approval safety monitoring, also known as pharmacovigilance, might be requested by the regulatory agencies. These long-term “real-world” observations provide evidence on the efficacy and especially the safety of a compound in more extended and undefined patient cohorts. In general, these data provide evidence for rare side effects, potential long-term effects as well as drug-drug interactions. If the pharmacovigilance studies indicate an unfavorable risk-benefit profile, a drug might be withdrawn from market.[54,66–69]

1.3.2 Drug repurposing and off-target identification

Interestingly, it happens regularly that drugs are being repurposed for indications beyond their original therapeutic area. This typically occurs when side effects, previously unknown off-target interactions, or molecular mechanisms of a drug are identified, revealing potential therapeutic applications unrelated to the initial indication. A notable example is thalidomide, which was originally developed as a sedative but withdrawn from the market due to its teratogenic effects. Subsequently, thalidomide was found to be effective in treating conditions such as leprosy and multiple myeloma due to its immunomodulatory properties, which led to the development of more targeted analogs, including lenalidomide and pomalidomide.[66,70]

Novel drug indications are often discovered by coincidence during clinical application. However, more systematic and targeted techniques are emerging to identify previously unknown molecular drug mechanisms, including the holistic "-omics" approaches. These methodologies include the systemic analysis of an organisms DNA (genomics), RNA expression (transcriptomics), protein abundance (proteomics), and metabolite quantities (metabolomics). Thus, these techniques not only enable the discovery of novel interaction partners of clinically used drugs for potential label expansion but also help characterizing toxicological risks that may have been unidentified beforehand.[71,72]

An important example is the use of proteomic approaches to examine an organism's protein response to the treatment with a given compound. This involves comparing the protein expression profiles of treated versus untreated organisms to identify significant differences.[73] Furthermore, derivatized tool compounds can directly identify molecular binding partners of the investigated molecule in a comprehensive proteome context. One such technique, affinity-based protein profiling (ABPP), uses probes, equipped with a photo-affinity linker (e.g., diazirine, azide, or benzophenone) and a click-

chemistry partner like an alkyne moiety, to treat bacterial or eukaryotic cells. Upon UV irradiation, the photo-crosslinker covalently binds the probe to target and off-target proteins. Following cell lysis, the alkyne moiety is coupled to biotin via azide-alkyne cycloaddition, enabling enrichment of labeled proteins on avidin beads. These enriched proteins are subsequently digested and analyzed via LC-MS/MS and computational methods to identify and quantify the interaction partners.[74] **(Figure I.3**)

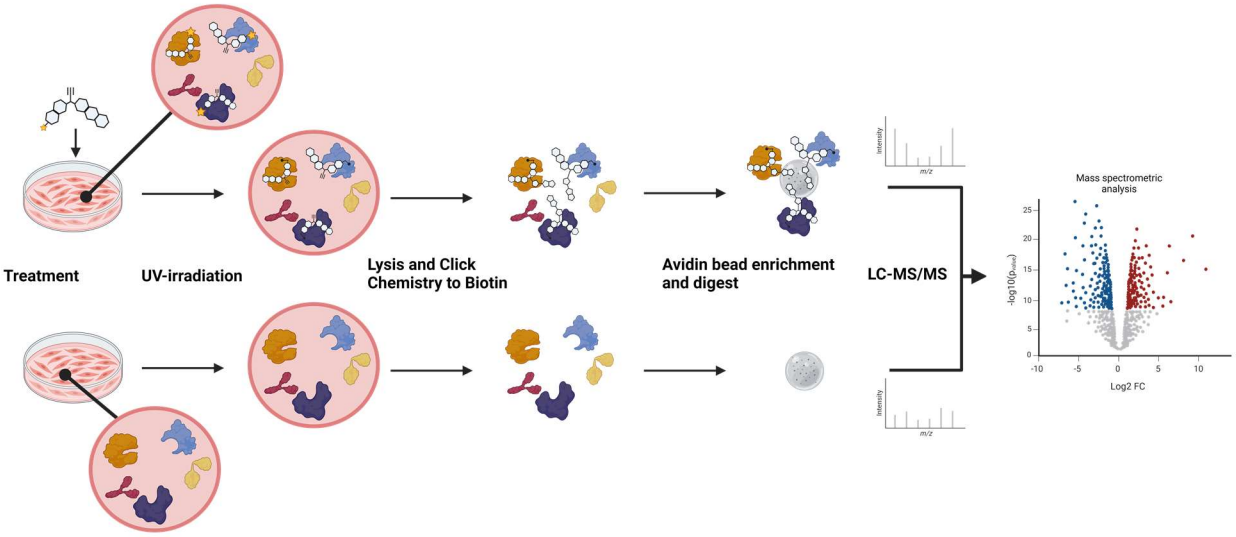

Figure I.3 Affinity-based protein profiling workflow for cystobactamids. Cells are treated with a photo-affinity probe or vehicle control (DMSO) and subsequently UV-irradiated to activate the photo-reactive moiety, enabling covalent binding of the probe to off-target proteins. After cell lysis, the probe-protein complex is conjugated to biotin via azide-alkyne click chemistry, followed by enrichment using avidin-coated beads. Proteins are digested with trypsin, and off-target proteins are identified by relative enrichment in LC-MS/MS analysis, compared to the vehicle-treated control. (Created with BioRender.com)

Such advanced techniques not only enhance the ability to detect and characterize overlooked toxicological properties of compounds but also provide insights into cellular responses to treatments, thus, offering opportunities to uncover previously unknown therapeutic potentials.

1.3.3 Challenges for a successful antibiotic candidate

In the (pre-) clinical development process of a novel antibiotic, some critical hallmarks need to be addressed for a successful candidate. These hallmarks include (broad-spectrum) *in vivo* activity, low tendency for resistance development, selectivity for bacterial targets and cost-effective production.[19]

Unlike for drugs targeting conserved human proteins, bacterial target proteins can vary significantly between species and even among strains within the same species. Consequently, broad-spectrum antibiotics must be optimized to interact with multiple functionally related, yet distinct, target proteins across a wide range of biologically diverse bacterial species. Furthermore, many antibiotics in the (pre-) clinical pipeline are derived from secondary metabolites. These compounds are naturally designed to exhibit antimicrobial activity. However, these natural products often require structural modifications to optimize key pharmacokinetic parameters, including bioavailability, metabolic stability, and potentially reduced plasma protein binding to achieve sufficient target exposure. These enhancements are crucial for ensuring effective *in vivo* therapy, while simultaneously maintaining their broad-spectrum activity.[1,75]

A further hurdle for effective broad-spectrum therapy is the prevalence of pre-existing cross-resistances, potentially rendering the antimicrobial agent ineffective against resistant bacterial populations. This might pose a risk for the future clinical application of the developed antimicrobial agent and can potentially be de-risked by assessing the minimal inhibitory concentration (MIC) against various clinically relevant multi-resistant strains.[76] To further estimate the bacterial adaptation rate due to the use of an antimicrobial compound under development, it is essential to thoroughly evaluate the mode and frequency of resistances (FoR) in response to the novel antimicrobial to prevent rapid resistance emergence and subsequent loss of efficacy.[19]

Another critical parameter for a successful candidate is the selectivity index (SI), which reflects the compound's ability to specifically target bacterial cells while minimizing harm to animals and human. For an antibiotic to be effective *in vivo*, it must achieve sufficient exposure in the target compartment, with concentrations exceeding the MIC and maintaining extended exposure times to effectively clear the infection. Simultaneously, the treatment must not pose a severe risk of toxic events for the infected host.[77,78]

A candidate meeting the efficacy and safety criteria advances in the development process, where cost-effective production scale-up becomes essential for successful progression, due to the relatively low revenue of antibiotics. The advanced production process of these natural products include synthetic and/or biotechnological scale up, where synthetic yield and/or production titer need to be optimized (often in g/L range)[60], with subsequent downstream processing and sufficient developability from drug substance (active ingredient) into the actual drug product (embedded in the formulation).

Furthermore, the compound and its manufacturing process must be reproducible to meet the Chemistry, Manufacturing, and Controls (CMC) requirements, ensuring drug product batch-to-batch consistency and thereby its safety, efficacy and quality.[62,65,79,80]

A successful candidate must meet these criteria while also offering the potential for economic benefit to the producing company. Achieving this, however, may prove to be the most challenging aspect, as discussed at the end of section 1.1.[16]

1.4 CYSTOBACTAMIDS

Cystobactamids are a class of microbial natural products originally isolated from the soil-dwelling myxobacterium *Cystobacter sp.*.[81] Myxobacteria are known for their unique ability to degrade insoluble organic materials and exhibit coordinated swarm behavior, acting as microbial predators against other bacteria.[82] These characteristics, combined with their comparatively large genomes (typically more than 10 million base pairs, with some reaching up to 16 million base pairs)[83] in contrast to smaller bacterial genomes, such as that of *E. coli* (3.5 to almost 8 million base pairs)[84], make myxobacteria particularly promising for the discovery of novel secondary metabolites. The diversity and prevalence of biosynthetic gene clusters (BGCs), within their genomes highlight their potential as a rich source of structural diverse bioactive natural products. BGCs are genes in close genetic proximity with often co-regulated expression. They mostly encode for proteins participating in a common, discrete metabolic pathway for producing secondary metabolites, which may mediate an ecological advantage for the producer over competitors.[85]

These include not only antimicrobial agents but also molecules with potential applications in anticancer, antiviral, anthelmintic, and immunomodulatory therapies. The potential of myxobacteria is thereby comparable to that of the well-characterized *Streptomyces* species. However, continuous thorough investigations are required to explore their value as a source of pharmaceutically relevant substances.[7,86]

Cystobactamids are biosynthesized through non-ribosomal peptide synthetases, encoded by a 52-kilobase biosynthetic gene cluster. The formation of the *para*-aminobenzoic acid (pABA) containing backbone is directed by six modules encoded by the genes *cysK* and *cysG*. These assemble the pABA chain around a methoxylated asparagine linker, which is initially processed by CysH with various tailoring enzymes,

prior to the transfer to CysK by CysB. Additionally, CysC, CysF, and CysS likely mediate the modification of the D-ring pABA unit to form 2-isopropoxy-3-hydroxy-pABA, while CysR catalyzes the conversion of the *N*-terminal pABA unit to *para*-nitrobenzoic acid (pNBA) (**Figure I.4**).[81,87] Structurally, cystobactamids show significant similarity to other natural product classes, including coralmycin and albicidin. Coralmycin, isolated from the myxobacteria *Corallococcus coralloides*, only differs in some stereoisomers of the central amino acid and may exhibit variations in the alkoxy and hydroxyl substitution of rings D and E, as shown for Coralmycin B. As a result, coralmycins can be considered as rediscovered analogs of cystobactamids.[88] As opposed to coralmycin, albicidin was isolated from the myxobacteria unrelated sugarcane pathogen *Xanthomonas albilineans*. Its structure incorporates an N-terminal *para*-methylcoumaric acid with a β-L-cyanoalanine linker and ring D and E substitution patterns different to cystobactamids. Nevertheless, insights into the biological activity of cystobactamids may thereby have implications for related compounds with potential therapeutic applications.[88,89]

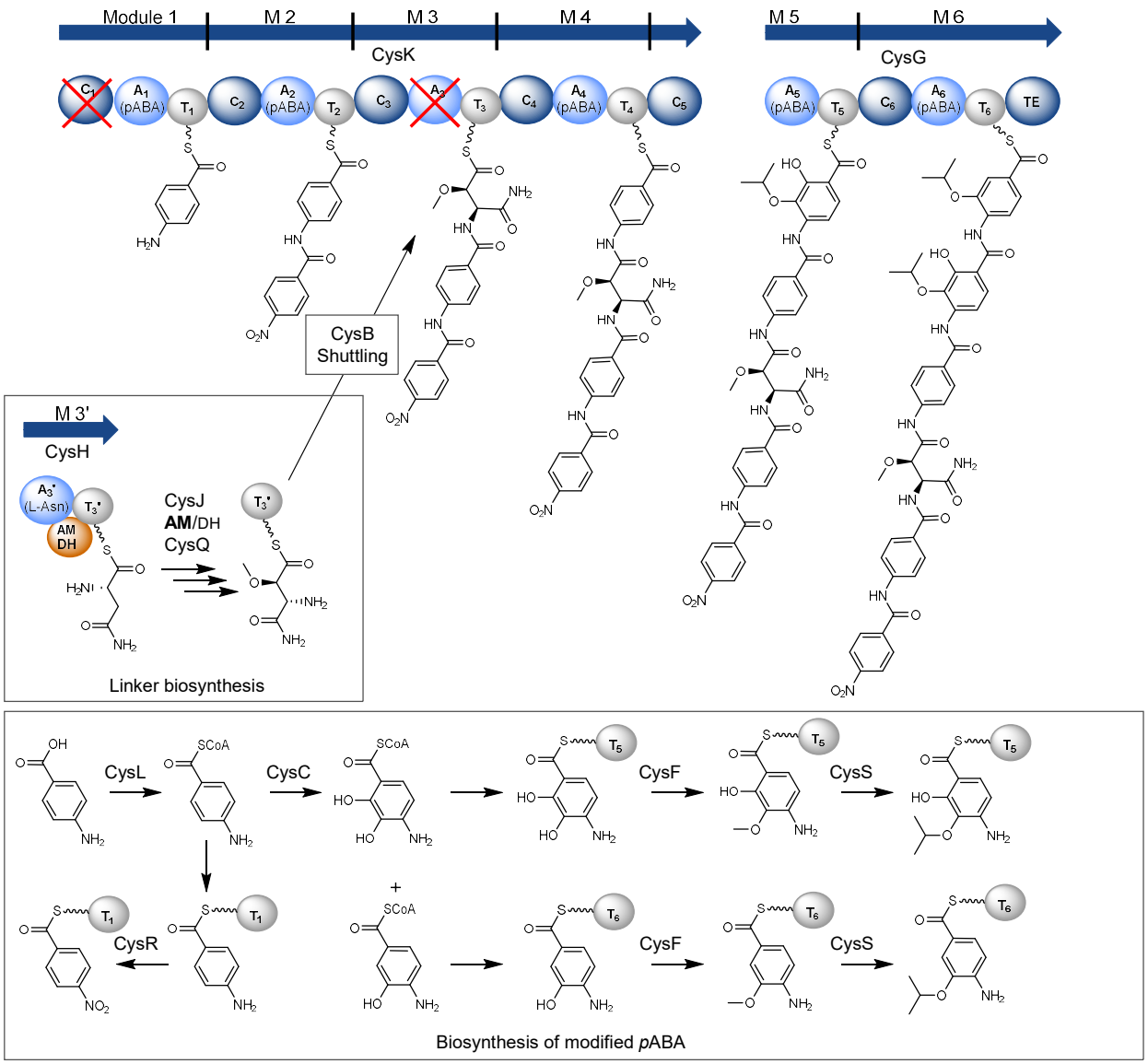

Figure I.4 Biosynthesis of cystobactamids through a 52-kilobase non-ribosomal peptide synthetase (NRPS) gene cluster. The *para*-aminobenzoic acid (pABA) backbone with central methoxylated asparagine moiety is assembled by six modules encoded within *cysK* and *cysG*. The modified amino acid linker is processed by CysH with various tailoring enzymes, with subsequent transfer to CysK by CysB. Modifications of the D-ring pABA unit to 2-isopropoxy-3-hydroxy-pABA are likely catalyzed by CysC, CysF, and CysS, while CysR converts the *N*-terminal pABA to *para*-nitrobenzoic acid (pNBA). Red cross indicates inactive domains. (Figure taken from *Groß et al., Nature Communication, 2021)*[87]

Notably, the *cysO* gene within the genetic locus of the cystobactamid BGC encodes a pentapeptide repeat protein. This protein family is known for mimicking the structure of DNA and thus, its role in conferring (self-) resistance to topoisomerase poisons,

including fluoroquinolones (Qnr and MfpA), microcin B17 (McbG), and the structurally similar albicidin (AlbG).[81,90]

Indeed, cystobactamids have been shown to inhibit bacterial gyrase and topoisomerase IV through a mechanism distinct from that of quinolone antibiotics.[81,91] The compound class exhibits broad-spectrum antibacterial activity against both Gram-positive and Gram-negative bacteria, including all ESKAPE pathogens (*Enterococcus faecium, Staphylococcus aureus, Klebsiella pneumoniae, Acinetobacter baumannii, Pseudomonas aeruginosa*, and *Enterobacter* spp.)[92], with inhibitory concentrations in the low micromolar to nanomolar range.[93] Early stage derivatives exhibited a slight cross-resistance to quinolone antibiotics, likely due to the spatial proximity of their binding sites and the contribution of efflux mechanisms.[81] However, the novel chemical structure of cystobactamids may contribute to their ability to overcome bacterial resistance, as no substantial cross- or co-resistances with existing clinical antibiotic classes have been reported for the more advanced derivatives.[93] Cystobactamids have demonstrated *in vivo* efficacy in an *E. coli* thigh infection model, although with slightly reduced potency compared to the quinolone reference drug levofloxacin. Additionally, cystobactamids have shown a favorable safety profile in mammalian cell lines, supporting selective inhibition of bacterial enzymes.[94–97]

The promising properties of cystobactamids have driven ongoing development efforts through a collaboration between the Helmholtz Center for Infection Research (HZI), the Helmholtz-Institute for Pharmaceutical Research Saarland (HIPS), Leibniz University Hannover, and Evotec. This partnership has focused on a synthetic hit-to-lead optimization strategy, generating over 300 derivatives through a thorough investigation of structure-activity and structure-property relationships (**Figure I.5**). These efforts have yielded derivatives with enhanced broad-spectrum activity in the

low nanomolar range, particularly against carbapenem-resistant *Acinetobacter baumannii*, as well as improved *in vivo* tissue exposure, increased water solubility, and an acceptable frequency of resistance (FoR) between 10^{-7} and 10^{-9}.[93,95–102] However, challenges remain, including high plasma protein binding, relatively short *in vivo* half-lives ($t_{1/2}$~0.5 h), and the generally low hydrophilicity of most derivatives.

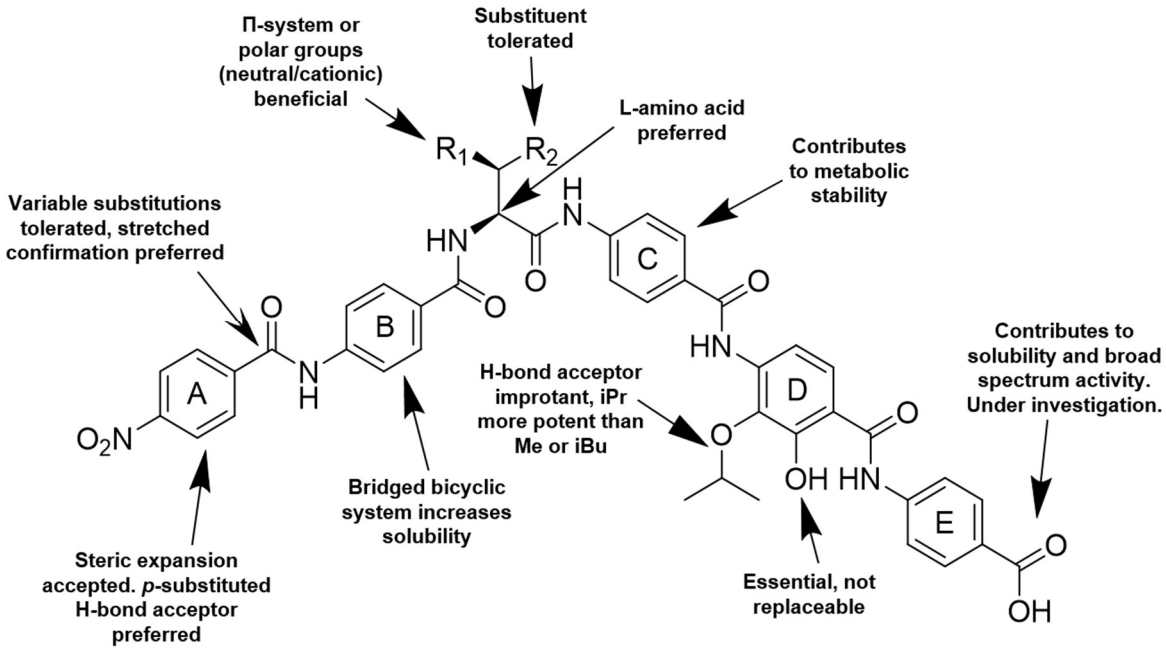

Figure I.5 Structure-activity and structure-property relationships of cystobactamids.[94,95,100,103,104]

1.5 OUTLINE OF THIS THESIS

This thesis investigates the microbiological, pharmacological and toxicological properties of cystobactamids as novel bioactive natural product class. Cystobactamids show promising potential as novel antimicrobial therapy, with the capability to contribute to the fight against the escalating silent pandemic of antimicrobial resistance. Since the majority of compounds in clinical development fail due to insufficient safety profiles and/or lack of efficacy, this thesis aims to de-risk some critical challenges of this compound class in the development pipeline.

Given their properties to overcome cross-resistances to the antimicrobial classes in clinical use, this thesis will explore the so far unknown mechanisms by which the high priority pathogen *E. coli* develops resistance to cystobactamids. To elucidate these resistance mechanisms, *E. coli* will be analyzed at both, the genomic and proteomic levels, identifying molecular mechanisms associated with resistance. The findings will provide critical insights into the bacterial pathways that contribute to cystobactamid resistance. (Chapter 1)

This work will further elucidate the pharmacological interactions of cystobactamids with eukaryotes. Therefore, potential toxicological effects on the protein, cellular and organismal level will be examined phenotypically and on a molecular basis, with the aim to characterize eukaryotic off-target effects. Additionally, metabolic vulnerabilities of cystobactamids will be identified, with the intention to develop strategies for improved metabolic stability, decreased cystobactamids biodegradation and potentially extended exposure duration. (Chapter 2)

2. Chapter 1: YgiV promoter mutations cause resistance to cystobactamids and reduced virulence factor expression in *Escherichia coli*

Published in *npj Antimicrobials and Resistance* – DOI: 10.1038/s44259-024-00050-7

Timo Risch[1, 2], Dominik Kolling[1], Dietrich Mostert[3], Tim Seedorf[4], Dominik Heimann[2, 5], Daniel Kohnhäuser[2, 5], Felix Deschner[1, 2], Franziska Fries[1, 2], Danny Solga[4], Jil-Sophie Hilgers[1], Jan Dastbaz[1, 2], Stefano Mancini[6], Anna K. H. Hirsch[1, 2], Mark Brönstrup[2, 5], Andreas Kirschning[4, 7], Stephan A. Sieber[1, 3], Jennifer Herrmann*[1, 2], and Rolf Müller*[1, 2]

(1) T. Risch, D. Kolling, F. Deschner, F. Fries, J. Dastbaz, J. Hilgers, Prof. Dr. A. K. H. Hirsch, Dr. J. Herrmann, Prof. Dr. S. A. Sieber, Prof. Dr. R. Müller
Helmholtz Institute for Pharmaceutical Research Saarland (HIPS)
Helmholtz Centre for Infection Research (HZI) and Saarland University Department of Pharmacy
Campus Building E8.1, 66123 Saarbrücken, Germany
E-mail: rolf.mueller@helmholtz-hips.de

(2) T. Risch, F. Deschner, F. Fries, J. Dastbaz, Dr. D. Kohnhäuser, D. Heimann, Prof. Dr. M. Brönstrup, Prof. Dr. A. K. H. Hirsch, Dr. J. Herrmann, Prof. Dr. R. Müller
German Centre for Infection Research (DZIF)
Inhoffenstraße 7, 38124 Braunschweig, Germany

(3) D. Mostert, Prof. Dr. S. A. Sieber
Center for Functional Protein Assemblies (CPA), Department of Chemistry, Chair of Organic Chemistry II, Technical University of Munich, 85748 Garching, Germany
Ernst-Otto-Fischer-Straße 8, 85748 Garching, Germany

(4) Dr. T. Seedorf, Dr. D. Solga, Prof. Dr. A. Kirschning
Leibniz University Hannover
Institute of Organic Chemistry
Schneiderberg 1B, 30167 Hannover, Germany

(5) Dr. D. Kohnhäuser, D. Heimann, Prof. Dr. M. Brönstrup
Helmholtz Centre for Infection Research (HZI)
Inhoffenstraße 7, 38124 Braunschweig, Germany

(6) PD Dr. Stefano Mancini
Institute of Medical Microbiology, University of Zürich
Vladimir-Prelog-Weg 4, 8049 Zürich, Switzerland

(7) Prof. Dr. A. Kirschning
Uppsala Biomedical Center (BMC), University Uppsala, Husargatan 3, 752 37 Uppsala, Sweden

(*) Co-corresponding Author

Supplementary information (SI) can be found at the end of this chapter. Synthesis and NMR spectra for Cysto-180 [**3**] and Cysto-33 [**5**] are not included in the SI and can be found online.

Contributions to the presented work

TR designed, performed and analyzed the majority of mentioned experiments. This included experiments to determine the frequency of resistance, mutant generation, minimal inhibitory concentration, growth curves and metabolic heat flow, genomic DNA extraction and analysis, full proteome profiling, motility assays, cloning of the overexpressing strain, gyrase supercoiling and cleavage assays, compound degradation assay, native protein mass spectrometry, microscale thermophoresis, affinity-based protein profiling and statistical evaluation. He wrote and edited the manuscript and handled the submission and revision process.

DKol optimized the expression, purified, and provided the YgiV protein. DH, TS, DS, DKoh synthesized and provided mentioned cystobactamid derivatives important for the manuscript. FF partly performed FoR testing. DM partially measured and helped analyzing proteomic samples. FD supported genomic data analysis. JSH supported MIC testing. JD supported cloning of *ygiV*. SM provided the clinically isolated *E. coli* strains. JH, RM, MB, AH, AK and SS provided supervision and funding. TR, JH and RM designed the project. All authors were involved in reviewing and editing the manuscript and approved the final version.

2.1 ABSTRACT

Antimicrobial resistance is one of the major health threats of the modern world. Thus, new structural classes of antimicrobial compounds are needed in order to overcome existing resistance. Cystobactamids represent one such new compound class that inhibit the well-established target bacterial type II topoisomerases while exhibiting superior antibacterial and resistance-breaking properties. Understanding potential mechanisms of emerging resistances is crucial in the development of novel antibiotics as they directly impact the future therapeutic application and market success. Therefore, the frequency and molecular basis of cystobactamid resistance in *Escherichia coli* was analyzed. High-level resistant *E. coli* mutants were selected and found to harbor single nucleotide polymorphisms in the promotor region of the *ygiV* gene, causing an upregulation of the respective protein. These stable mutations are contrary to what was observed as a resistance genotype for the structurally related albicidins, where *ygiV* gene amplifications were identified as causing resistance. Overexpression of YgiV in the mutants was additionally amplified upon cystobactamid exposition, showing further adaptation to this compound class under treatment. YgiV binds cystobactamids with high binding affinity, thereby preventing their interaction with the antimicrobial targets topoisomerase IV and DNA gyrase. In addition, we observed a substantial impact of YgiV on *in vitro* gyrase activity by leading to increased DNA cleavage and concurrent reduction in the efficacy of cystobactamids in inhibiting gyrase supercoiling activity. Furthermore, we identified co-upregulation of membrane-modifying proteins, such as EptC, and the transcriptional regulator QseB. This presumably contributes to the observed reduced motility and fimbrial protein expression in resistant mutants, resulting in a reduced expression of virulence factors and potentially pathogenicity, associated with *ygiV* promotor mutations.

2.2 INTRODUCTION

Antimicrobial resistance (AMR) is a major threat for modern medicine, influencing not only primary therapeutic intervention but also essential treatments such as surgery, cancer chemotherapy and prevention of secondary infections. This silent pandemic, mainly driven by misuse of existing antimicrobials and lack of novel antibiotics, causes prolonged hospitalization, higher treatment costs and increased mortality.[105] Recent studies show that AMR was associated with 4.95 million deaths in 2019, with increasing numbers potentially reaching 10 million deaths in 2050.[106] Multidrug-resistant (MDR) *Escherichia coli* was found to be the leading cause of deadly infections associated with or attributed to antimicrobial resistance in 2019.[10] This pathogen shows high adaptability to a broad spectrum of known antimicrobial classes such as beta-lactams, quinolone antibiotics, sulfonamides and many more. The spread of AMR results in decreased treatment options, prolonged treatment time leading to treatment complications and finally increased mortality.[107,108]

Cystobactamids (CYSs) have a high potential to be developed as a new antibiotic class due to their novel structural scaffold and mode of action. This natural compound class was first isolated from *Cystobacter* spp. and their biosynthetic pathway, as well as their total synthetic route, have been investigated and optimized.[99,87] Natural CYS derivatives incorporate multiple *para*-aminobenzoic acid (PABA) units and an *N*-terminal *para*-nitrobenzoic acid linked through a central amino acid, similar to the structurally related natural compounds albicidin, which carries in contrast to CYSs an N-terminal *para*-methylcoumaric acid, and coralmycin.[89,88] A number of structure-activity guided chemical optimization studies led to the discovery of new derivatives with favorable properties in terms of antibacterial spectrum coverage and potency.[10] CYSs show broad activity against multi-drug resistant (MDR) Gram-negative and

Gram-positive pathogens such as *Acinetobacter baumannii*, *E. coli*, *Staphylococcus aureus*, and *Enterococcus* spp. mediated by inhibition of the bacterial gyrase and topoisomerase IV. This potent activity coupled with the lack of cytotoxic effects on eukaryotic cells, render CYSs as highly valuable for the development of a potential novel antibiotic class.

During the development of a novel antimicrobial compound, it is of utmost importance to understand the mechanism(s) of resistance in target pathogens. In contrast to the structurally related albicidins, where the tsx-encoded outer membrane channel mutation was found as a major cause for stable resistance in *E. coli*, the resistance mechanism for CYSs remained unknown.[47] In this study, the CYS mode of resistance in *E. coli* as the target pathogen was investigated. To this end we generated resistant mutants and subsequently characterized the mutants using genomic and proteomic analyses. Previous studies already suggested that, in contrast to fluoroquinolones, CYS resistance (CYS^R) in *E. coli* is barely affected by efflux through the AcrAB-TolC pump or by typical target mutations in the quinolone resistance determining region (QRDR) of gyrase and topoisomerase IV.[98,93] Here, we could confirm this finding and identified the YgiV protein as major cause of high-level resistance. YgiV is a soluble 17.8 kDa protein consisting of 160 amino acids, whose biological function is described as a repressor of the *mcbR* biofilm gene.[109] Furthermore, it incorporates a DNA binding domain and shows homology to GyrI-like proteins.[110] GyrI-like proteins are known for their protective effect on bacterial cells via numerous mechanisms, including gyrase protection or binding as well as modification of harmful xenobiotics.[111] With further characterization we have been able to conclude CYS neutralization is due to competitive binding to YgiV rather than an efflux-mediated mode of resistance. As opposed to recently published literature on albicidin resistance, YgiV overexpression

in CYS^R is caused by point mutations in its promotor region, which in turn also affect bacterial virulence factor expression.[112]

2.3 RESULTS AND DISCUSSION

2.3.1 Resistance development leads to stable high-level resistance against different CYS derivatives.

Among many synthetic and natural CYS derivatives, the early-stage CYS derivative CN-861-2 [**1**] was used as the major reference compound in this study, because of its typical CYS structural composition, which is closely related to the natural products and its well-studied biological behaviour.[101,98] CNDM-861 [**2**] and Cysto-180 [**3**] (synthesis see **Supplementary Figure 1.1** to **1.10**) were further chosen as control CYSs. The early stage derivative CNDM-861 [**2**] is closely related to CN-861-2 [**1**], missing a single methoxy-group in the linker region. Cysto-180 [**3**] is a later stage CYS derivative with a highly modified B-ring and linker region, leading to superior physicochemical properties (**Figure 1.1**). The well characterized *E. coli* K12 (BW25113) strain was used for generating CYS^R mutants because of its outstanding annotation and comparability with single gene knockout (KO) strains from the Keio library.[113] Single bacterial colonies were selected after overnight incubation on CYS CN-861-2-[**1**]-containing solid medium, with a moderate to low frequency of resistance (FoR) of 2.6×10^{-8} at 4-fold MIC and no resistance development at 8-, 16- and 32-fold MIC (FoR < 10^{-9}) (**Supplementary Table 1.1**). Eight individual mutant clones were selected and tested for susceptibility to three CYS derivatives, as well as to the clinically approved topoisomerase poisons ciprofloxacin (CIP) and levofloxacin (LEV). All isolated mutants showed high-level resistance against tested CYS derivatives with 20- to ≥ 640-fold shifts in the minimum inhibitory concentration (MIC). No shift in MIC was

observed for these mutants when tested against quinolone antibiotics (**Table 1.1**), however, high-level cross-resistance to the structurally related albicidin [**4**] was detected (**Supplementary Table 1.2**). This indicated that the occurring resistance mechanism is highly specific for CYS and structurally related compounds, and does not rely on the specific linker or ring composition, nor the physicochemical properties of the derivatives. This specificity is supported by the lack of cross-resistance to the quinolone topoisomerase poisons, sharing the same targets. When MICs were re-evaluated after ten days of serial passaging without selective pressure, reversibility of resistance was not observed, suggesting a stable mutant genotype. To study whether the underlying resistance mechanism is accompanied by a fitness cost, we analyzed the *in vitro* growth and metabolic heat profiles of CYS^R mutants. There were no considerable differences between the mutants and the wild-type (WT) (**Supplementary Figure 1.11),** indicating that there is no evolutionary disadvantage such as metabolic fitness loss resulting from the resistance-causing mutations, and explaining the stability of the occurring resistance.

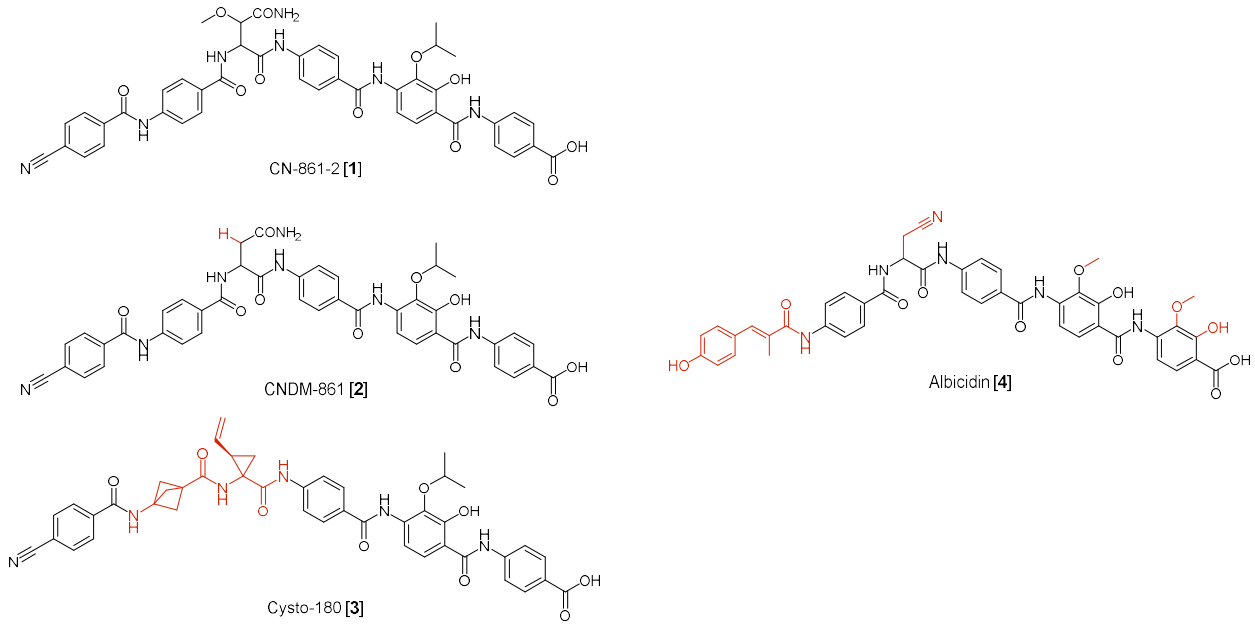

Figure 1.1: Chemical structures of tested cystobactamid derivatives CN-861-2 [1], CNDM-861 [2] and Cysto-180 [3] in comparison to the structurally related albicidin [4]. Structural differences to cystobactamid CN-861-2 [**1**] (reference in this study) are marked in red.

Table 1.1: Minimal inhibitory concentrations (MIC) of cystobactamids and quinolone antibiotics against *Escherichia coli* BW25113 wild type (WT) and generated cystobactamid-resistant mutants (M1-8). Generated cystobactamid-resistant mutants showed high-level MIC shifts (≥20-fold) to all tested cystobactamids. M3 and M6 show the highest MIC shift. Cross-resistance with topoisomerase poisons ciprofloxacin (CIP) and levofloxacin (LEV) was not observed.

	MIC [µg/mL]				
	CN-861-2 [1]	CNDM-861 [2]	Cysto-180 [3]	CIP	LEV
***E. coli* WT**	0.2	0.1	0.2	0.08	0.16
M1	8	4	4	0.08	0.16
M2	8	4	8	0.08	0.08
M3	32	4	16	0.08	0.08
M4	8	4	8	0.08	0.16
M5	8	2	8	0.08	0.08
M6	> 64	> 64	64	0.04	0.08
M7	8	4	8	0.08	0.16
M8	8	4	8	0.08	0.16

CIP: Ciprofloxacin, LEV: Levofloxacin

2.3.2 Genome analysis revealed SNPs in the potential promotor region of the *ygiV* gene.

Whole-genome sequencing of CYS^R *E. coli* enabled the identification of two major mutation sites in close proximity to each other, that are associated to resistance (**Figure 1.2**). All eight mutants showed SNPs upstream of the *ygiV* gene. Mutants M3 and M6, showing the highest MIC shifts, differed in SNP location from the other CYS^R mutants. This is contrary to a recently published report on the related albicidin [**4**], where gene amplification events in the genetic locus of *ygiV* were identified to cause resistance[112]. Gene amplifications are intrinsically unstable due to higher fitness costs[114], explaining the difference in stability of albicidin [**4**] and CYS resistance in *E. coli*, respectively. The previously investigated albicidin-[**4**]-resistant mutants lost their higher copy number of the respective genetic area in the absence of selective pressure[112], whereas CYS^R mutants carrying SNPs maintained high-level resistance under similar experimental conditions. When testing the Keio *ygiV* KO strain, we did not detect a shift in MIC compared to the parent strain (**Supplementary Table 1.3**). However, when trying to evaluate the FoR for this strain, it was not possible to generate resistant mutants and a FoR of $<10^{-10}$ was determined (**Supplementary Table 1.4**). Moreover, our attempts to induce resistance in the *ygiV* KO strain through prolonged antibiotic exposure over 5 days, utilizing parallel serial passaging in low to high CYS concentrations (0.25-, 0.5-, 1.0-, 2-, 4-fold MIC) remained unsuccessful, indicating an essential role of this gene for CYS resistance in *E. coli,* which cannot be compensated by other resistance mechanisms such as target mutation.

Furthermore, six out of eight CYS^R *E. coli* showed mutations in *qseC*, encoding for the sensor histidine kinase of the two-component system (TCS) QseBC[115], leading to a change in the amino acid sequence, a frameshift or an insertion of a premature stop

codon (**Table 1.2**). These mutations were located in the direct genetic neighborhood to *ygiV*, probably mutually influencing their transcription due to a shared promotor site.[115] However, the level of resistance of individual mutants did not correlate with the presence or absence of mutations in the *qseC* gene.

Figure 1.2: Cystobactamid induced mutations in *Escherichia coli* are located in direct genetic neighborhood. Single nucleotide polymorphisms were found in the promotor region of *ygiV* of all cystobactamid-resistant mutants, with some carrying additional mutations in *qseC* (cp. Table 1.2) (created with BioRender.com).

Table 1.2: Identified mutations in cystobactamid-resistant *Escherichia coli* were found upstream of *ygiV* as well as in *qseC*.

	M1	M2	M3	M4	M5	M6	M7	M8
ygiV	-4 G>T	-4 G>T	-13 C>T	-4 G>T	-4 G>A	-9 C>A	-4 G>T	-4 G>T
qseC	ΔG892 Val321*	-	IS T221 Asn75*	ΔG1246 M331*	-	98 G>A W33*	-	Ile159>Leu Val160>Arg

Point mutations were indicated as e.g., -4 G>T, describing a G to T transition four bases upstream of *ygiV*. Insertion and deletions were indicated by IS and Δ with the respective base position. Frameshift mutations that cause early stop of translation were indicated with the native amino acid position and * as translational stop.

2.3.3 Full-proteome analysis revealed extensive overexpression of YgiV in CYS^R mutants compared to the WT.

Three CYS^R mutants M3, M6 and M8 with varying mutation sites (**Table 1.2**) and resistance phenotype (**Table 1.1**) were selected to study their differential proteome expression. All selected mutants carry mutations in the promotor region of *ygiV*, with M8 representing the most common genotype, and additionally carrying *qseC*

mutations. The analyzed mutants showed a high consensus of significantly upregulated proteins (*p*-value [$-\log_{10}$] > 1.3, difference [$\log_2$] > 1.5). Eighteen out of 32 proteins were overexpressed in all analyzed mutants, and two functional clusters were identified (**Figure 1.3a** and **b**). One cluster represented phage-shock proteins (Psp), which are related to survival under nutrient- or energy-limited conditions and known for stabilizing the cell membrane.[116,117] The second cluster comprised upregulated proteins known to play a role in resistance against cationic antimicrobial peptides (AMPs) by affecting bacterial membranes. This includes the transcriptional regulator protein QseB, the undecaprenyl-phosphate 4-deoxy-4-formamido-L-arabinose transferase ArnC, the phosphoethanolamine transferase EptC, the bifunctional polymyxin resistance protein ArnA, the transcriptional regulatory protein BasR and the lipopolysaccharide core heptose(II)-phosphate phosphatase Ais (**Figure 1.3b**).[118,119,120] This upregulation of proteins, potentially causing cationic peptide resistance due to positively charged membrane modifications, can be explained as a downstream effect of detected QseB overexpression, which is known to influence the expression of ArnA, ArnC and EptC.[118] This overexpression of QseB in CYS^R mutant bacteria was very likely caused by the identified mutations (**Table 1.2**), suggesting a shared transcriptional regulatory region between *ygiVW* and *qseBC*.[115] However, no cross-resistance to colistin and polymyxin B was identified, which led us to conclude that, although being significantly upregulated, these membrane modifying proteins only play a minor role in contributing to the CYS resistance phenotype of *E. coli*, further highlighting a very specific mode of resistance that occurs also independent of *qseC* mutation (**Supplementary Table 1.2**). In case of the most resistant CYS^R M6, YgiV was the most highly overexpressed protein compared to the WT proteome (**Figure 1.3c**). Additionally, relative YgiV expression levels differ significantly between mutants

with different SNP positions (*p*-value < 0.0001, two-tailed student´s t-test, n = 4) and correlated with observed MIC shifts for tested CYS^R strains (M6>M3>M8) (**Figure 1.3d**), indicating a crucial role of the protein in CYS^R. YgiV expression levels in WT bacteria were below the limit of detection (LoD), hence its abundance for relative quantification was based on imputed values. This suggests that found SNPs, occurring in the promotor region of the *ygiV* gene, potentially cause a change in affinity for a yet unknown transcriptional regulator, resulting in upregulation of the protein. This hypothesis is supported by the differences we identified in overexpression and the degree of CYS^R, seen for mutants with different SNP positions in the *ygiV* promotor region. In addition, we analogously generated resistant mutants from a set of three clinically relevant *E. coli* strains and performed a full proteome analysis of these mutants with the highest level of CYS resistance in order to determine the relevance of YgiV overexpression in clinical isolates.[121] Firstly, multiple MDR clinical isolates were tested for their susceptibility to CYS, showing sensitivity with no pre-existing resistances (**Supplementary Table 1.5** and **1.6**). Secondly, resistance to CYS was generated and the differential proteome expressions of the most resistant CYS^R mutants was analyzed, revealing highly consistent differential proteome profiles to those generated from BW25113, including YgiV overexpression (**Supplementary Figure 1.12**).

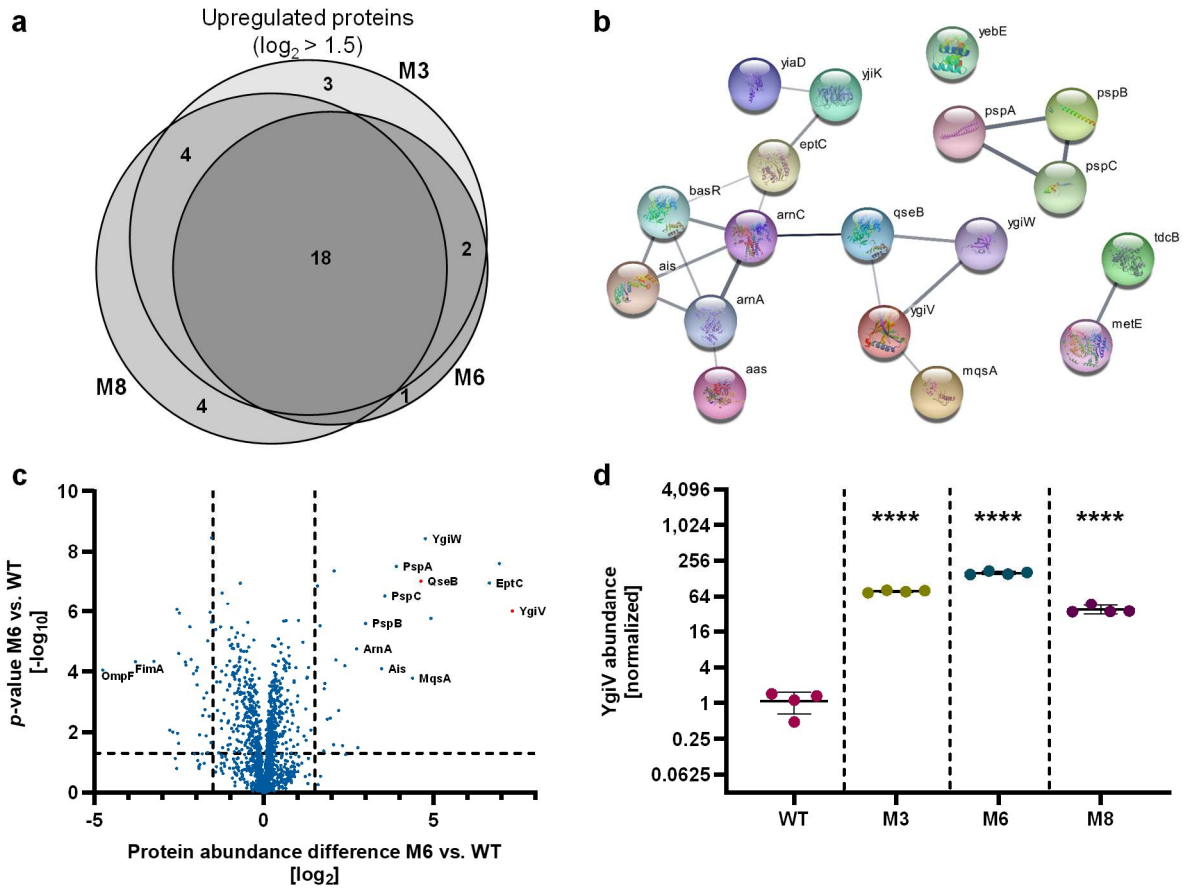

Figure 1.3: Full-proteome analysis revealed high consensus in upregulated proteins of tested mutants and indicate an important role of YgiV in resistance. a Comparison of upregulated proteins in mutants M3, M6 and M8 showed an intersection of 18 out of 32 proteins. (created using BioVenn). **b** Two main functional clusters were identified, including phage-shock proteins and membrane modifying proteins (created using STRING database). **c** Volcano plot shows that YgiV was the most upregulated protein in highly resistant strain M6 and major downregulated proteins in all tested mutants were found to be OmpF and FimA. **d** YgiV expression levels correlated to the level of resistance (M6>M3>M8). Data shown are mean ± SD of n = 4 (**** *p*-value < 0.0001). Significant up-/downregulation was analyzed by two-tailed student's t-test with *p*-value [$-\log_{10}$] > 1.3 and abundance difference [$\log_2$] > 1.5 as cut-offs (n = 4).

Intriguingly, we found two proteins, namely the porin OmpF and the type-1 fimbrial protein A (FimA), to be substantially underexpressed in all three tested mutants (**Figure 1.3c**). In order to study the possible involvement of OmpF in cell entry of CYS we tested an *ompF* knockout strain for susceptibility to the antibiotics. However, no

MIC shift was observed compared to the WT (**Supplementary Table 1.3**). The FimA protein was abundant in all WT samples but was below or close to the LoD in mutant samples, showing a strongly reduced FimA expression level for CYS^R mutants. FimA is a key building protein of fimbriae or pili, which are responsible for cell adhesion and involved in pathogenicity. The influence of the observed FimA downregulation in CYS^R mutant proteomes, might result in reduced pathogenicity due to loss of ability to colonize epithelial cells of specific organs.[122] As an additional virulence marker, we tested the bacterial cell motilities of CYS^R mutants and confirmed highly reduced swarming behavior of resistant mutants (**Supplementary Figure 1.13**). The flagellin protein, the primary structural component of bacterial flagella responsible for motility, could not be quantified and compared in *E. coli* BL21 WT and CYS^R mutant strains, as its abundances were below the LoD. However, in all three tested CYS^R clinical isolates, flagellin expression was significantly reduced compared to their respective WT strain, which may account for the observed loss of motility **(Supplementary Figure 1.12)**. It is known that *qseC* defects and *qseB* upregulation cause reduction of flagellar motility and fimbrial hemagglutination.[115,123] This observation supports the notion that development of resistance to CYSs, caused by SNPs located upstream of the *ygiV* gene, contribute to the upregulation of QseB due to formation of open promotor complexes for both gene loci[115], which, in turn, influences FimA expression and cell motility.[123] This molecular cascade very likely results in a reduced expression of these specific virulence factors in *E. coli*. In the context of infection, reduction in FimA expression might result in less effective epithelial attachment of the pathogen. Accompanied by the observed decrease in cell motility and migration, this reduction could enhance the host´s ability to clear the pathogen. These expression changes of FimA and flagellin might be of particular advantage for the infected host in the context

of urinary tract infections, where epithelial adhesion and bacterial motility are critical determinants of pathogenicity.[124] However, this needs to be confirmed *in vivo* before firm conclusions can be drawn.

2.3.4 Overexpression of YgiV caused high-level CYS^R.

The *ygiV* sequence was isolated from *E. coli* WT genomic DNA and cloned into a vector for protein overexpression via an inducible T7 promotor (pET-28b) (**Supplementary Figure 1.12**). This inducible vector was transformed into *E. coli* Lemo21 (DE3) suitable for protein expression of a wide range of proteins. Following induction of YgiV overexpression with IPTG (isopropyl-β-*D*-thiogalactopyranoside), the MIC of CYSs increased 1,600- to 6,400-fold, compared to the strain containing the empty vector (**Table 1.3**). These susceptibility shifts confirm that overexpression of YgiV in CYS^R mutants is the leading cause for their high-level resistance.

Table 1.3: High-level cystobactamid resistance was achieved by induced YgiV overexpression.

	MIC [µg/mL]		
	pET-28b empty	pET-28b +*ygiV*	Fold MIC-shift
CN-861-2 [**1**]	0.005	8	1,600
CNDM-861 [**2**]	0.0025	16	6,400
Cysto-180 [**3**]	0.0025	4	1,600

The biological function of YgiV is barely described in literature but is known as a transcriptional repressor of *mcbR*.[109] McbR is known to bind in the promotor region of *mcbA* and thereby inhibits its transcription, which prevents overproduction of colonic acid and mucoidy.[109] To test if this repression of *mcbR* causes CYS^R, the respective Keio knockout strain was tested and no shift in CYS antimicrobial activity was observed compared to the WT (**Supplementary Table 1.3**), excluding this pathway as a major mode of resistance.

2.3.5 CYS inhibitory activity on gyrase was lost in the presence of YgiV.

To further characterize the resistance determinant we purified YgiV after expression in *E. coli* Lemo21 (DE3) by affinity and size exclusion chromatography (**Supplementary Figure 1.15**). On-target activity of CYS in a gel-based assay in the presence and absence of YgiV showed a clear YgiV-concentration dependent shift in the IC_{50} (half maximal inhibitory concentration) in the presence of 0.6 µM YgiV and completely abolished activity with 20 µM YgiV (**Figure 1.4a**). When YgiV is present in a similar molarity as CYS, the inhibitory effect of CYS was neutralized. To rule out that YgiV degrades CYSs, we incubated YgiV and CN-861-2 [**1**] for 1 hour and measured compound concentration. No reduction in the CYS amount was detected, excluding compound degradation as the YgiV-mediated mode of resistance (**Supplementary Figure 1.16**). Thus, we view it as likely that CYS binding by YgiV prevents the antibiotics from interacting with its target, resulting in inactivity towards the gyrase. Native protein mass spectrometry (native MS) revealed seemingly stoichiometric binding of YgiV to all tested CYSs (**Figure 1.4b**, **Supplementary Figure 1.17**) after equimolar incubation. Subsequently, by using microscale thermophoresis (MST), a two-digit nanomolar K_D (36.41 ± 16.86 nM) (equilibrium dissociation constant) was determined (**Figure 1.4c, Supplementary Figure 1.18** and **1.19**), identifying the high-affinity binding of CYS to YgiV as a major cause for neutralization. This high-affinity binding is in line, with the previously reported binding of YgiV to the structurally related albicidin [**4**].[112] In addition, due to multiple *m/z* shifts in the native protein MS with the mass of tested CYS derivatives, multiple binding sites per YgiV molecule seem to be possible. The exact binding mode will be further investigated by co-structure elucidation using cryo-EM and/or X-ray crystallography.

Intriguingly, addition of 20 µM YgiV to the gyrase supercoiling assay seemed to reduce the conversion of relaxed to supercoiled plasmid. However, without gyrase enzyme (negative controls in **Supplementary Figure 1.20**) it became apparent that YgiV has an influence on the plasmid DNA by converting/cleaving the relaxed plasmid mainly to its linear form. Consequently, in the presence of YgiV, supercoiling activity of gyrase was generally less pronounced. Importantly, cystobactamids inhibit gyrase activity with an IC_{50} of 0.448 µM. In the presence of YgiV, where we observed less efficient gyrase supercoiling activity, much higher concentrations of cystobactamid were needed to block this reaction (**Supplementary Figure 1.20**). These findings led us to conclude that YgiV might play a dual role in the resistance mechanism of cystobactamids by on the one hand neutralizing the antibiotic through high-affinity binding and on the other hand interfering with the gyrase reactions. To further assess potential DNA cleavage properties of YgiV, we titrated the protein to relaxed and supercoiled plasmid DNA. The addition of YgiV resulted in a concentration dependent increase of OC/nicked and linearized plasmid DNA (**Figure 1.4d** and **Supplementary Figure 1.21**), thus confirming direct single- and double-stranded DNA-cleavage activity of YgiV. Furthermore, YgiV shows sequential and structural similarity to GyrI-like proteins such as SbmC, known for its protective effect against the topoisomerase poison microcin B17. Microcin B17 shows a similar molecular mechanism on DNA gyrase as CYSs and albicidin [**4**]. These compound classes require DNA strand passaging for binding to the DNA gyrase, a mechanism that differs from quinolone antibiotics.[125,91] It cannot be excluded that the YgiV-DNA interaction contributes to its properties in mediating CYS resistance. The hypothesis is supported by the finding that full length YgiV conveyed higher resistance against the structurally related

albicidin [**4**] than constructs lacking the DNA binding domain.[112] The underlying molecular mechanism needs to be investigated in future studies.

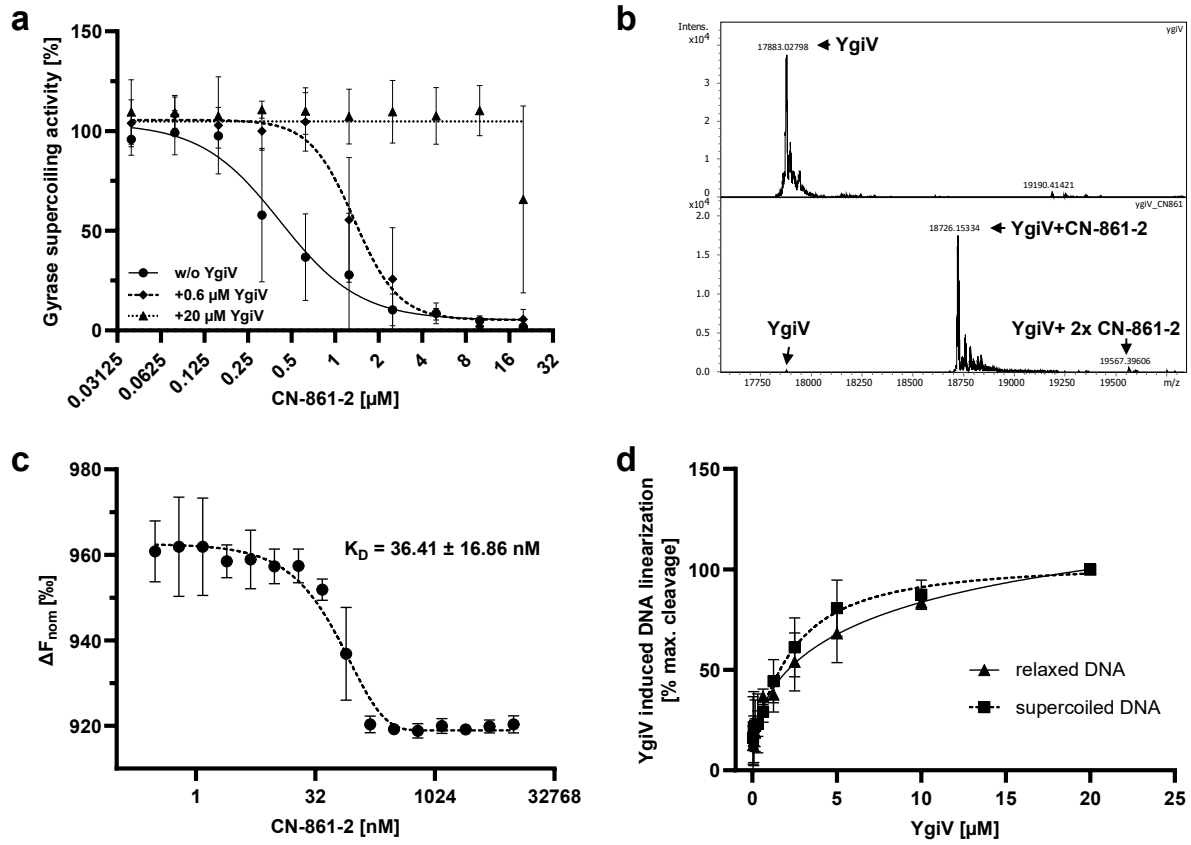

Figure 1.4: Cystobactamids lose their inhibitory activity on the bacterial gyrase in the presence of YgiV due to high-affinity binding and potentially by the DNA interaction of YgiV. a Gyrase supercoiling assay showed neutralization of CN-861-2 [**1**] inhibitory activity (mean ± SD of n = 3) by addition of YgiV. **b** Native MS measurements showed binding of CN-861-2 [**1**] to YgiV with at least one but potentially multiple binding sites. **c** Microscale thermophoresis revealed low nanomolar binding affinity (K_D = 36.41 ± 16.86 nM, mean ± SD of n = 3) of CN-861-2 [**1**] to YgiV. **d** YgiV induced linearization of plasmid DNA in a concentration dependent manner. Intensity after background subtraction of the linear plasmid band at 20 µM YgiV was set as 100 %. Negative control was set as 0 %. (n = 3)

2.3.6 YgiV expression in mutants was inducible via treatment with CYS.

To investigate how mutants react and adapt to CYS treatment, their differential proteome expression was analyzed under CYS stress. Full-proteome comparison of CYS^R and WT bacteria revealed a dependency of the YgiV expression to sub-MIC

CYS treatment. When treating CYS^R mutants with the CYS derivative CN-861-2 [**1**] at 0.25-fold MIC, YgiV expression was induced even further in comparison to the already elevated expression in the mutant without CYS treatment (**Figure 1.5a** and **b**). The elevated expression rates still correlated with the determined MIC shifts seen for tested CYS^R mutants (M6>M3>M8) (**Figure 1.5b**) and hint towards an adaptation of mutant bacteria under sub-MIC treatment, which probably allows the mutants to resist higher CYS concentrations in comparison to their basal YgiV expression level. In addition, the trimethylamine-*N*-oxide reductases TorA and TorC, which are coupled to energy yielding reactions, as well as the acyl-coenzyme A dehydrogenase FadE, catalyzing the first step in fatty acid beta-oxidation, were found to be induced by treatment. Furthermore, various proteins involved in the SOS response such as DinD and RecA, and the DNA gyrase inhibitor protein SbmC[126], were overexpressed in treated WT and mutant bacteria (**Figure 1.5a** and **c**). The remaining SOS response in mutant bacteria demonstrates that CYSs still reach their antimicrobial targets, DNA gyrase and topoisomerase IV. In order to test if DNA damage and SOS response cause induction of YgiV, we treated M6, the mutant with the highest YgiV overexpression, with ciprofloxacin (CIP) as a representative topoisomerase poison. We could not detect any additional upregulation of YgiV caused by the resulting SOS response. In fact, the relative YgiV abundance in CYS^R M6 was slightly reduced following treatment with CIP (**Figure 1.5d**). Therefore, it seems that the mechanism of *ygiV* induction is specific for the interaction with CYSs and potentially related compound classes. Due to the known repressor characteristics of YgiV itself[109], it might be possible that binding of CYS to YgiV (**Figure 1.4c** and **d**) directly influences its own transcription in the form of abolishing a potential negative transcriptional

feedback loop. However, the detailed understanding of this mechanism is outside the scope of this paper and will be further investigated.

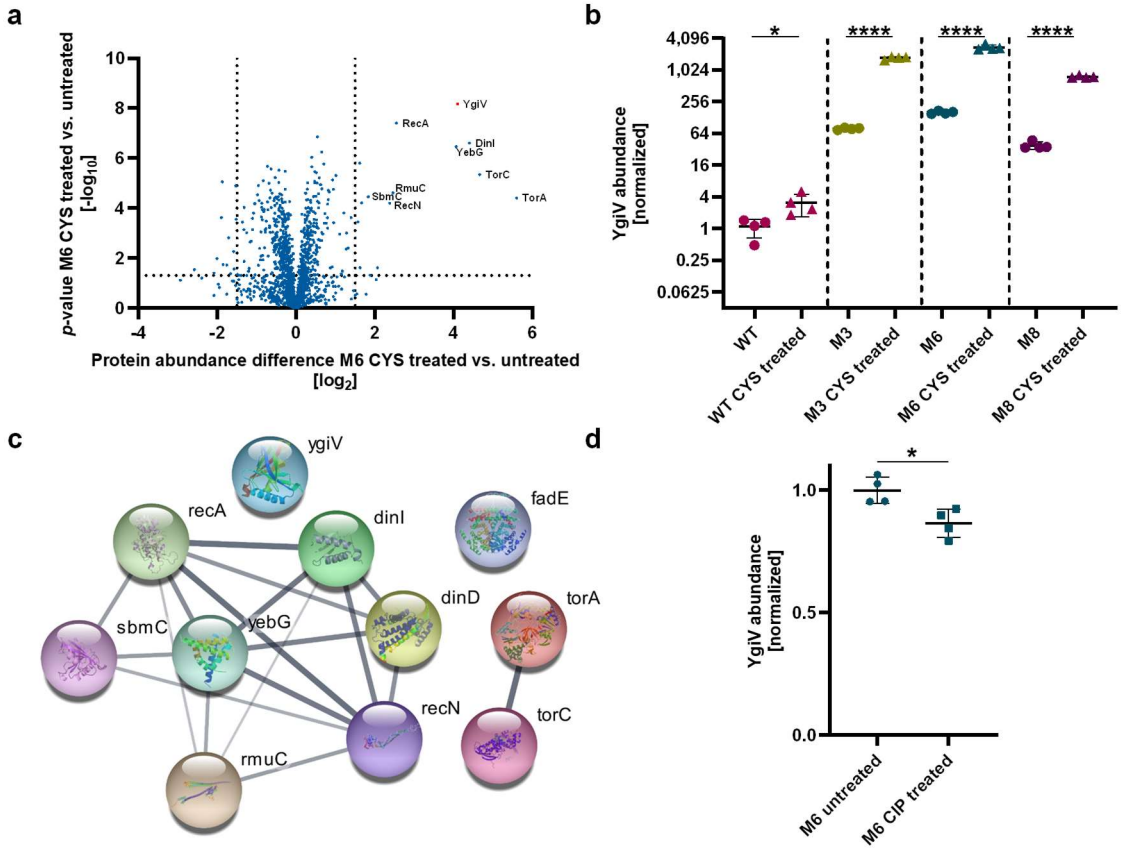

Figure 1.5: YgiV overexpression in cystobactamid-resistant mutants was significantly induced by treatment with cystobactamid. **a** Volcano plot, and **c** string protein network show protein expression profile of cystobactamid treated vs untreated mutant M6, mainly identifying DNA repair as part of SOS response commonly upregulated (created using STRING database). **b** YgiV overexpression in cystobactamid-resistant mutants was induced via cystobactamid treatment, whereas only minor effects were observed in WT cells (* *p*-value =0.0344, **** *p*-value < 0.0001). **d** YgiV upregulation could not be induced via CIP treatment (* *p*-value = 0.0142). Data shown are mean ± SD of n = 4. Significant up-/downregulation was analyzed by two-tailed unpaired student's t-test (cut-offs: *p*-value [$-\log_{10}$] > 1.3 and abundance difference [$\log_2$] > 1.5) (n = 4).

2.3.7 Affinity-based protein profiling confirmed binding of CYSs to YgiV in the whole cell environment and revealed additional binding partners.

The CYS photo-affinity probe Cysto-33 [**5**] (synthesis see **Supplementary Figure 1.22 to 1.26**) was designed and used to check whether binding to YgiV plays a role in the complex environment of the whole cell. The incorporation of a diazirine group for photo-reactive coupling and the alkyne moiety for click-chemistry in the CYS photo probe [**5**] relied on current structure-activity relationship (SAR) studies of CYSs.[101] These functional groups were used during the affinity-based protein profiling (AfBPP) to couple the CYS derivative covalently to binding proteins after UV-irradiation with subsequent linking to biotin via click-chemistry. This complex of CYS binding proteins linked to biotin was used for enrichment on avidin beads, which were relatively quantified against the untreated vehicle control after tryptic digest using mass spectrometry (**Figure 1.6a**). Using this approach we aimed at identifying potential additional target proteins and binding partners of CYSs. The probe was first tested for bioactivity on WT and CYS^R mutants (**Supplementary Table 1.2**) as well as for inhibition of gyrase supercoiling activity (**Supplementary Figure 1.27**), thus showing activity in the same range as other CYSs. Affinity-based protein profiling using CYS^R *E. coli* mutant M6 showed significant enrichment (*p*-value [$-\log_{10}$] > 1.3, difference [$\log_2$] > 1.0) of YgiV, thereby confirming binding of CYS to the upregulated protein in the whole-cell environment (**Figure 1.6b**). Co-incubation with CN-861-2 [**1**] during AfBPP was used to check for competition for the same binding site with Cysto-33 [**5**]. Thereby, YgiV enrichment was not competed by addition of sub-MIC CN-861-2 [**1**], indicating a high extent of YgiV CYS binding capacity in M6. Additionally, target proteins (gyrase subunit B, ParE (topoisomerase IV subunit B)) were confirmed by enrichment and competition as direct interaction partners of CYSs, confirming the

remaining binding to these proteins by sub-MIC CYS treatment, which ultimately explains the identified SOS response in mutants (**Figure 1.4a and c**). Moreover, the efflux pump protein AcrB, the probable protease SohB and the plasma membrane protein YdgA were identified as potential additional binding partners of CYS via competition assays (**Figure 1.6c**). Knockout (KO) strains of these proteins were tested to check if CYS binding to these proteins influences its biological activity. For Δs*ohB* and Δ*ydgA*, no activity shift was found. However, the KO-strain of the efflux pump AcrB, which is part of the AcrAB-TolC tripartite efflux pump, showed a slight increase in activity (4x). Using a KO-strain of the negative regulator of the multidrug efflux pump AcrAB-TolC (Δ*marR*)[127], a fourfold decrease in activity compared to the WT could be shown. Interestingly, only the Δ*acrB* but not the tested Δ*tolC* strain showed a slight increase of CYS susceptibility (**Supplementary Table 1.3**). These findings are in line with previously published data where it could be shown that natural CYS derivatives are effluxed through *E. coli* AcrAB-TolC, whereas this liability could be overcome with some natural derivatives that inspired the total synthesis of advanced CYS compounds overcoming this resistance mechanism[93].

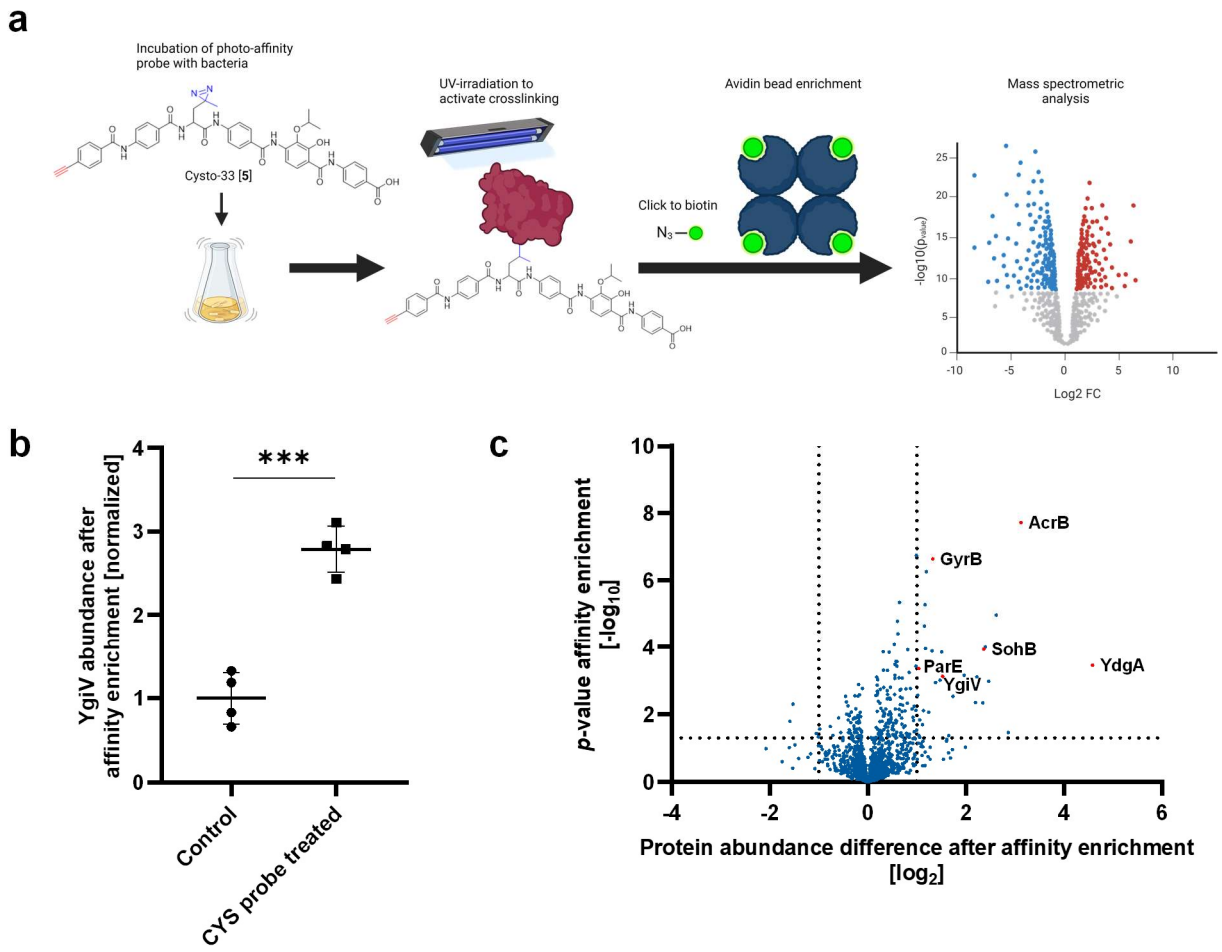

Figure 1.6: Affinity-based protein profiling (AfBPP) in M6 revealed intracellular binding of cystobactamid to YgiV and other proteins. a AfBPP cross-linked the photo-affinity probe Cysto-33 [**5**] to target proteins after UV-irradiation with following click-reaction to biotin used for avidin-bead enrichment of bound proteins. After tryptic digest, the samples were measured using nanoElute-timsTOF (Bruker) and analyzed using DIA-NN and Perseus (created with BioRender.com). **b** YgiV was significantly enriched (*p*-value [-$\log_{10}$] > 1.3, difference [$\log_2$] > 1.0), thereby confirming binding to the cystobactamid probe [**5**] inside the whole cell environment (*** *p*-value = 0.0001, two-tailed unpaired t-test, mean ± SD of n = 4). **c** Known target proteins, gyrase and topoisomerase IV, could be identified, as well as AcrB, SohB and YdgA as potential cystobactamid binding proteins. However, of these only the efflux pump protein AcrB seemed to have an effect on cystobactamid´s bioactivity (**Supplementary Table 1.3**).

However, the observed activity shifts by KO or overexpression of AcrB through Δ*marR* disruption are rather low, compared to the large shift in MIC in the presence of elevated

YgiV expression. Additionally, overexpression of AcrB or other components of the tripartite efflux pump was not observed in tested mutants. It cannot be excluded that efflux may play a role in (low-level) resistance to CYSs in clinical application against *E. coli*, since the AcrAB-TolC efflux pump is common.[49] However, overexpression of YgiV is very likely the major cause of high-level resistance in *E. coli*. Furthermore, high-level resistance development in a YgiV homolog expressing pathogens like *Salmonella*, *Vibrio* and *Pseudomonas* is probable.[112] In the event that homologous modes of resistance emerge in related pathogens, it would be of scientific and clinical interest to investigate whether a demonstrated reduced expression of virulence factors associated with CYS^R, could effectively reduce the pathogenicity of these bacterial isolates *in vivo*.

2.4 CONCLUSION

Cystobactamid resistance in *E. coli* is mediated through mutations in the promotor region of *ygiV*, leading to significant overexpression of the protein. Mutants further adapt against cystobactamids during treatment via substantial amplification of YgiV overexpression. The efflux pump AcrB was identified as an off-target protein but only influences cystobactamid bioactivity slightly. Furthermore, we observed that cystobactamid-resistant mutants show a reduction of fimbrial protein expression and cell motility, associated with cystobactamid induced *ygiV* promotor mutations.

2.5 MATERIALS AND METHODS

2.5.1 Bacterial strains and culture conditions.

The parent strain *E. coli* K12 (BW25113) WT was used for mutant generation. KO mutants Δ*sohB*, Δ*ydgA*, Δ*acrB* and Δ*ompF* were provided from the in-house *E. coli* K12 Keio collection.[113] *E. coli* AB100 parent and *E. coli* AB100 Δ*marR* were provided by Prof. Peter Heisig (University of Hamburg). Clinically isolated *E. coli* strains were provided by PD Dr. Stefano Mancini (University of Zürich). Routine culture was performed in lysogeny broth (LB-Lennox) media under ambient conditions (37 °C, 180 rpm). MALDI-biotyping (Ultraflex III, Bruker) was regularly used to ensure quality of used strains.

2.5.2 Frequency of resistance (FoR) and mutant generation.

For FoR and mutant generation, an overnight culture (ONC) of *E. coli* K12 was inoculated and grown at 37 °C, 180 rpm. The next day, bacteria were centrifuged, washed and suspended in PBS with an OD_{600} of 12 (5.15x 10^9 CFU/mL). 100 µL of this bacteria suspension was used to inoculate selective LB-agar plates containing CN-861-2 [**1**] (4x, 8x, 16x and 32x MIC) and cultured overnight (37 °C) to determine the FoR. Bacterial dilution series and unselective agar plates were used to determine the exact bacterial load. Single colonies were picked and isolated in CN-861-2 [**1**] (10x WT MIC) containing LB-media and plated again. Cryo-stocks were made by mixing bacteria with 1:1 LB-media and 50% glycerol.

2.5.3 Minimal inhibitory concentration (MIC).

Bacteria were cultivated on agar for 24 h at 37 °C. Bacteria were suspended in 0.9% (w/v) sterile NaCl to obtain 0.5 McFarland. Pure media as well as media including bacteria suspension (1:50 dilution) were prepared. A serial compound dilution was

prepared in 96 well plates, after which bacterial suspension was added. The plates were incubated for 24 h at 37 °C. The MIC was reported as the concentration where no bacterial growth was observable.

2.5.4 Growth curves and metabolic heat flow.

For the evaluation of the growth profile of *E. coli* BW25113 WT and CYS^R mutants, strains were incubated overnight. Overnight cultures of the respective strains were inoculated in fresh LB-media with an OD_{600} of 0.001 and 4x120 µL per strain was pipetted in a 96 well plate. The plate was incubated at 37 °C for 24 h. OD_{600} measurement was done using a plate reader (Tecan) in kinetics mode. Same procedure was followed for microcalorimetry measurements using calScreener (Symcel). (**Supplementary Figure 1.11**)

2.5.5 Genomic DNA analysis.

Genomic DNA (gDNA) was isolated by phenol-chloroform extraction. Briefly, ONC was washed with 10 mL MilliQ water and suspended in 1.8 mL Tris-buffer (10 mM, pH=8.0). 100 µL RNase A (20 mg/mL) was added, followed by 30 min incubation at 37 °C before 200 µL proteinase K (20 mg/mL) with 20 µL SDS (20%) was added. This mixture was incubated additional 1.5 h at 55°C. Afterwards, samples were poured to 2 mL phenol:chloroform:isoamylalcohol mix, and the supernatant was extracted multiple times before the gDNA was precipitated by the addition of 200 µL sodium acetate (3 M, pH = 4.8) and 5 mL ethanol (100%), followed by incubation overnight at -20 °C. Subsequently, the resulting pellet was washed using 5 mL 70% ethanol and dried, followed by reconstitution in 100 µL MilliQ water. Isolated gDNA was send for Illumina sequencing (MiSeq PE 300, PE 2x300 bp reads). Reads were analyzed using Geneious Prime (version 2022) by assembling to the *E. coli* K12 reference sequence

(NC_000913). Consensus regions were generated and mauve alignment was completed comparing WT and mutant sequences, followed by manual SNP calling.

2.5.6 Full-proteome analysis.

ONC of each strain was inoculated in 4x fresh media and incubated until early stationary phase. The samples were washed with 1 mL cold PBS, and the pellet was stored at -80°C until lysis. Lysis was done by adding 210 µL 0.4% SDS in PBS and four rounds of sonication with an amplitude of 70% for 30 s (Bandelin Sonoplus). Subsequently, samples were centrifuged and supernatant was used for BCA assay (Thermo). Proteome concentrations of the samples were adjusted to 100 µg/200 µL per sample. Afterwards, the proteome was precipitated by adding 1 mL ice-cold acetone and incubation overnight at -20°C. Next, the samples were centrifuged (16900xg, 15 min, 4°C), and the supernatant was discarded. Samples were washed two times with 1 mL ice-cold methanol. Preparation for protein digest was done by resuspension in 200 µL X-buffer (7 M urea, 2 M thiourea, 20 mM HEPES, pH = 7.5) followed by reduction of cysteine with 0.8 µL DTT (250 mM) (dithiothreitol) for 45 min at 25°C, capping with 2 µL IAA (550 mM) (iodoacetic acid) for 30 min at 25°C and adding additional 3.2 µL DTT (250 mM) for 30 min at 25°C. 600 µL ammonium bicarbonate buffer (pH = 8.5) and trypsin (1 µg) (MS grade, Promega) were added for digest overnight. Digestion was stopped by adding 8 µL formic acid. Peptide samples were desalted on SepPak C18 columns (Waters) using the following protocol. Columns were primed by adding 1 mL 100% and 80% acetonitrile (ACN) with 0.5% FA, followed by equilibration with 3x 1 mL H_2O + 0.1% TFA, before samples were loaded and washed with 3x 0.1% TFA. Subsequently, samples were eluted into 2 mL LoBind (Eppendorf) by adding 3x 250 µL 80% ACN + 0.5% FA and dried using a speedVac (Eppendorf) before dissolving in 1% FA with a proteome concentration of

1 µg/µL. Samples were filtered with Ultrafree centrifugal filters (Merck Millipore, UFC30GV0S) and transferred to QuanRecovery autosampler vials (Waters). Peptide samples were analyzed using an UltiMate 3000 nano HPLC system (Dionex) with an Acclaim C18 PepMap100 (75 µm ID x 2 cm) (Thermo) trap column and an Aurora Ultimate (25 cm x 75 µm ID, 1.6 µm FSC C18) (Ionoptics) separation column coupled to an Orbitrap Fusion (Thermo Fisher) in EASY-spray mode. 1 µL sample was loaded on the trap column and washed for 10 min with 0.1% TFA at 5 µL/min. Afterwards, peptides were transferred on the separation column, and analysis was done using a 132 min gradient (Buffer A: H2O + 0.1% FA; B: ACN + 0.1% FA) with a flow rate of 0.300 µL/min: in 7 min from 0% to 5% B, in 105 min from 5% to 22%, in 10 min from 22 to 35% and in another 10 min to 90% B. MS settings were adjusted as follows: ion transfer tube temperature at 275°C, RF lens amplitude 60%, scan range from 300-1500 *m/z*, automatic gain control (AGC) target of $4.0x10^5$, 3 s cycle time and 50 ms maximal injection time. Lower intensity cut-off was set to 5.0×10^3 and charge states between 2 and 7 were selected for fragmentation at 30% collision energy, before subsequent analysis in the ion trap using rapid scan rate. The isolation window was set to 1.6 *m/z*. AGC target was set to standard with a maximal injection time of 35 ms. Raw data were processed using MaxQuant (version 2.2.0.0) with *E. coli* K12 as reference proteome (Proteome ID: UP000000625). Subsequent analyses was performed using Perseus (version 2.0.5.0). GraphPad Prism (Version 9.1.1) was used for visual representation and further statistical analysis.

2.5.7 Motility assay.

Motility agar (25 mL; 30 g/L tryptic soy broth, 3.4 g/L bacto agar, 9.0 g/L glucose) was poured in petri dishes and 5 µL of bacterial suspension with OD_{600} = 1 was spotted in

the middle of the plate. Plates were incubated overnight at 37 °C. Photos were taken with transmission light and a top view camera. (**Supplementary Figure 1.13**)

2.5.8 Cloning.

Forward primer$_{ygiV}$ (5´ATATCATATGGAAAACCTGTATTTTCAGGGCATGACAAACCTGACACTGGA) and reverse primer$_{ygiV}$ (5´TATAAAGCTTTCACGCCAACGGCACATAA) were designed based on sequenced WT DNA (Geneious Prime) followed by PCR to amplify the *ygiV* sequence from isolated gDNA. Subsequently, PCR product and pET-28b vector were restricted by NdeI and HindIII followed by ligation of both digests. Ligation mix was transformed into *E. coli* HS996 by electroporation to amplify the *ygiV*-carrying plasmid. Kanamycin was used as selectivity marker. The plasmid was isolated using midiprep as described by the manufacturer (Thermo). The plasmid was LGC-sequenced as quality control of the edit genetic code (**Supplementary Figure 1.14**). The construct pET-28b-YgiV with a N-terminal His-Tag and TEV protease cleavage site (ENLYFGQ) was transformed into electrocompetent *E. coli* Lemo 21 and plated on agar plates containing both selection antibiotics kanamycin (50 µg/mL) and chloramphenicol (25 µg/mL). Preculture in LB medium supplemented with the appropriate antibiotics was inoculated with a single colony, and the flask was incubated overnight at 37°C with shaking at 180 rpm. The following day, this culture was used to inoculate the main culture (1:100) in TB medium. The culture was incubated at 37°C and 180 rpm until an OD_{600} of 0.8 was reached, and protein expression was then induced with 1 mM IPTG and incubated at 18°C and 180 rpm overnight. The following day, the cells were harvested by centrifugation at 12,800 × g at 4°C for 15 min, and the cell pellet was flash frozen in liquid nitrogen and stored at -80°C until further use.

2.5.9 Protein purification.

YgiV and His-YgiV were purified using lysis buffer A (50 mM Tris, pH 8.0, 500 mM NaCl, 10% glycerol, 20 mM imidazole, and 2 mM BME) supplemented with DNAse (0.4 mg/g wet cell pellet, Sigma) and cOmplete EDTA-free protease inhibitor tablets (Roche). The bacterial cell pellet was resuspended in lysis buffer and lysed by passing it through a cell disruptor twice at 24.5 kPSI and cooling at 4 °C. Cell debris was removed by centrifugation at 35,000 × g at 4 °C for 30 min. The lysate was filtered through a filter with a pore size of 0.45 µm and loaded onto a HisTrap HP 5 mL column pre-equilibrated with buffer A using a Äkta pure at 4 °C. The column was then washed with five CV of buffer A, and protein elution was performed with 100 % buffer B (50 mM Tris, pH 8.0, 500 mM NaCl, 10 % glycerol, 300 mM imidazole, and 2 mM BME). The YgiV-containing fractions were collected, and an aliquot was concentrated using a 10 kDA cut-off Amicon concentrator. This aliquot was used to purify His-YgiV by loading it onto a Superdex S200 16/600 column pre-equilibrated with storage buffer C (30 mM HEPES, pH 8.0, 200 mM NaCl and 2 mM DTT). The protein fractions containing His-YgiV were pooled and concentrated to 1.5 mg/mL. The remaining YgiV protein sample after the HisTrap HP column was buffer-exchanged into buffer A without imidazole using a HiPrepTM 26/10 desalting column. Subsequently, digestion with TEV protease was performed at a ratio of 1:10 at 4 °C overnight to remove His-tag. At the following day the protein sample was loaded onto a HisTrap HP column pre-equilibrated with buffer A. The flow-through containing the YgiV protein was concentrated and applied to a Superdex S200 16/600 column pre-equilibrated with final storage buffer D (10 mM Tris pH 7.0, 150 mM NaCl, and 2 mM DTT). The protein fractions were pooled together, and YgiV was concentrated to 3.4 mg/mL (190 µM). Protein concentrations were determined by the specific absorption coefficient at A280

using a Nanodrop, and purity was checked by SDS-PAGE (**Supplementary Figure 1.15**).

2.5.10 Gyrase supercoiling and cleavage assay.

Inhibition of gyrase activity was examined using gyrase supercoiling activity kit (Inspriralis) as indicated by the manufacturer. Briefly, a compound dilution series was prepared in water. Water, dilution buffer, assay buffer, plasmid and enzyme were mixed with compound solution and incubated. YgiV was added in indicated amounts. A positive control was prepared without compound and a negative control was prepared without compound and enzyme. The reaction was stopped by adding chloroform/isoamylalcohol and STEB-buffer. The samples were vortexed and centrifuged before running gel-electrophoresis. The gel was stained in ethidium bromide and imaged using a Fusion Fx gel imager (Vilber Lourmat). Subsequent analysis was done using ImageJ and GraphPad Prism (Version 9.1.1). The same procedure was followed for the DNA cleavage assays, except that the samples did not contain gyrase but only YgiV and supercoiled or relaxed plasmid DNA, respectively (Inspiralis). Assays were independently repeated three times.

2.5.11 Degradation assay.

Cystobactamid CN-861-2 [**1**] (20 µM) was incubated with YgiV (20 µM) in gyrase assay buffer (35 mM Tris·HCl (pH 7.5), 24 mM KCl, 4 mM MgCl2, 2 mM DTT, 1.8 mM spermidine, 1 mM ATP, 6.5% (w/v) glycerol, and 0.1 mg/ml albumin) for 60 min at 37 °C. Afterwards, compound amount was measured using HPLC-UV/Vis-MS. (**Supplementary Figure 1.16**)

2.5.12 Native protein mass spectrometry.

YgiV (10 µM) was buffered in ammonium acetate (10 mM) and incubated overnight with CYS (CN-861-2 [**1**], CNDM-861 [**2**] or Cysto-180 [**3**]) (10 µM) at 4°C. Afterwards, samples were measured using a solariX (Bruker) by direct infusion. Parameters for ionization were set as follows; flow rate: 5.0 µL/min, capillary voltage: 4500 V, nebulizer: 3 bar, dry gas: 5 L/min and dry temperature: 200°C. The recorded mass window was set between 988.97 to 5000.00 *m/z* and 64 scans with an accumulation time of 1 s. Measurements were analyzed by DataAnalysis (Bruker, version 5.3) using maximum entropy deconvolution.

2.5.13 Microscale thermophoresis.

A Monolith His-Tag Labelling Kit RED-tris-NTA 2nd Generation (NanoTemper) was used for K_D determination as recommended by the manufacturer. Briefly, YgiV concentration (200 nM) was adjusted in assay buffer and labeled by RED-tris-NTA dye (100 nM) for 30 min. This mixture was added to CYS dilution (c_{start} = 10 µM) series and measured using Monolith NT.115 (NanoTemper) with standard glass capillaries (NanoTemper). The assay was independently repeated three times with CN-861-2 [**1**].

2.5.14 Affinity-based proteome profiling.

Affinity enrichment in combination with competition by CN-861-2 [**1**] was done by inoculation of an ONC of M6 in 4x50 mL fresh LB-media and incubated until early stationary stage at 37 °C, 180 rpm. Bacteria were harvested (3000xg, 15 min) and washed with PBS followed by resuspension at an OD_{600} of 20. This suspension was treated with sub-MIC CN-861-2 [**1**] (25 µM) for competition or DMSO before adding Cysto-33 [**5**] photo-affinity probe (2.5 µM) or DMSO as control. Afterwards, samples were UV-irradiated for 10 min in 24 well plates, washed with 1 mL PBS and pellets

were stored until lysis. Lysis and proteome adjustment was done as described above. Subsequently, the click reaction was performed by adding 3 µL biotin-azide (10 µM), 10 µL copper(II) sulfate (50 mM), 10 µL TCEP (Tris(2-carboxyethyl)phosphin – hydrochlorid) (15 µg/mL) and 3 µL THPTA (Tris((1-benzyl-4-triazolyl)methyl)amine) (10 mM) and incubating for 1h at room temperature. Precipitation and washing were performed as described above. Samples were reconstituted in 0.2% SDS in PBS followed by avidin-bead enrichment (Merck) by coupling biotin labeled proteins to the avidin-agarose for 1 h under continuous mixing, followed by 3x washing steps with 1 mL 0.2% SDS in PBS, 2x 1 mL urea (6 mM) and 3x 1 mL PBS (centrifuge 3 min, 400xg, RT). Subsequent protein digest, desalting and preparation for HPLC was done as described above. Sample analysis was done by using nanoElute nano flow liquid chromatography system (Bruker, Germany) coupled with a timsTOF Pro (Bruker, Germany). Samples were loaded to the trap column (Thermo Trap Cartridge 5 mm) and washed with 6 µL 0.1% FA with a flow rate of 10 µL/min. Peptides were then transferred to the analytical column (Aurora Ultimate CSI 25 cm x 75 µm ID, 1.6 µm FSC C18, IonOpticks) and separated by a gradient elution (eluent A: H_2O + 0.1% FA, B: ACN + 0.1% FA; 0% to 3% in 1 min, 3% to 17% in 57 min, 17% to 25% in 21 min, 25% to 34% in 13 min, 34% to 85% in 1 min, 85% kept for 8 min) with a flow rate of 400 nL/min. A Captive Spray nanoESI source (Bruker, Germany) was used to ionize the peptides at 1.5 kV with 180°C dry temperature at 3 L/min gas flow. The timsTOF Pro (Bruker, Germany) was operated in default dia-PASEF long gradient mode with TIMS set between 1/K0 0.6 Vs/cm2 and 1.6 Vs/cm2 with a ramp and accumulation time of 100 ms each and a ramp rate of 9.43 Hz. The mass range was set from 100.0 Da to 1700 Da with positive ion polarity. Dia-PASEF mass range was set to 400.0 Da to 1201.0 Da with a mobility range of 0.60 1/K0 to 1.43 1/K0 and a cycle time of 1.80

s. The collision energy for 0.60 1/K0 was set to 20.00 eV and for 1.6 1/K0 to 59.00 eV. Tuning MIX ESI-TOF (Agilent) was used for calibration of m/z and mobility. Data were processed using DIA-NN (version 1.8.1), and proteins were identified against Uniprot *E. coli* reference proteome (Proteome ID: UP000000625, downloaded 18/01/2023). Settings were used as default except precursor charge range was changed from 2 to 4. C carbamidomethylation was set as a fixed modification. "--relaxed-prot-inf" was added in additional options to allow further data processing with Perseus Software. In Perseus (version 2.0.5.0) the values were transformed to their $\log_2$-value and the replicates were grouped. Missing values were imputed by the default settings and the differential protein abundance between different conditions were evaluated using two-tailed student's t-test. The cut-off for $-\log_{10}$ *p*-value was set to 1.3 (*p*-value = 0.05) and $\log_2$ t-test difference >1.0. Proteins fitting these thresholds were seen as significantly over- or underexpressed compared to the wild type.

2.5.15 Data and Statistics.

Proteomics data were analyzed using Perseus software (version 2.0.5.0) with two-tailed student's t-test to determine significant expression changes or enrichment as indicated. Dissociation constants (K_D) were identified using MO.Control (v1.6, NanoTemper) and MO.Affinity Analysis (v2.3, NanoTemper) software. GraphPad Prism (Version 9.1.1) was used for visual data representation and IC_{50} determination. Statistical significance for direct comparisons was determined by GraphPad Prism (Version 9.1.1) using two-tailed, unpaired student´s t-test with statistical significance given to a *p*-value < 0.05.

2.6 DATA AVAILABILITY

Datasets and further information of current and ongoing related studies are available upon request from the corresponding author. Genomic data were deposited in the NCBI SRA database and can be accessed using the BioProject ID PRJNA1049158. The mass spectrometry proteomics data have been deposited to the ProteomeXchange Consortium via the PRIDE partner repository with the data set identifiers PXD047566, PXD051732 and PXD047539.

2.6.1 Code availability

The open-source software DIA-NN (version 1.8.1) and Perseus (version 2.0.5.0) used for proteomic data analysis can be downloaded via github.com and maxquant.net, respectively.

2.7 ACKNOWLEDGEMENT

We thank Dr. F.P. Jake Haeckl (HIPS) and Dr. Katarina Cirnski (HIPS) for proof-reading of the manuscript, Julia Christmann (HIPS) for her work on EptC and Prof. Peter Heisig (University of Hamburg) for providing the *marR* KO strain. We also thank Prof. Dr. Andreas Keller (HIPS, UdS) and Leidy Alejandra Gonzalez Molano (HIPS, UdS) for their support in genome analysis. The authors also want to thank Dr. Sari Rasheed (HIPS) for help with binding affinity measurements. This study was funded by the German Federal Ministry of Education and Research (OpCyBac-project grant number: 16GW0219K). The funder played no role in study design, data collection, analysis and interpretation of data, or writing of this manuscript.

2.8 AUTHOR CONTRIBUTIONS

TR designed, performed and analyzed the majority of mentioned experiments and wrote the manuscript. FF performed FoR testing. DKol purified the YgiV Protein. DH, TS, DS, DKoh synthesized and provided cystobactamid derivatives. DM and FD supported genomic and proteomic data analysis. JSH and JD performed MIC testing and supported cloning of *ygiV*. SM provided the clinically isolated *E. coli* strains. JH, RM, MB, AH, AK and SS provided supervision and funding. TR, JH and RM designed the project. All authors were involved in reviewing and editing the manuscript and approved the final version.

2.9 COMPETING INTERESTS

All authors declare no financial or non-financial competing interests.

2.10 SUPPLEMENTARY INFORMATION CHAPTER 1

Synthesis and NMR spectra for Cysto-180 [**3**] and Cysto-33 [**5**] (Supplementary Figures 1.1-1.10 and Supplementary Figures 1.22-1.26, respectively) are not included in the SI shown here and can be found online.

2.10.1 Synthesis of CN-861-2 [1] and CNDM-861 [2]

CN-861-2 [**1**] was synthesized according to published literature.[93,94]

HRMS (ESI) calculated 842.2780 [M+H$^+$], 842.2759 found.

Purity (LC-MS): 99%.

CNDM-861 [**2**] was synthesized according to published literature.[93,94]

HRMS (ESI) calculated 812.2675 [M+H$^+$], 812.2675 found.

Purity (LC-MS): 99%.

2.10.2 Growth curves of CYS^R mutants compared to WT.

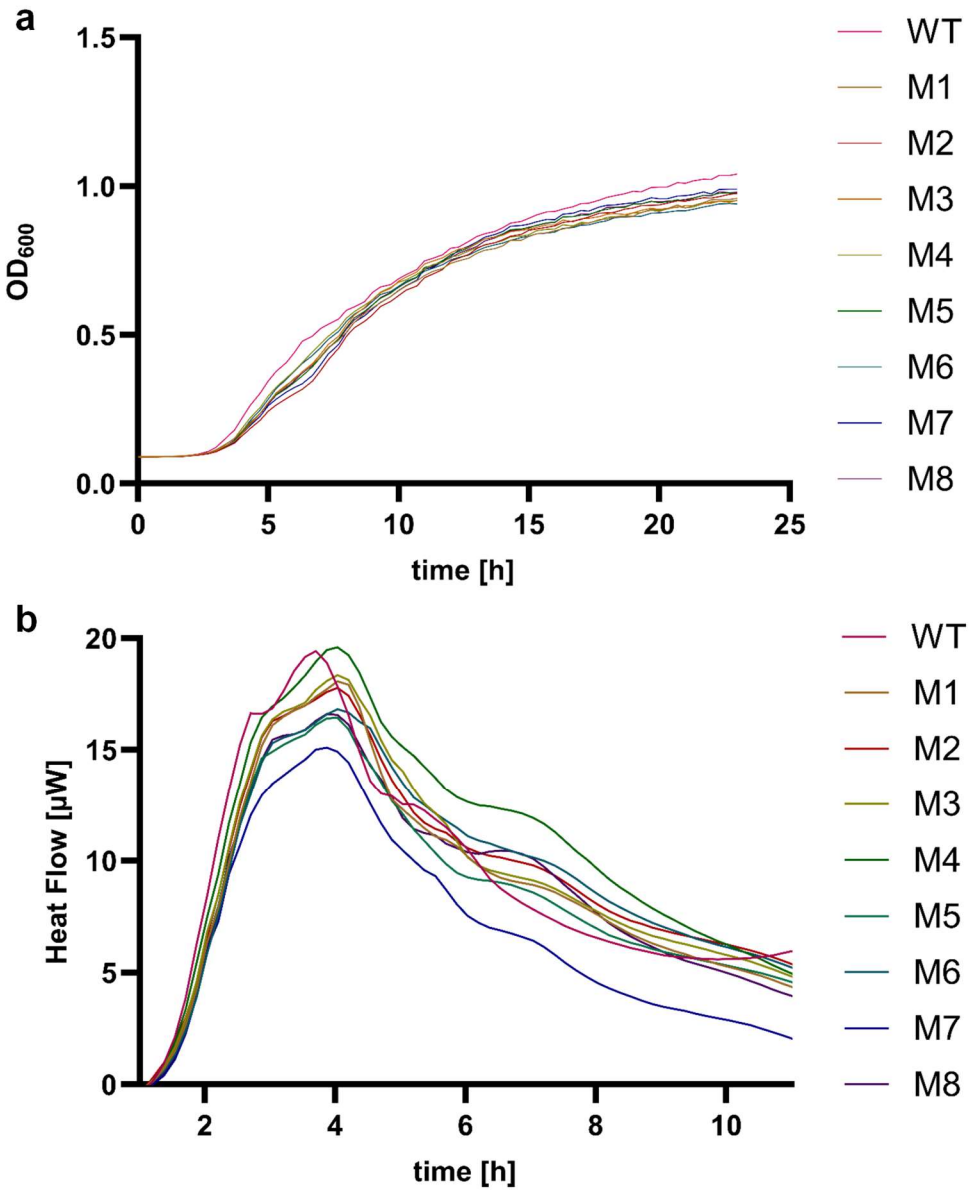

Supplementary Figure 1.11: **a** Growth curves (n=4 technical replicates) and **b** heat flow during growth (n = 2 technical replicates) show no considerable differences between CYS^R mutant and WT bacteria.

2.10.3 Frequency of Resistance of CN-861-2 [1], CNDM-861 [2] and Cysto-180 [3].

Supplementary Table 1.1: Frequency of resistance for used cystobactamid derivatives on *E. coli* K12 (BW25113).

Derivative	MIC multiple	FoR
Cysto-180 [3]	4x	$6.42x10^{-08}$
	8x	$< 10^{-9}$
	16x	$< 10^{-9}$
	32x	$< 10^{-9}$
CNDM-861 [2]	4x	$< 10^{-9}$
	8x	$< 10^{-9}$
	16x	$< 10^{-9}$
	32x	$< 10^{-9}$
CN-861-2 [1]	4x	$2.62x10^{-08}$
	8x	$< 10^{-9}$
	16x	$< 10^{-9}$
	32x	$< 10^{-9}$

2.10.4 Minimal inhibitory concentrations of KO-strains and check for cross-resistance to other antibiotic classes.

Supplementary Table 1.2: CYS^R mutants show no cross-resistance to polymyxins and quinolone antibiotics but to albicidin.

[µg/mL]	CN-861-2 [1]	CNDM-861 [2]	Cysto-180 [3]	Cipro	Levo	Cysto-33 [5]	Albicidin [4]	Polymyxin B	Colistin
***E. coli* BW25113 WT**	0.2	0.1	0.2	0.08	0.16	<0.03	<0.03	4	8
M1	8	4	4	0.08	0.16	n.d.	n.d.	4	8
M2	8	4	8	0.08	0.08	>64	n.d.	4	8
M3	32	4	16	0.08	0.08	>64	0.25	4	8
M4	8	4	8	0.08	0.16	n.d.	n.d.	4	8
M5	8	2	8	0.08	0.08	n.d.	n.d.	4	4
M6	>64	>64	64	0.04	0.08	>64	64	4	8
M7	8	4	8	0.08	0.16	n.d.	n.d.	4	4
M8	8	4	8	0.08	0.16	n.d.	0.125	4	8

Supplementary Table 1.3: Minimal inhibitory concentrations (MIC) of genetic knockout strains.

MIC [µg/mL] in MHBII	CN-861-2 [1]	CNDM-861 [2]	Cysto-180 [3]	Cipro	Levo
***E. coli* BW25113 WT**	0.16	0.025	0.04	0.02	0.04
E. coli* BW25113 *ΔacrB	0.04	n.d.	0.01	0.005	n.d.
E. coli* BW25113 *ΔtolC	0.08	n.d.	0.04	0.02	n.d.
E. coli* BW25113 *ΔacrR	0.2	0.1	0.1	0.02	0.04
E. coli* BW25113 *ΔydgA	0.1	0.025	0.1	0.16	n.d.
E. coli* BW25113 *ΔsohB	0.16	n.d.	0.04	0.01	n.d.
E. coli* BW25113 *ΔompF	0.2	<0.05	0.1	<0.05	n.d.
E. coli* BW25113 *ΔmcbR	0.2	<0.05	0.2	0.02	n.d.
E. coli* BW25113 *ΔygiV	0.08	0.02	0.04	0.03	n.d.
E. coli AG 100 Parent	0.4	0.1	0.2	0.02	0.04
E. coli AG 100 ΔmarR	1.6	0.4-0-8	0.4-0.8	0.04	0.08

2.10.5 Frequency of Resistance of CN-861-2 [1] on BW25113 Δ*ygiV.*

Supplementary Table 1.4: FoR *E. coli* BW25113 Δ*ygiV* for CN-861-2

CN-861-2			
strain	**plated [CFU]**	**colonies 4x MIC**	**FoR**
***E. coli* BW25113** Δ*ygiV*	1.05E+10	0	< 1.0E-10
	1.05E+09	0	< 1.0E-9

2.10.6 Minimal inhibitory concentrations of clinically isolated *E. coli* and generated CYS^R mutants.

Supplementary Table 1.5: MIC clinical *E. coli* isolates.

Clinical isolates IMM Zürich										
µg/mL	CN-861-2	CNDM-861	Cysto-180	Tobramycin	Amikacin	Tetracyline	Colistin	Ciprofloxacin	Levofloxacin	Trimethoprim
CI#3	0.2	0.05	0.1	32	8	2	0.25	0.03	0.06	>64
CI#6	0.0625	0.125	<0.03	4	8	>64	0.25	0.03	0.06	>64
CI#19	0.25	0.25	<0.03	64	8	64	0.5	1	0.5	>64
CI#23	0.4	0.1	0.2	>64	>64	>64	0.25	>8	>16	>64
CI#24	0.0625	<0.03	<0.03	>64	4	>64	0.25	0.03	0.125	0.5
CI#39	0.4	0.2	0.2	4	4	>64	0.25	>8	>16	>64

Supplementary Table 1.6: MICs of generated CYS^R clinical isolates.

µg/mL	CN-861-2	CNDM-861	Cysto-180
CI#3 WT	0.2	0.05	0.1
CI#3 M1	>6.4	3.2	6.4
CI#3 M2	>6.4	1.6	6.4
CI#3 M3	>6.4	1.6	6.4
CI#3 M4	>6.4	6.4	>6.4
CI#3 M5	>6.4	>6.4	>6.4
CI#23 WT	0.4	0.1	0.2
CI#23 M1	6.4	1.6	6.4
CI#23 M2	6.4	0.8	3.2
CI#23 M3	>6.4	3.2	6.4
CI#23 M4	6.4	1.6	3.2
CI#23 M5	6.4	1.6	3.2
CI#39 WT	0.4	0.2	0.2
CI#39 M1	>6.4	3.2	6.4
CI#39 M2	>6.4	3.2	>6.4
CI#39 M3	>6.4	>6.4	>6.4
CI#39 M4	>6.4	1.6	6.4
CI#39 M5	>6.4	1.6	6.4

2.10.7 Differential proteome expression of CYS^R mutants generated from clinical *E. coli* isolates.

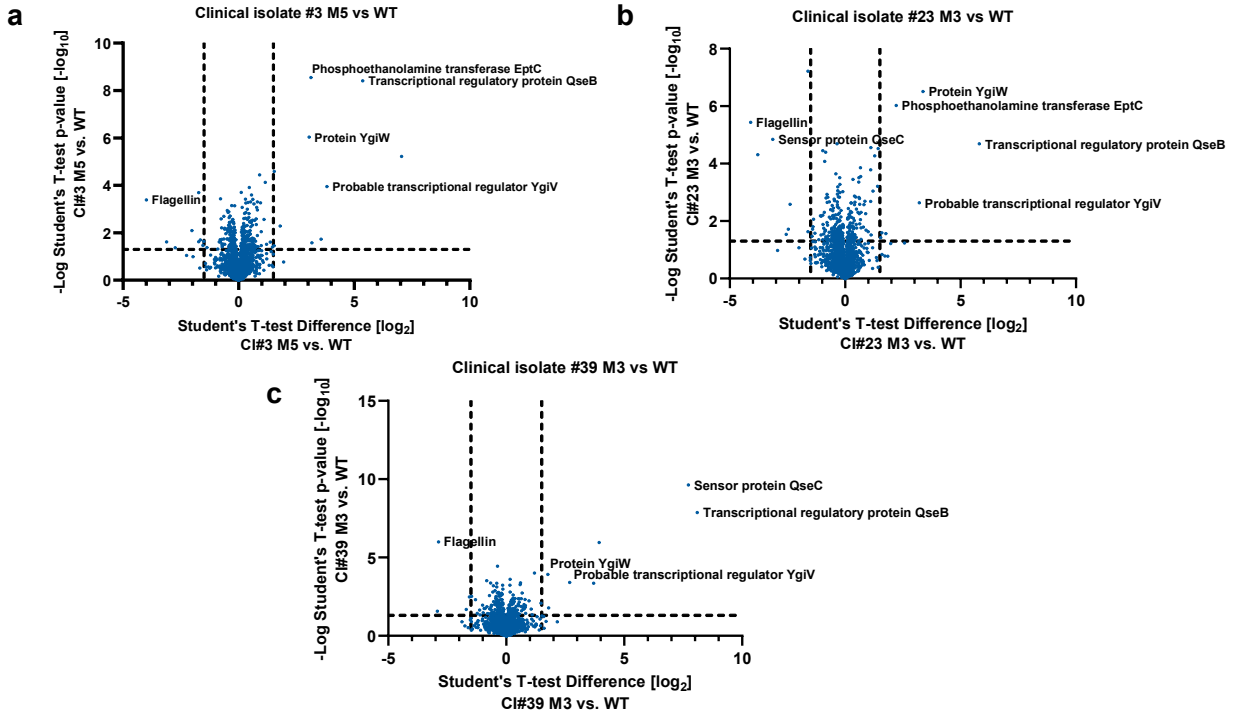

Supplementary Figure 1.12: Differential proteome expression of CYS^R mutants generated from clinical *E. coli* isolates (CI). **a** CI#3 M5 compared to CI#3 WT. **b** CI#23 M3 compared to CI#23 WT. **c** CI#39 M3 compared to CI#39 WT. Significant up-/downregulation was analyzed by two-tailed student's t-test with *p*-value [$-\log_{10}$] > 1.3 and abundance difference [$\log_2$] > 1.5 as cut-offs (n = 4).

2.10.8 Motility assay of CYS^R mutants compared to WT.

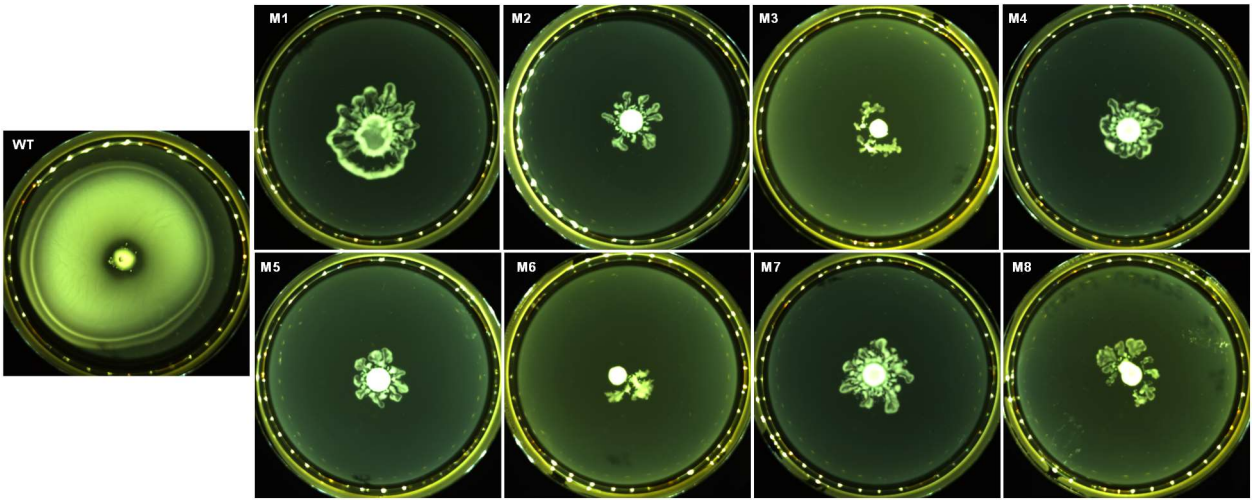

Supplementary Figure 1.13: Bacterial motility assay shows reduced swarming behavior of CYS^R mutants compared to WT.

2.10.9 Cloning and Expression of YgiV.

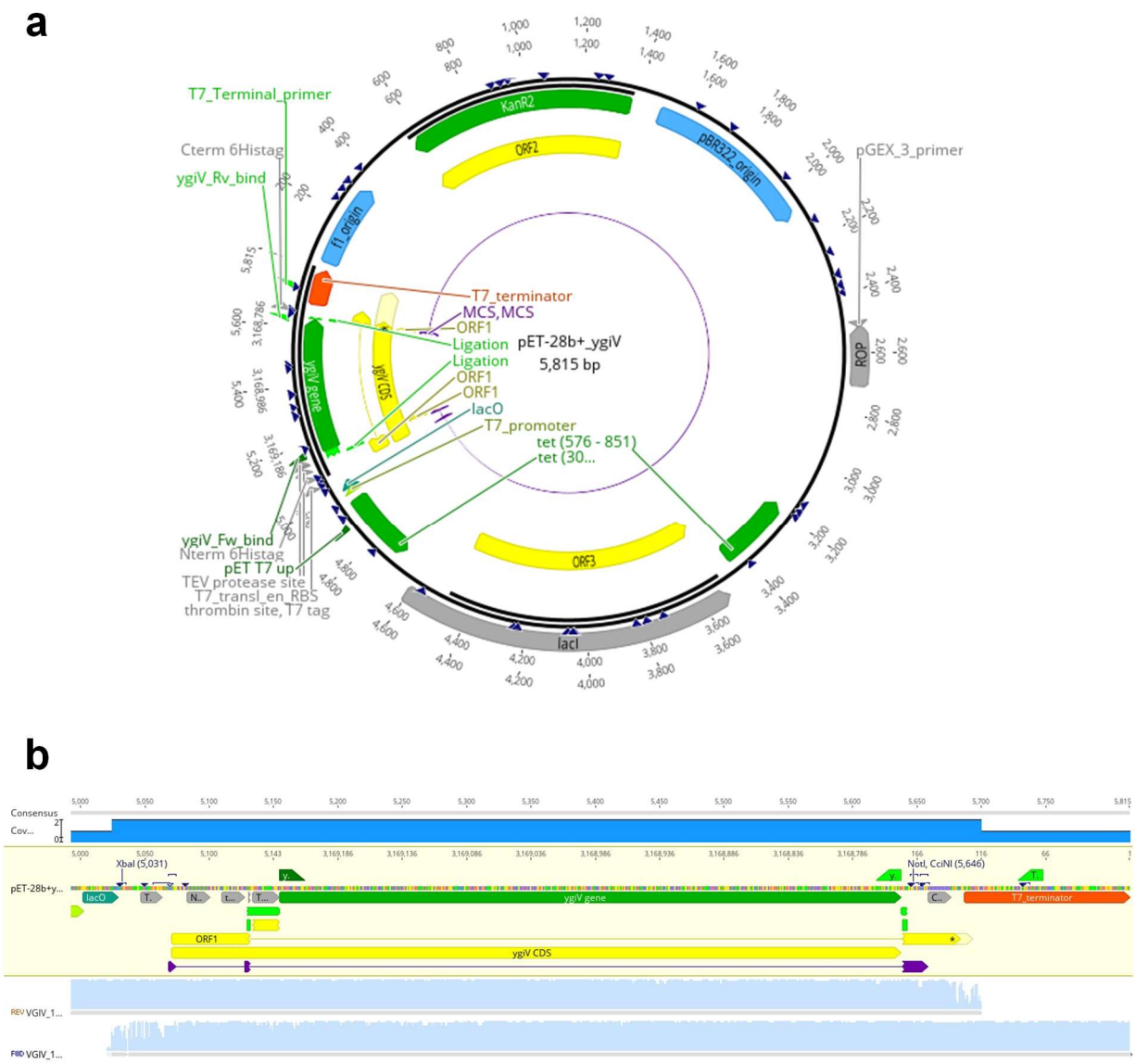

Supplementary Figure 1.14: **a** Plasmid map and **b** sequencing control of *ygiV* carrying pET-28b vector. The *ygiV* gene sequence with TEV-protease cleavage site was inserted downstream of the Nterm-6Histag and the IPTG inducible T7 promotor with lacO. The plasmid carries a kanamycin resistance gene for selectivity. Figures were created using Geneious Prime 2023.0.1 software.

2.10.10 Purification of His-YgiV and YgiV.

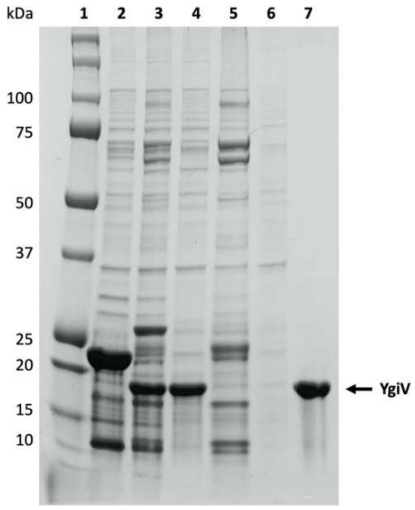

Supplementary Figure 1.15: YgiV protein purification. SDS-gel shows sequential steps of YgiV purification. Molecular weight marker (lane 1), elution of the first HisTrap affinity chromatography step (lane 2), protein sample after incubation with TEV protease overnight (1:10) at 4°C (lane 3), flow-through of the second HisTrap affinity chromatography step (lane 4), elution of the second HisTrap purification run (lane 5), fraction one of the final size-exclusion chromatography run (lane 6) and YgiV (17.8 kDa) containing fraction of the size-exclusion chromatography run.

2.10.11 Degradation assay.

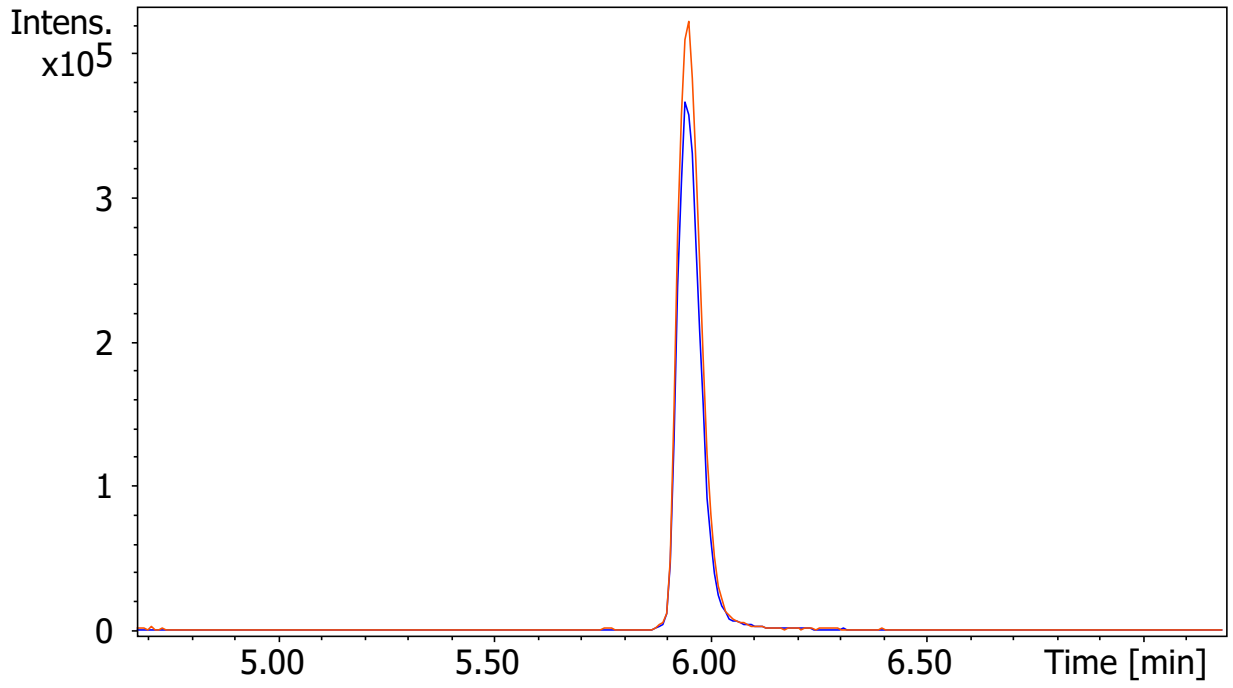

Supplementary Figure 1.16: Overlaid EICs (842.26773 ± 0.1 m/z) of CN-861-2 [**1**] incubated with (orange) and without (blue) YgiV in assay buffer showed no CN-861-2 [**1**] degradation due to catabolic activity of the protein.

2.10.12 Native MS of YgiV incubated with CN-861-2 [1], CNDM-861 [2] and Cysto-180 [3].

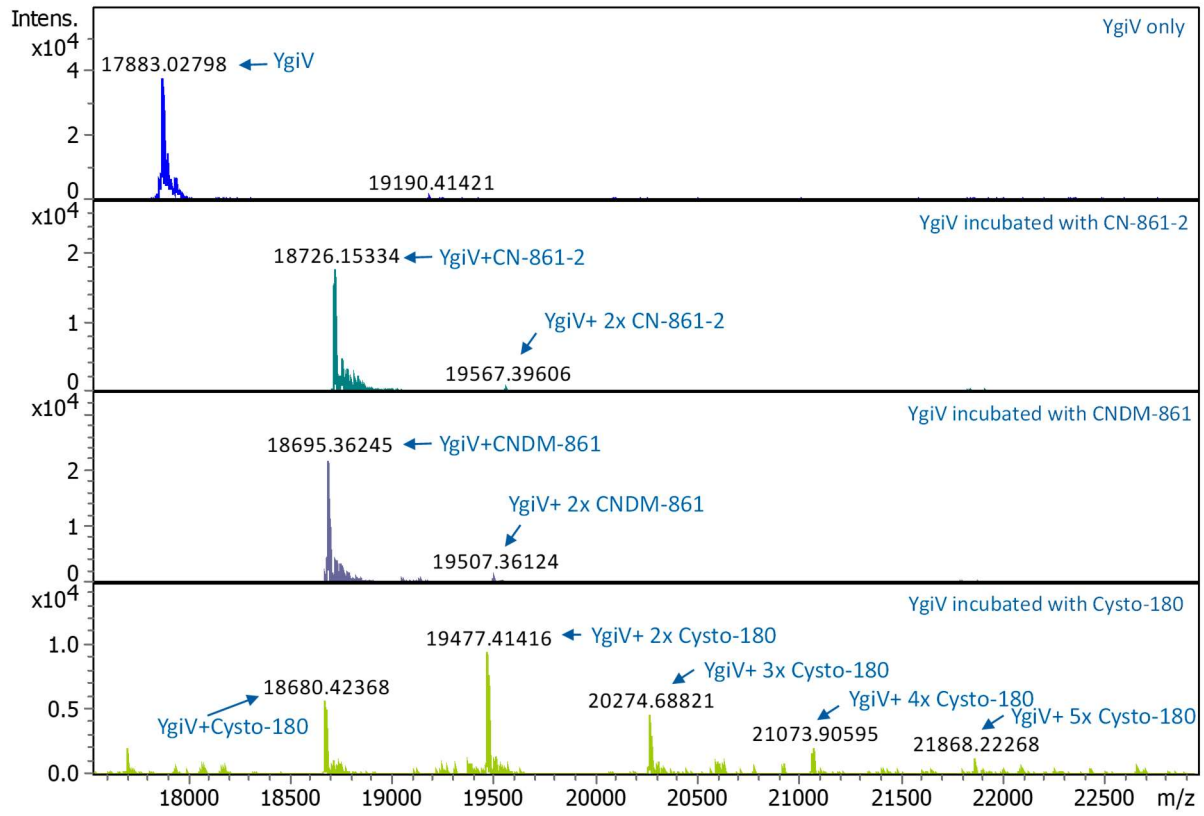

Supplementary Figure 1.17: Native protein mass spectrometry of YgiV (10 µM in ammonium acetate) incubated with CN-861-2 [**1**] (1:1 ratio), CNDM-861 [**2**] (1:1 ratio) and Cysto-180 [**3**] (1:10 ratio) suggests binding of CYS to the protein with potentially multiple binding sites due to seen *m/z* shifts.

2.10.13 MST of YgiV with CNDM-861 [2] and Cysto-180 [3].

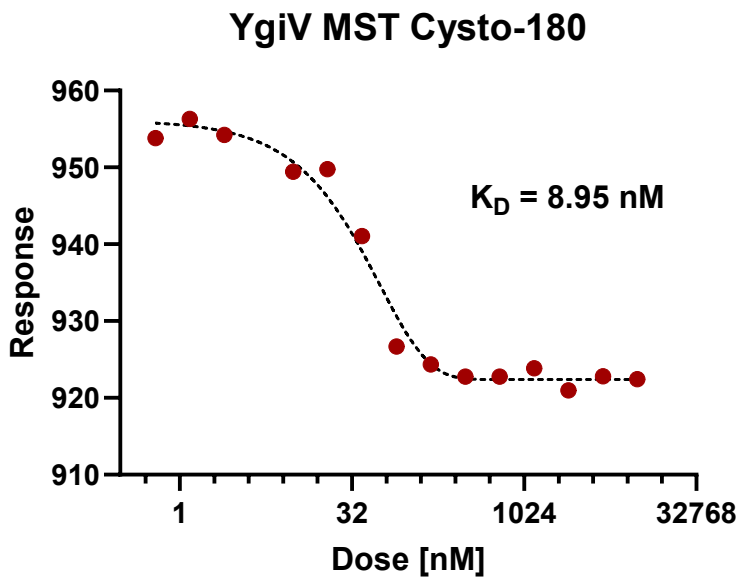

Supplementary Figure 1.18: Microscale thermophoresis shows a nano-molar binding affinity of Cysto-180 [**3**] to YgiV with a K_D of 8.95 nM (n=1).

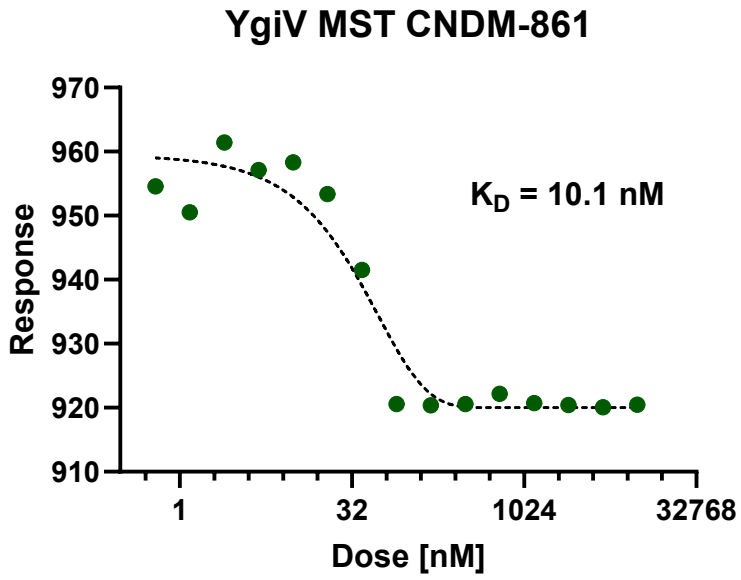

Supplementary Figure 1.19: Microscale thermophoresis shows a nano-molar binding affinity of CNDM-861 [**2**] to YgiV with a K_D of 10.1 nM (n=1).

2.10.14 Gel-images of supercoiling and cleavage assay with and without YgiV addition.

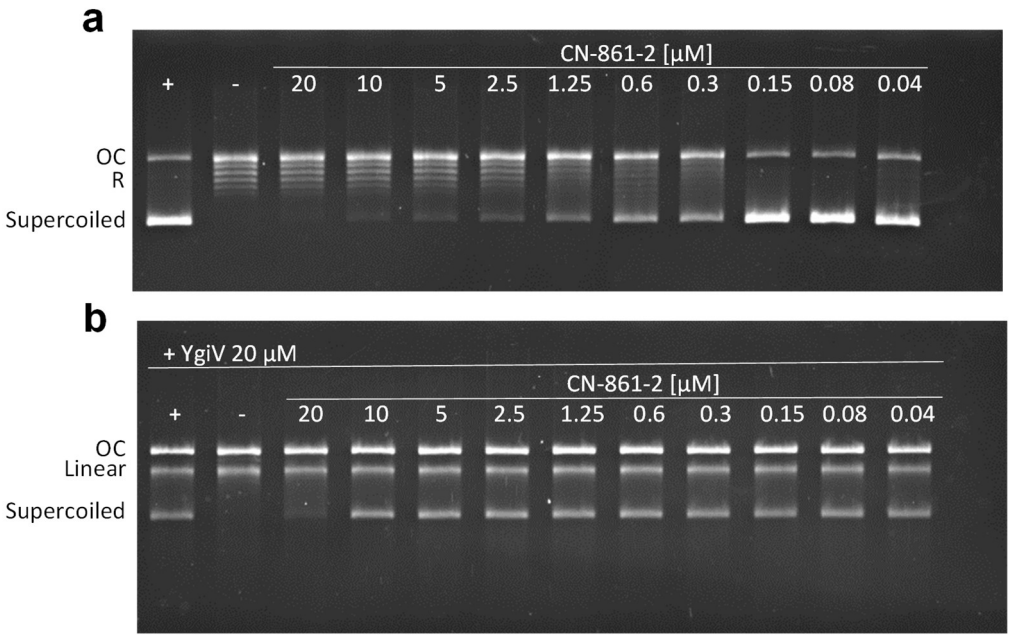

Supplementary Figure 1.20: DNA gyrase supercoiling assay without (**a**) and with (**b**) YgiV addition. The addition of 20 µM YgiV counteracted the inhibitory effect of CN-861-2 [**1**] on gyrase supercoiling activity. This was seen by an IC_{50} shift (**Figure 1.4a**), seen as more pronounced appearance of the supercoiled band at higher concentrations of CN-861-2 [**1**] by addition of YgiV (**b**). It has to be noted here that upon addition of YgiV, gyrase supercoiling activity seemed to be reduced, the relaxed topoisomers (R) disappeared and linearized plasmid appeared between the more pronounced open circular/nicked (OC) and supercoiled plasmid form, indicating a cleavage of the plasmid by YgiV. Plus (+) indicates plasmid with gyrase, but without compound, as positive control, which was used as basis for normalization (set to 100%). Minus (-) indicates the relaxed plasmid incubated without gyrase as negative control (set as 0%). Supercoiling inhibition assays without (**a**) and with (**b**) YgiV were processed in parallel and loaded on the same gel for comparison.

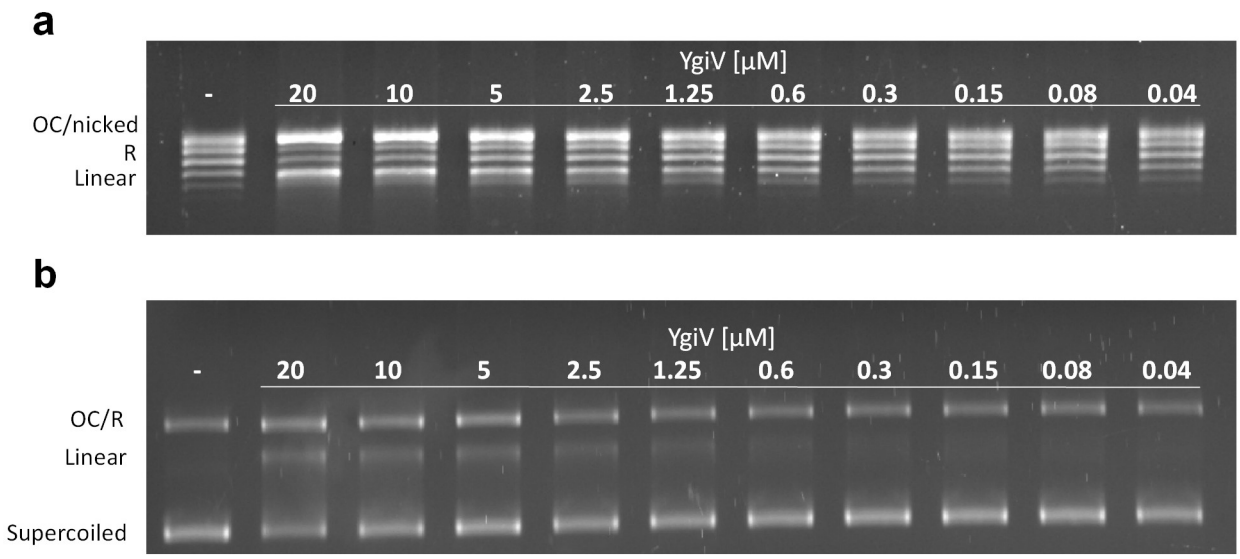

Supplementary Figure 1.21: DNA cleavage assay showed concentration dependent cleavage of the relaxed (**a**) and supercoiled (**b**) plasmid form by YgiV. **a** Relaxed plasmid DNA was added to the assay, which got converted into the open circular/nicked (OC) and linear form by addition of YgiV. **b** Negative supercoiled plasmid DNA was incubated with and without YgiV, resulting in partial linearization of the plasmid upon YgiV addition. These products were then analyzed by gel electrophoresis. Partial impurities of the negative supercoiled plasmid (**b**) with the OC/R form were visible in the negative control. A concentration dependent cleavage to the OC/nicked as well as the linear plasmid form by YgiV could be observed. Negative control without enzyme is marked with minus (-).

2.10.15 Gyrase Supercoiling Inhibition Assay Cysto-33 [5].

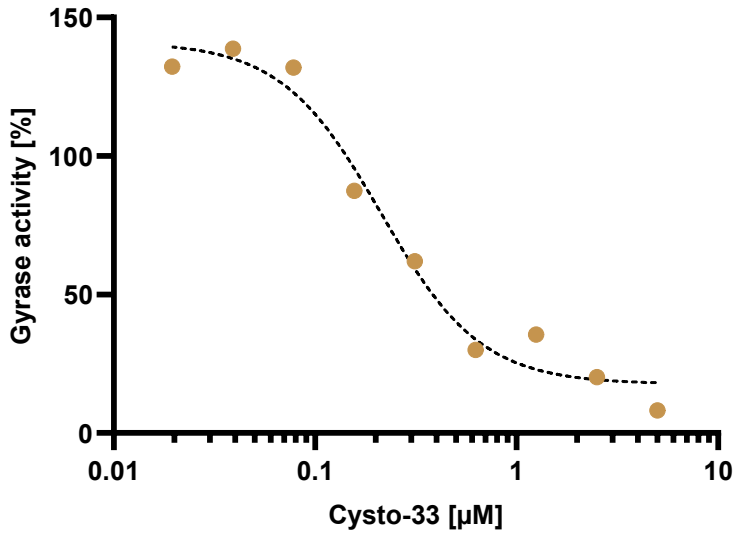

Supplementary Figure 1.27: Cysto-33 [**5**] shows inhibitory effect in the gyrase supercoiling inhibition assay with an IC_{50} of 0.25 µM (n=1).

3. Chapter 2: Cystobactamid off-target profiling reveals favorable safety, superoxide reduction, and SCARB1 inhibition in eukaryotes

Under review in *npj Drug Discovery*

Timo Risch[1,2], Benedikt Hellwinkel[3], Dietrich Mostert[4], Andreas M. Kany[1,2], Danny Solga[5], Tim Seedorf[5], Dominik Heimann[2,6], Jessica Hoppstädter[7], Daniel Kohnhäuser[2,6], Jil-Sophie Hilgers[1], Franziska Fries[1,2], Felix Deschner[1,2], Mark Brönstrup[2,6], Andreas Kirschning[5,8], Stephan A. Sieber[1,4], Thomas Pietschmann[2,3,6,9], Alexandra K. Kiemer[7], Jennifer Herrmann*[1,2], and Rolf Müller*[1,2]

[1]T. Risch, Dr. A. M. Kany, J. Hilgers, F. Fries, F. Deschner, Dr. J. Herrmann, Prof. Dr. S. A. Sieber, Prof. Dr. R. Müller
Helmholtz Institute for Pharmaceutical Research Saarland (HIPS), Helmholtz Centre for Infection Research (HZI) and Saarland University Department of Pharmacy, Campus Building E8.1, 66123 Saarbrücken, Germany, E-mail: rolf.mueller@helmholtz-hips.de
[2]T. Risch, Dr. A. M. Kany, Dr. D. Kohnhäuser, D. Heimann, F. Fries, F. Deschner, Prof. Dr. M. Brönstrup, Prof. Dr. Thomas Pietschmann, Dr. J. Herrmann, Prof. Dr. R. Müller
German Centre for Infection Research (DZIF), Inhoffenstraße 7, 38124 Braunschweig, Germany
[3]B. Hellwinkel, Prof. Dr. Thomas Pietschmann
TWINCORE, Centre for Experimental and Clinical Infection Research, a joint venture between the Helmholtz Centre for Infection Research and the Hannover Medical School, Hannover, Germany
[4]Dr. D. Mostert, Prof. Dr. S. A. Sieber
Center for Functional Protein Assemblies (CPA), Department of Chemistry, Chair of Organic Chemistry II, Technical University of Munich, Ernst-Otto-Fischer-Straße 8, 85748 Garching, Germany
[5]Dr. D. Solga, Dr. T. Seedorf, Prof. Dr. A. Kirschning
Leibniz University Hannover, Institute of Organic Chemistry, Schneiderberg 1B, 30167 Hannover, Germany
[6]Dr. D. Kohnhäuser, D. Heimann, Prof. Dr. M. Brönstrup, Prof. Dr. Thomas Pietschmann
Helmholtz Centre for Infection Research (HZI), Inhoffenstraße 7, 38124 Braunschweig, Germany
[7]Dr. J. Hoppstädter, Prof. Dr. A. K. Kiemer
Institute for Pharmaceutical Biology, Department of Pharmacy, Saarland University
Campus C2 3, 66123 Saarbruecken, Germany
[8]Prof. Dr. Andreas Kirschning
Uppsala Biomedical Center (BMC), Uppsala University, Husargatan 3, 752 37 Uppsala, Sweden
[9]Prof. Dr. Thomas Pietschmann
Cluster of Excellence RESIST (EXC 2155), Hanover Medical School, Hanover, Germany
*Co-corresponding Author

Supplementary information (SI) can be found at the end of this chapter. Synthesis and NMR spectra for Cysto-354 are not included in the SI and can be found online.

Contributions to the presented work

TR designed, performed and analyzed the majority of mentioned experiments. This included experiments to determine topoisomerase inhibition of cystobactamids, cytotoxicity, micronucleus testing, mitochondrial toxicity using seahorse and investigations of mitochondrial superoxide formation. Furthermore, he helped designing the experiments for DMPK profiling. Additionally, he designed, performed and analyzed zebrafish embryo experiments for evaluation of the maximum tolerated dose, cardiotoxicity and hepatotoxicity. He helped designing the probe for affinity-based protein profiling and performed and analyzed the affinity-based proteomic workflow in the mentioned human cell lines. Moreover, he evaluated SCARB1 as a target using surface plasmon resonance and did the molecular docking studies on the modeled protein. He wrote and edited the manuscript and handled the submission process.

DH, TS, DS, DK synthesized and provided the mentioned cystobactamid derivatives important for the manuscript. AMK performed and analyzed the *in vitro* DMPK experiments. JHo supported the seahorse assay. JSH and DM supported proteomic sample preparation and data analysis. BH performed and analyzed the HCVpp assay and cytotoxicity testing on Huh-7.5 cells. FF supported the topoisomerase assays and helped writing the manuscript. FD helped with scientific advice and manuscript revision. JH, RM, MB, AK, AKK, TP and SS provided supervision and funding. TR, JH and RM designed the project. All authors were involved in reviewing and editing the manuscript and approved the final version.

3.1 ABSTRACT

Antimicrobial resistance (AMR) poses a fundamental global threat, necessitating new strategies for effective therapies. Cystobactamids (CYS), a class of antibacterial agents targeting bacterial gyrase and topoisomerase IV, represent a non-traditional chemical scaffold with broad-spectrum activity. For toxicological de-risking, we performed a comprehensive profiling on eukaryotic cells, focusing on cytotoxicity, genotoxicity, and mitochondrial toxicity, demonstrating cellular safety and superoxide scavenging properties. Studies in zebrafish embryos assessed developmental, cardiovascular, and hepatic toxicity, indicating a favorable *in vivo* safety profile. Metabolism studies revealed glucuronidation and amide bond hydrolysis as key pathways, whereby CYS metabolic stability substantially improved by cobicistat co-treatment. Affinity-based protein profiling identified the cholesterol- and HCV-receptor scavenger receptor class B member 1 (SCARB1) as a primary eukaryotic off-target protein, with cystobactamids shown to inhibit SCARB1´s function, preventing hepatitis C virus pseudoparticle entry into cells. These findings suggest a high therapeutic potential for cystobactamids and highlight SCARB1 as a primary eukaryotic target.

3.2 INTRODUCTION

Leading health institutions, including the European medicine agency (EMA) and the World Health Organization (WHO), call attention to antimicrobial resistance (AMR) as an increasing global risk to patients and healthcare systems.[128,129,130,131] The misuse and overuse of antibiotics in humans and also in animals drive the emergence and spread of multidrug-resistant (MDR) bacteria. At the same time, the number of future treatment options using novel antibiotics with innovative structures and mechanisms of action is insufficient.[17,131] The development of previously identified cystobactamids (CYS) might help to fill this gap, as they represent promising broad-spectrum antibiotics comprising a novel scaffold.[81]

CYS are natural products derived from *Cystobacter and Myxococcus* spp.[93] They exhibit antibacterial activity against a broad spectrum of clinically relevant Gram-negative and Gram-positive bacteria including MDR isolates of *Acinetobacter baumannii*, *Enterococcus faecalis*, *Streptococcus pneumoniae*, *Staphylococcus aureus* and *Escherichia coli*.[81,93] CYS act through a new mechanism of action by inhibiting bacterial type IIa topoisomerases (gyrase and topoisomerase IV).[81] A dual mode of binding for the structurally related albicidin and CYS was recently described with one part of the molecule blocking the gyrase dimer interface and the other end intercalating between cleaved DNA fragments, hence preventing DNA religation.[91] Importantly, CYS and the structurally related compound classes of albicidin and coralmycin represent a novel chemical scaffold consisting of *para*-nitrobenzoic acid (PNBA) and multiple *para*-aminobenzoic acid (PABA) units connected through an amino acid linker.[88,89] The novel structure, the lack of cross-resistance with commercially used drugs and their new mechanism of action contribute to the observed resistance-breaking properties within clinical isolates of MDR

pathogens.[81,93,96,97,132] Furthermore, CYS were shown to have a low frequency of resistance (FoR)[132], which is of utmost importance for the wide and sustainable use as an antibiotic. Several total syntheses of CYS were established and modified to successfully yield more than hundred derivatives.[93,96–98,101] This allowed for large-scale production and structural modifications to derive structure-activity and structure-property relationships for optimization of potency, antibacterial spectrum coverage, on-target activity, and physicochemical properties.[94,98]

To ensure efficacy and safety, pharmacological and toxicological properties need to be determined before entering clinical studies. In fact, leading causes for failure of drug candidates in the drug development process are lack of efficacy (52%) or an unfavorable safety profile (24%) (2013-2015).[63,133] Drug approval requires three key properties, namely high quality standards during the production procedure, efficacy against the target disease or symptoms, and a favorable safety profile.[61] Overall, the benefit of using a certain drug must exceed the risk of serious adverse effects.[134] Adverse or side effects include innumerable symptoms, which can range from uncritical effects like dizziness or headaches to live-threatening events such as liver damage or arrhythmia.[135,136]

In the presented study, we evaluated the cyto-, geno- and mitotoxicity of CYS derivatives CN-861-2, CN-DM-861 and Cysto-180 using *in vitro* cell culture models, and we investigated more complex organotoxicity with regards to general developmental, cardio- and hepatotoxicity by *in vivo* zebrafish embryo models. Furthermore, the metabolic pathways and biotransformations of CYS were investigated *in vitro,* and a strategy to improve their *in vivo* exposure was proposed. Moreover, eukaryotic off-target proteins of CYS were identified and analyzed on a molecular level by affinity-based proteome profiling and functional inhibition assays,

surprisingly uncovering yet unexplored potential therapeutic areas for CYS outside their use as antibacterial agents.

3.3 RESULTS AND DISCUSSION

3.3.1 CYS demonstrate general safety in cytotoxicity and genotoxicity assays, with a mild effect on uncoupling the mitochondrial electron transfer chain (ETC)

Three CYS derivatives (CN-861-2, CN-DM-861 and Cysto-180; **Figure 2.1A**) were chosen to further investigate properties of the class with respect to their biological activity on eukaryotic cells. The selected derivatives comprise early stage frontrunner molecules with improved antibacterial properties (CN-861-2 and CN-DM-861[94]; the former served as main reference compound in this study due to its availability) and a further improved derivative (Cysto-180[132]).

Since CYS are bacterial topoisomerase II inhibitors and thus, affect DNA synthesis and repair[137], an obvious potential molecular off-target of CYS is the human DNA topoisomerase IIα (TOP2A). Half inhibitory concentrations (IC_{50}) of 6.26-12.22 µM (**Figure 2.1B**) against TOP2A were determined (CN-861-2 IC_{50} = 6.26 ± 4.69 µM, CN-DM-861 IC_{50} = 10.83 ± 2.38 µM, Cysto-180 IC_{50} = 12.22 ± 0.63µM), which range far beyond (~100 fold) previously observed minimal inhibitory concentrations (MIC) of CYS for their target pathogens as well as identified IC_{50} on *E. coli* gyrase (CN-DM-861 IC_{50} = 0.08 µM).[101,132]

Cell culture models are widely used to determine the cytotoxicity of compounds and to initially assess whether molecules interact with fundamental cellular functions affecting cell division and viability.[138] Interestingly, though their inhibitory effect on the isolated TOP2A activity, CYS did not show any reduction of cell viability in their tested solubility range (≤ 20 µM) for any tested human and non-human cell line (**Figure 2.1C**).

Cysto-180 was more soluble than CN-861-2 and CN-DM-861 and could be tested at higher concentrations. Cysto-180 did not exert cytotoxic effects in Huh-7.5 or CHO-K1 cells with an IC_{50} > 100 µM, underlining the safety of this compound class in the cell viability assay. False negatives resulting from CYS binding to FBS present in the cell media can be excluded, since we observed only a negligible shift in MIC (2-fold) when supplementing the bacterial growth media (MHCII) with FBS (10 %).

In order to assess whether topoisomerase inhibition or previously observed minor groove binding would translate into genotoxicity in a cellular context, a micronucleus assay was performed.[96,91] The DNA cross-linker mitomycin C (0.05 µM), the intercalator doxorubicin (0.05 µM) and the topoisomerase II poison etoposide (0.25 µM) showed a high amount of nuclear bud/micronuclei formation. Interestingly, etoposide as TOP2 poison showed substantial micronuclei formation far below its IC_{50} for TOP2A (46.3 µM, determined by Inspiralis). Cells treated with CYS at concentrations exceeding their TOP2A IC_{50} (20 µM, 100 µM for Cysto-180) also exhibit some micronuclei/nuclear bud formation, but the extent was comparable to that observed in the DMSO control (**Figure 2.1D**, **Figure S2.1**). Despite the topoisomerase inhibition observed on the isolated protein, these results suggest a relatively safe genotoxic profile in a whole cell environment, potentially explainable by poor passive eukaryotic membrane permeability of tested CYS derivatives. Nevertheless, further de-risking measures in the development of CYS are highly recommended, as the possibility of a genotoxic effect cannot be excluded.[139,140]

Given the known risk of quinolone antibiotics interfering with the mitochondrial topoisomerases and ETC-proteins, thereby harming mitochondrial functions[141,142], CYS were further tested in a Seahorse XF Mito Tox Assay (Agilent) to evaluate mitotoxic risks. This assay measures the oxygen consumption rate (OCR) of HepG2

cells treated with the test compounds. During the assay, oligomycin is added as an inhibitor of the oxidative phosphorylation, thus oversaturating the electrochemical gradient at the inner mitochondrial membrane and thereby causing a decrease in the OCR. Subsequently, carbonyl cyanide-p-trifluoromethoxyphenylhydrazone (FCCP) (ionophore) addition leads to an uncoupling of the ETC from the oxidative phosphorylation, thereby increasing the OCR. Inhibition of the oxidative phosphorylation can be seen as a decrease of the starting OCR, whereas uncoupling is defined as an increase in OCR after oligomycin addition. Furthermore, a reduction of the starting OCR and after FCCP addition indicates an inhibition of the ETC caused by the test compound. CYS showed neither inhibition of the oxidative phosphorylation, nor of the ETC due to reduced oxygen consumption at the starting conditions or after FCCP addition, respectively.[143] However, CYS showed a slight but significant uncoupling of the ETC from the oxidative phosphorylation after oligomycin addition with an uncoupling mitochondrial toxicity index (MTI) of 13-17% at their highest soluble concentrations (**Figure 2.1E** and **F**). This indicates that CYS as lipophilic weak acids might act as mitochondrial protonophores, shuttling protons across the inner mitochondrial membrane.[144] CYS are likely to be present in a neutral charge form in the acidic environment of the mitochondrial intermembrane space. This protonation could enhance their membrane migration into the mitochondrial matrix, where the carboxylic acid group is subsequently deprotonated. This process might partially restore the electrochemical gradient and thereby the functionality of the ETC. However, this slight uncoupling did not seem to have a direct harming effect for cell growth and viability as shown above.

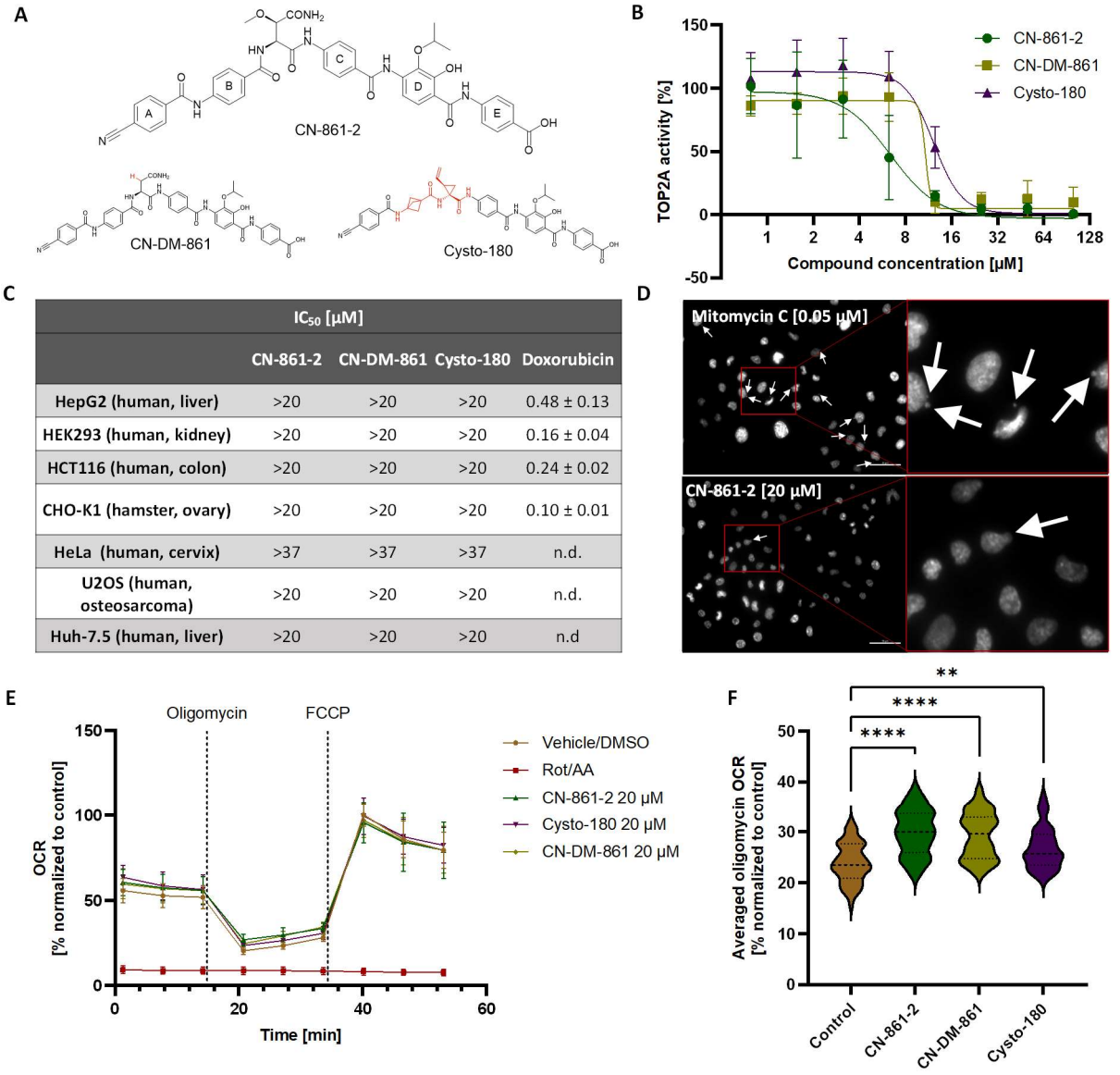

IC_{50} [µM]	CN-861-2	CN-DM-861	Cysto-180	Doxorubicin
HepG2 (human, liver)	>20	>20	>20	0.48 ± 0.13
HEK293 (human, kidney)	>20	>20	>20	0.16 ± 0.04
HCT116 (human, colon)	>20	>20	>20	0.24 ± 0.02
CHO-K1 (hamster, ovary)	>20	>20	>20	0.10 ± 0.01
HeLa (human, cervix)	>37	>37	>37	n.d.
U2OS (human, osteosarcoma)	>20	>20	>20	n.d.
Huh-7.5 (human, liver)	>20	>20	>20	n.d

Figure 2.1. CYS demonstrate general safety in cytotoxicity and genotoxicity assays, with a mild effect on uncoupling the mitochondrial electron transfer chain (ETC). (**A**) Chemical structures of tested CYS derivatives CN-861-2 (top), CN-DM-861 (bottom left) and Cysto-180 (bottom right) in comparison. N-terminal rings A and B are connected via an amino-acid linker with C-terminal rings C to E. Structural differences to CN-861-2 (reference in this study) are marked in red. (**B**) Cystobactamids show concentration dependent inhibition of the human topoisomerase IIα. Data are represented as mean values with standard deviation. IC_{50} was evaluated using non-linear regression (*n* = 3). (**C**) CYS derivatives showed no harming effect on cell viability on human and non-human immortalized cell lines in their solubility range (*n* = 3) (n.d., not determined). (**D**) CYS treated cells showed micronucleus formation comparable to the DMSO control (see also Figure S1.1), while mitomycin C treated cells showed extensive micronucleus formation. (nuclei colored in white, white arrows indicate micronuclei,

scale bar = 50 µm) (*n* = 3). (**E**) Seahorse mitotoxicity assay revealed a slight uncoupling effect of CYS, determined as an increased oxygen consumption rate (OCR) following oligomycin addition. Data are represented as mean values with standard deviation (*n* = 3 x 6 wells). (**F**) Normalized mean values (% normalized to max OCR of control group) with standard deviations are shown (*n* = 3 x 6). Statistically significant differences of the oligomycin OCR were analyzed by ordinary one-way ANOVA with multiple comparison to the DMSO treated control group. (**, $p < 0.005$; ****, $p < 0.0001$). Violin plot is used for data representation.

3.3.2 CYS treatment resulted in a significant reduction of superoxide radical formation

It has been shown that anti-infective agents frequently influence the mitochondrial function.[141] To investigate potential mitochondrial toxicity caused by increased levels of reactive oxygen species (ROS) due to interruption of the ETC upon CYS treatment, superoxide radical ($O_2^{\bullet-}$) production was examined using MitoSOX Red. ROS are byproducts of various essential biological functions and are involved in cell homeostasis and signaling. However, excess of ROS due to cellular stress, (UV-)irradiation or xenobiotics leads to oxidation of biological components such as lipids, proteins and DNA, which ultimately interrupt their physiological function.[145] It has been shown that an increase in ROS *in vivo* can lead to *e.g.* heart or liver failure with increased mortality, as seen *e.g*. for the cancer chemotherapeutic class of anthracyclines.[146–148] The superoxide radical is the precursor of most ROS and thus, represents an indicator used for quantification of ROS formation.

When comparing the superoxide formation of the DMSO control with the CYS treated cells, there was no increase observable. To our surprise, a decrease of superoxide radical levels was observed in CN-861-2 and Cysto-180 treated samples compared to the control group. We also noticed precipitation of CN-DM-861, probably contributing to increased variation in measured fluorescence intensity caused by light scattering at

the particles (**Figure 2.2A top row**, **Figure 2.2B**). In order to investigate whether CYS are able to intercept superoxide radicals, ROS formation via treatment with the redox-cycler menadione was induced and cells were co-treated with CYS.[149] Indeed, in the presence of CN-DM-861 and Cysto-180 no significant increase of superoxide was observed. CN-861-2 co-treated cells exhibited a slight yet statistically significant increase in superoxide production, though the induction remained considerably lower compared to the menadione control (**Figure 2.2A bottom row**, **Figure 2.2C**).

Nevertheless, some minor morphological abnormalities were also observed in CYS co-treated cells, indicating that a comprehensive ROS-protection was not achieved. However, these results show that CYS are able to counteract superoxide radical formation induced by menadione, and suggest that CYS generally prevent ROS formation to a certain extent. This effect might partially be explained by the observed slight uncoupling of the ETC. It was previously reported that mild uncoupling by mitochondrial uncoupling proteins (UCPs) reduces superoxide formation due to a slight proton leakage.[150] This proton leakage potentially decreases the transfer of excess electrons in the ETC to oxygen (electron leakage), which would subsequently lead to superoxide formation.[151] Furthermore, the structure of CYS could additionally serve as a radical scavenger due to radical resonance stabilization captured in its aromatic moieties.[152] These findings indicate that CYS do not induce ROS formation but serve as protective agents against oxidative cell stress.

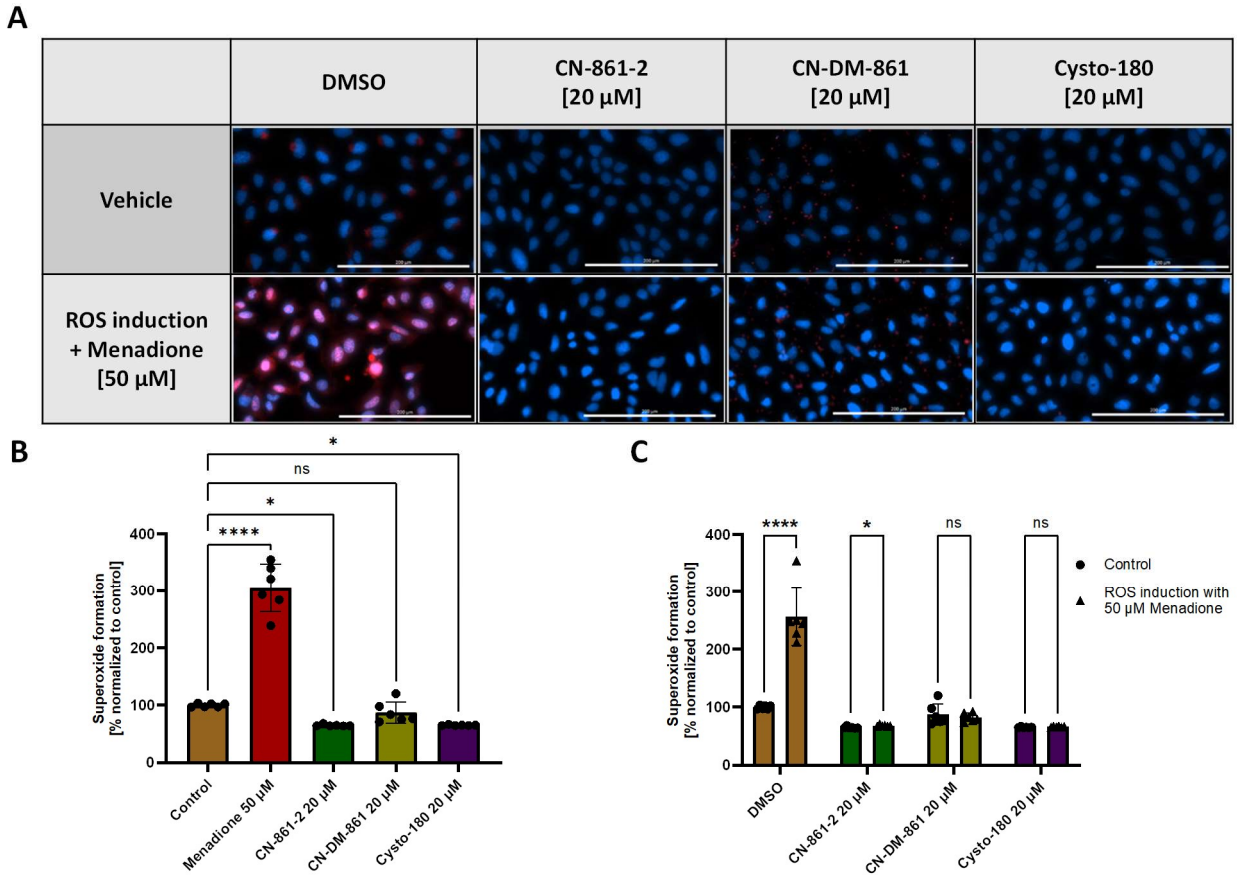

Figure 2.2. CYS treatment resulted in a significant reduction of superoxide radical formation. (**A**) Superoxide formation in U-2 OS cells (indicated by MitoSOX-red fluorescence (pseudocolor red), Hoechst-stained nuclei (pseudocolor blue)) (scale bars are set to 200 µm). (**B**) Cells showed significantly reduced basal levels of superoxide, when treated with CN-861-2 and Cysto-180. (**C**) Co-treatment with CYS suppresses menadione-induced ROS formation. Mean values with standard deviation are shown. Statistical significance was analyzed by ordinary one-way ANOVA with multiple comparison to the control group (A) and multiple unpaired two-stage step-up t-test (B) (n = 6) (ns, non-significant; *, $p < 0.05$; ****, $p < 0.0001$).

3.3.3 CYS are metabolized in hepatocytes by amide bond hydrolysis and glucuronidation, which can be suppressed by cobicistat supplementation

Investigation of the *in vitro* drug metabolism and pharmacokinetic (DMPK) properties of potential new drugs is a crucial aspect of its pharmacological and toxicological assessment that is essential for evaluating an efficacy and safety profile. The characterization of new molecules comprises *e.g.* plasma or metabolic half-life and thereby the drug's ability to reach sufficient exposure *in vivo* in relevant compartments. In addition, the metabolic pathway of a compound can guide compound optimization and has potential impact on toxicological properties, *e.g.* by formation of reactive or toxic intermediates, or by depleting detoxifying agents like glutathione.[153,154]

In vitro evaluations revealed metabolic stability of tested CYS in mouse plasma ($t_{1/2}$ > 240 min). In mouse liver microsomes (MLM), some turnover was observed with slight differences between the derivatives. Cysto-180 and CN-861-2 were stable with $t_{1/2}$ > 120 min and 81 % and 59 % of parent compound remaining after 120 min, respectively, while CN-DM-861 had a half-life of 89 min (**Table S2.1**). When tested in murine hepatocytes containing the full complement of phase I and phase II drug metabolizing enzymes, degradation was observed for CN-DM-861 ($t_{1/2}$ 94 ± 15 min), and Cysto-180 ($t_{1/2}$ 41 ± 16 min), while CN-861-2 was stable for over > 3 h (**Table S2.1**). In order to obtain information about the metabolic pathways of CYS, the metabolites of CN-DM-861 and Cysto-180 in mouse hepatocytes were analyzed qualitatively. These studies revealed amide bond hydrolysis and glucuronidation of the parent compound as the major metabolic pathways (**Figure S2.2-S2.5**). In particular, the amide bond between ring C and ring D appeared to be metabolically labile.

With the aim of reducing the turnover of CYS *in vivo* by reducing hepatic uptake, we investigated its metabolic stability in the presence of cobicistat. This drug is known as

an OATP1B and CYP3A inhibitor and is used as a co-treatment with HIV therapeutics to enhance their metabolic stability.[155,156]

Supplementation substantially increased the metabolic stability of CN-DM-861 in mouse hepatocytes in a concentration-dependent manner. Whether the observed increase in CYS stability is solely related to reduced transport into hepatocytes via OATP inhibition or also influenced by reduced CYP-mediated amide cleavage[157], cannot be fully answered by these assays. The fact that CN-DM-861 metabolism was also reduced by cobicistat in liver microsomes shows that in principle, reduction of CYS metabolism via CYP inhibition is feasible (**Figure S2.6**).[157] In any case, combination of CYS with cobicistat represents a promising strategy to enhance their metabolic stability and availability *in vivo*. However, verification in murine pharmacokinetic studies is required to determine whether a combination with cobicistat leads to improved *in vivo* stability.

All compounds showed high plasma protein binding (PPB ~ 96-100%, **Table S2.1**), which might raise an issue *in vivo* due to reduced availability of free drug. Only the free compound fraction is capable of interacting with its antimicrobial target and thus, capable of causing a pharmacological effect. However, previous experiments demonstrated the capability of CYS for being efficacious *in vivo* as assessed in various murine infection models.[94,95] It is also important to consider that partial PPB might even be beneficial for increased metabolic half-life and prolonged exposure at the site of infection.

3.3.4 *In vivo* toxicity evaluation of CYS in zebrafish embryos revealed no abnormalities in development, cardiac function, or liver morphology

In vitro assays are sufficient in providing a basic understanding of the pharmacological properties of a new compound on a cellular level but can often not cover the complexity

of a whole organism. Zebrafish embryos can be used as a more complex *in vivo* model *e.g.*, for the early evaluation of potential (organo-)toxicity of a compound and its potential phase I and phase II metabolites.[158–160] In compliance with the 3R principle on the reduction, refinement and replacement of animal experiments, we applied this model since zebrafish at early developmental stages (≤ 120 hours post-fertilization, hpf) are not classified as animal models according to Directive 2010/63/EU.[161]

Developmental toxicity can be caused by various mechanisms including interference of the compound with gene expression, cell growth and differentiation, homeostasis or inhibition of angiogenesis.[69,162] To investigate potential developmental and *in vivo* genotoxicity, zebrafish embryos were incubated in the presence of CYS from a very early developmental stage (1 day post fertilization (dpf)) until most organs are fully developed (5 dpf). For the positive control 3,4-dichloroaniline[163] various malformations including spinal curvature and edema were observed, which ultimately led to death. CYS-treated zebrafish embryos did not develop malformations with 100% survival until 5 dpf at their highest tested soluble concentration (20 µM) (**Figure 2.3A**). Due to its higher solubility in the incubation medium, Cysto-180 was tested up to 200 µM, showing the same outcome. Thus, the maximum tolerated concentration (MTC) of CYS in zebrafish embryos is above their solubility limit. In view of their potent antibacterial activity with minimum inhibitory concentrations (MICs) in the sub-µM range[94], these data suggest that CYS might have a large therapeutic window.

Furthermore, it was reported that substances, which are cardiotoxic in humans, show the same effect in zebrafish embryos with a very high accuracy.[164] Especially human ether-à-go-go-related gene (hERG) channel inhibition is regarded as a major risk factor being predictive for cardiotoxicity. Inhibition of this ion channel induces cardiac QT interval prolongation, resulting in a specific type of arrhythmia called torsades de

pointes, which is associated with high mortality rates.[136,165] The phenotypical endpoints determined in the zebrafish embryo assay included heartbeat rate, cardiac rhythm and the development of pericardial edema.[159] Upon treatment with the known hERG-inhibitor terfenadine, embryos showed a significant, concentration-dependent increase in pericardial area (**Figure 2.3B** and **C**). Additionally, examination of the heartbeat rate revealed a significant and concentration-dependent decrease of beats per minute with apparent arrhythmia in the vast majority of treated embryos (**Figure 2.3D**). CYS-treated embryos neither showed pericardial malformations, nor significant changes in pericardial area or heartbeat rate (**Figure 2.3B-D**). These results suggest a favorable cardiotoxic safety profile of CYS *in vivo*.

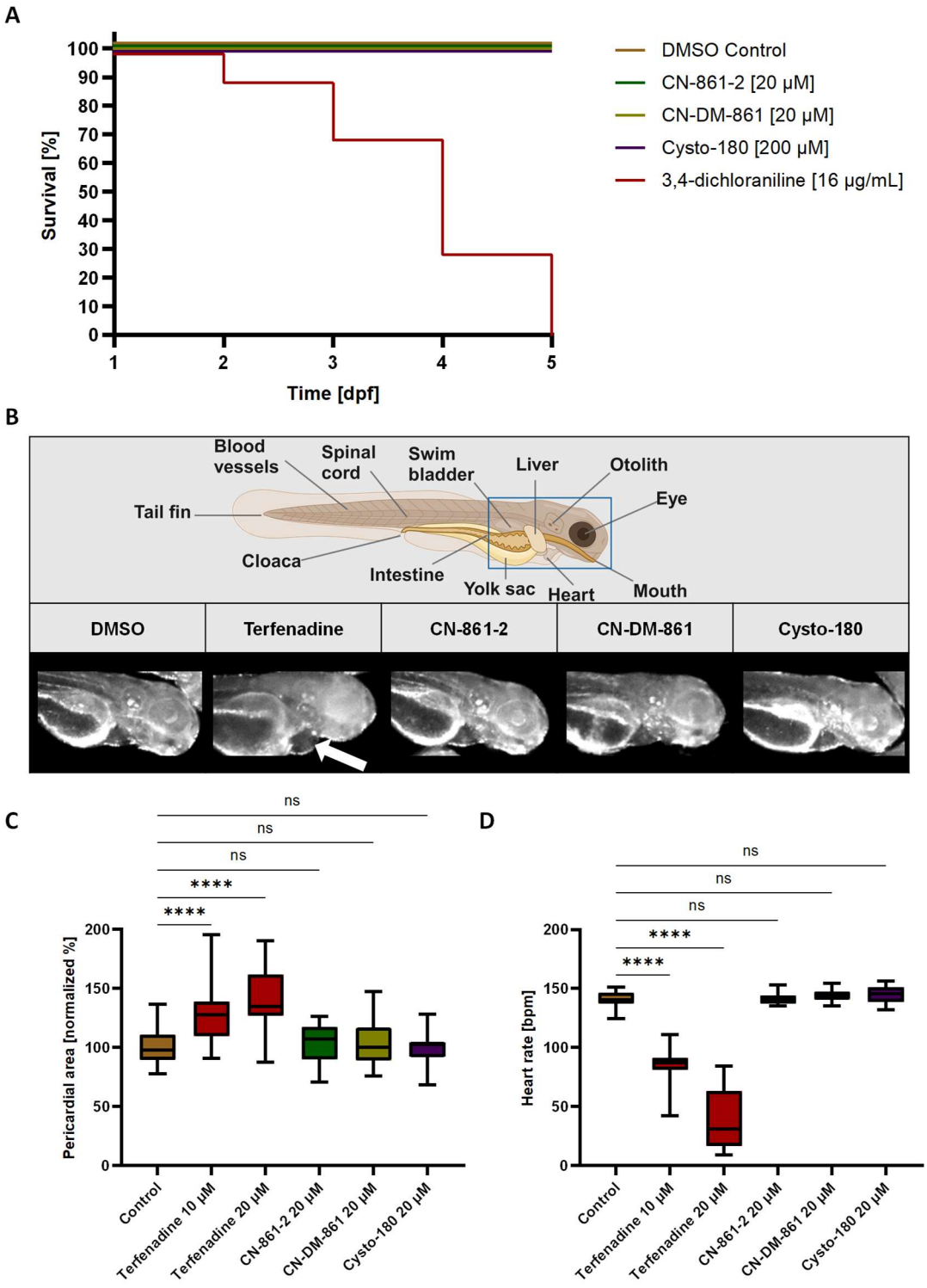

Figure 2.3. *In vivo* toxicity evaluation of CYS in zebrafish embryos revealed no abnormalities in development or cardiac function. (**A**) CYS showed no developmental *in vivo* toxicity. All CYS treated zebrafish embryos survived and showed no abnormal development when exposed from 1 to 5 dpf. Maximum tolerated concentration (MTC) of CYS was shown to be above their solubility limit (*n* = 20). (**B**) For assessment of cardiotoxicity, zebrafish embryos were treated from 2 to 3 dpf with no observable

pathological cardiac morphology for CYS. For the positive control terfenadine, pericardial edemas were observable (white arrow) (created with BioRender.com). (**C**) Statistical evaluation of the pericardial area showed no abnormalities for CYS treated embryos, but an increase in pericardial area after terfenadine treatment. (**D**) Statistical evaluation of the embryo´s heart rates showed no abnormalities after CYS treatment, but a decreased heart rate after treatment with the positive control terfenadine. Box plot (quartiles Q1 to Q3, including median) with whiskers (min to max) is shown. Statistical significance was analyzed by ordinary one-way ANOVA with multiple comparison to the control group ($n \geq 20$) (ns, non-significant; ****, $p < 0.0001$).

The correlation between human and zebrafish toxicology was also observed for drug-induced hepatotoxicity. The assessment of *in vivo* hepatotoxicity offers the opportunity to identify not only toxic effects by the parent molecule but also potential toxicity of *in vivo* metabolites. At the same time the actual *in vivo* distribution of a drug and its metabolites is considered, which can cause adverse effects if a compound shows accumulation in certain compartments such as the liver. Functional toxicity, such as bile acid pump inhibition or steatosis, is also more effectively assessed *in vivo* than *in vitro*. For intoxicated zebrafish embryos, liver degradation can be easily observed by quantifying liver size reduction and observation of histological changes after treatment.[160]

Several mechanisms of drug-induced hepatotoxicity were proposed for the positive control valproic acid, namely formation of reactive metabolites, disturbance of the mitochondrial function and fatty acid metabolism and finally induction of oxidative stress.[146]

The transgenic fish line [Tg(fabp10a:DsRed; elaA:EGFP)] with fluorescent liver cells was used, facilitating the quantification of liver size.[160] Valproic acid-treated embryos showed significant liver size reduction, reflecting its hepatotoxicity. CYS did not show

any significant reduction in liver size, thus suggesting an advantageous and non-hepatotoxic profile *in vivo* (**Figure 2.4A** and **B**).

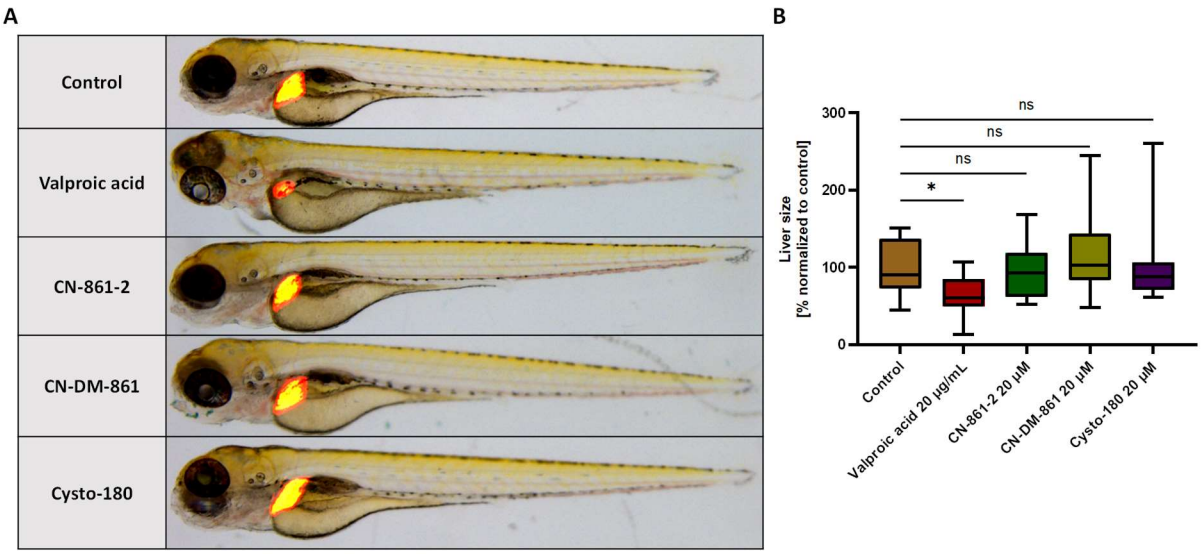

Figure 2.4. *In vivo* toxicity evaluation of CYS in zebrafish embryos revealed no abnormalities in liver morphology. (**A**) No *in vivo* hepatotoxic effect was observed for CYS treated zebrafish embryos. Transgenic zebrafish embryos [Tg(fabp10a:DsRed; elaA:EGFP)] were checked for liver size reduction after treatment as endpoint readout. Liver degeneration was examined by comparing the fluorescent liver area to the control group. (**B**) CYS treated embryos did not show a significant reduction in liver size, in contrast to the positive control valproic acid. Box plot (quartiles Q1 to Q3, including median) with whiskers (min to max) is shown for a quantitative representation of liver size. Statistical significance was analyzed by ordinary one-way ANOVA with multiple comparison to the control group ($n \geq 15$) (ns, non-significant; *, $p < 0.05$).

3.3.5 Molecular off-target identification revealed SCARB1 as primary binding partner of CYS in eukaryotes

Phenotypical assays offer a comprehensive overview of potential intoxications; nevertheless, they frequently fail to provide insights into molecular mechanisms including binding partners of the investigated compounds.

For this purpose we designed and synthesized the CYS photo-probe Cysto-354 to investigate eukaryotic target proteins of CYS via affinity-based protein profiling

(AfBPP) (**Figure S2.7–S2.27**).[74] Cysto-354 was tested for potential cytotoxicity, revealing a slight effect on cell viability at the highest assay concentration (37 µM) and no effect at any of the lower concentrations tested (≤ 12.3 µM) (**Figure S2.28**).

AfBPP aims to identify molecular binding partners via photo-reactive cross-linking followed by enrichment of the bound proteins. In order to exclude enriched but unspecifically bound proteins, competition of the binding site was performed by co-treatment with the unfunctionalized parent compound (here: CN-861-2). In such cases, specific binding is identified by reduction of enrichment in the presence of the parent compound.

By performing the AfBPP assay with Cysto-354-treated HepG2 cells, an immortalized liver cell line which is widely used in early toxicity profiling of drug candidates, we were able to identify significantly enriched proteins, which belong to a functional cluster of cholesterol transfer activity due to lipoprotein and lipid binding (**Figure 2.5A** and **B**). Proteins within this functional cluster had in common, that they interact with the highly enriched cholesterol-, lipid- and lipoprotein-receptor scavenger receptor class B member 1 (SCARB1).

By comparing significantly enriched and competed proteins, we were able to identify SCARB1 (**Figure 2.5C**) and LPCAT3 as potential specific binding partners of CYS. To gain insights across diverse cell types, this assay was replicated utilizing both HEK293 (kidney) and HeLa (cervix) cells. SCARB1 was observed to be enriched in all tested cell types, whereas LPCAT3 was not enriched in HEK293 or HeLa cells (**Figure 2.5D** and **E**). The transcriptional coregulator pirin (PIR) and the acyltransferase AGPAT2 were observed to be enriched in all cell types (**Figure 2.5E**), however, the proteins were not competed by CN-861-2 addition, indicating only unspecific binding of Cysto-354.[166] Noteworthy, human topoisomerase (TOP1, TOP2A, TOP2B) enrichment was

not observed in the whole cell environment of HepG2, HeLa and HEK293, potentially explaining the lack of observable cellular (geno-)toxicity (**Figure S2.29**).

In conclusion, SCARB1 appears to be the primary off-target protein of CYS in eukaryotic cells. Biophysical binding analysis via surface plasmon resonance (SPR) (Biacore X100, Cytiva) was used to characterize and confirm the direct interaction of CYS and SCARB1. For this, biotinylated SCARB1 (Acrobiosystems) was immobilized on a SPR sensorchip, coated with streptavidin (sensor chip SA, Cytiva). All tested CYS derivatives (20 µM) showed interaction with the immobilized SCARB1 protein, exhibiting different binding kinetics (**Figure 2.5F**). However, CYS appeared to not only interact specifically, as indicated in the competition assay, but also unspecifically with SCARB1. This can be concluded from the observed exceeding of the theoretical maximal response R_{max} (~41 RU) with increasing CYS contact time and concentration, which did not result in saturation. This effect is most likely mediated by the previously observed π-π-stacking of CYS´s aromatic systems, which occurs subsequently to initial specific binding.[99] Consequently, we were not able to determine the equilibrium dissociation constant (K_D) of CYS to SCARB1 reliably.

Nevertheless, encouraged by this finding, we further characterized SCARB1 binding and functional inhibition with regards to a potential novel therapeutic indication of CYS.

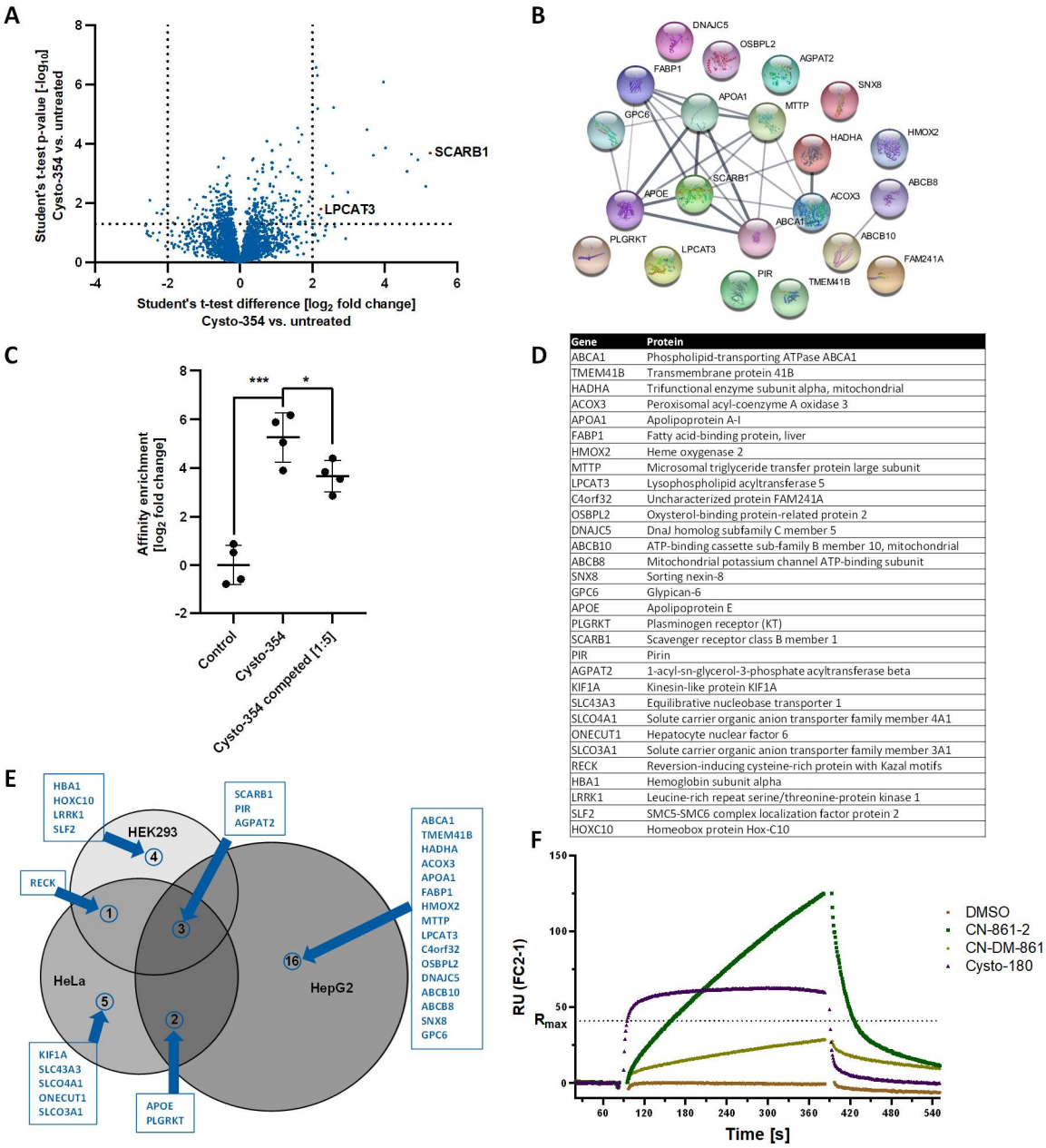

Gene	Protein
ABCA1	Phospholipid-transporting ATPase ABCA1
TMEM41B	Transmembrane protein 41B
HADHA	Trifunctional enzyme subunit alpha, mitochondrial
ACOX3	Peroxisomal acyl-coenzyme A oxidase 3
APOA1	Apolipoprotein A-I
FABP1	Fatty acid-binding protein, liver
HMOX2	Heme oxygenase 2
MTTP	Microsomal triglyceride transfer protein large subunit
LPCAT3	Lysophospholipid acyltransferase 5
C4orf32	Uncharacterized protein FAM241A
OSBPL2	Oxysterol-binding protein-related protein 2
DNAJC5	DnaJ homolog subfamily C member 5
ABCB10	ATP-binding cassette sub-family B member 10, mitochondrial
ABCB8	Mitochondrial potassium channel ATP-binding subunit
SNX8	Sorting nexin-8
GPC6	Glypican-6
APOE	Apolipoprotein E
PLGRKT	Plasminogen receptor (KT)
SCARB1	Scavenger receptor class B member 1
PIR	Pirin
AGPAT2	1-acyl-sn-glycerol-3-phosphate acyltransferase beta
KIF1A	Kinesin-like protein KIF1A
SLC43A3	Equilibrative nucleobase transporter 1
SLCO4A1	Solute carrier organic anion transporter family member 4A1
ONECUT1	Hepatocyte nuclear factor 6
SLCO3A1	Solute carrier organic anion transporter family member 3A1
RECK	Reversion-inducing cysteine-rich protein with Kazal motifs
HBA1	Hemoglobin subunit alpha
LRRK1	Leucine-rich repeat serine/threonine-protein kinase 1
SLF2	SMC5-SMC6 complex localization factor protein 2
HOXC10	Homeobox protein Hox-C10

Figure 2.5. Molecular off-target identification revealed SCARB1 as primary binding partner of CYS in eukaryotes. (**A**) Affinity-based protein profiling (AfBPP) revealed significant enrichment of the SCARB1 protein. HepG2 cells were treated with the CYS photo-probe Cysto-354. After affinity enrichment, the protein abundances were compared to an untreated control (volcano plot). Significant enrichment was analyzed by two-tailed unpaired student's t-test (cut-offs for enrichment: p [$-\log_{10}$] > 1.3 and abundance difference [$\log_2$] > 2) (n = 4). (**B**) STRING database analysis of significantly enriched proteins showed functional clustering with respect to cholesterol transfer activity due to lipoprotein and lipid binding (GO-term false discovery rate: 5.05e-7) (created using STRING db (version 12.0)). (**C**) SCARB1 showed the highest enrichment and significant competition upon CN-861-2 addition, indicating

specific binding by CYS. Data are shown as mean ± standard deviation. Significant enrichment and competition was analyzed by two-tailed unpaired student's t-test (*, $p < 0.05$; ***, $p < 0.001$) ($n = 4$). (**D**) List of significantly enriched proteins after Cysto-354 treatment in HepG2, HeLa-CCL-2 and HEK293. (**E**) Venn diagram of enriched proteins for CYS AfBPP in HeLa, HEK293 and HepG2 cells (created using BioVenn). (**F**) Binding analysis using surface plasmon resonance (SPR) confirmed binding of CYS to the SCARB1 protein, exceeding theoretical maximal response (R_{max}).

3.3.6 Binding of CYS to SCARB1 leads to functional inhibition of HCVpp entry into hepatocytes

The functional inhibition of SCARB1 was evaluated to examine the effects of CYS interaction with the protein.

SCARB1 binds different ligands such as phospholipids, cholesterol esters, lipoproteins, phosphatidylserine, but especially high density lipoproteins (HDL) with high affinity. Thus, SCARB1 plays a dual role in cholesterol metabolism. Firstly, it promotes cholesterol efflux in peripheral tissues such as the arterial wall, aiding in the removal of excess cholesterol. Secondly, it serves as a substantial receptor for HDL cholesterol particles, facilitating the transfer of cholesterol, lipids and lipoproteins back into the liver.[167–169] Thus, it plays a crucial role in many physiological and pathophysiological processes including cholesterol and lipid homeostasis, cardiovascular disease, liver disease and cancer.[170–172] Importantly, SCARB1 also serves as a crucial entry receptor for the hepatitis C virus (HCV) into hepatocytes.[173,174]

Chronic hepatitis C is a viral infection that causes liver cirrhosis and hepatocellular carcinoma. In 2019, 1.5 million people were newly infected with the hepatitis C virus, with 290,000 infection-related deaths in the same year.[175] After infection, HCV circulates in the bloodstream as lipoviral particle and thereby gets in contact with the basolateral surface of hepatocytes to which it attaches by low affinity interaction of

lipoviral-associated ApoE to low-density lipoprotein (LDL) receptors and glycosaminoglycans (GAGs). Subsequently, SCARB1 binds the lipoviral-associated lipoproteins, initiating the lipid- and cholesterol-transfer activity of the protein, which probably mediates dissociation of the virus particle from its associated lipoproteins. Importantly, SCARB1 binds the HCV surface glycoprotein E2, causing a conformational change, which enables binding of E2 by CD81. Consequently, CD81 mediates lateral movement and interaction of HCV with claudin-1 (CLDN1), facilitating its endosomal cell entry and release of the viral genome (**Figure 2.6A**).[176]

We investigated the functional interaction of CYS with SCARB1 by examining the reduction of HCV pseudoparticle (HCVpp) cell entry into hepatocytes (Huh-7.5) upon CYS treatment. To this end, we used the lentivirus-based pseudotype assay, where the HCVpp was equipped with glycoproteins derived from two different genotypes (JFH1 from genotype 2a and Con1 from genotype 1b). The SCARB1-inhibitor ITX5061 was used as positive control.[172] The luciferase reporter gene was used to quantify HCVpp entry. CYS treatment successfully inhibited HCVpp cell-entry in a concentration-dependent manner for both tested genotypes. CN-861-2 and CN-DM-861 exhibited similar inhibitory capacities, while Cysto-180 was the most effective derivative with 50% entry inhibition at a concentration of ~3.3 µM (**Figure 2.6B** and **C**).

To elucidate the specificity of CYS in inhibiting SCARB1 as the entry receptor of HCVpp, we examined the effect of CYS to the SCARB1-independent entry of vesiculovirus pseudoparticles (VSVpp) equipped with respective viral glycoprotein. Indeed, we demonstrated that CYS exhibited no inhibitory effect on VSVpp cell entry (**Figure S2.30**). Hence, these results provide evidence for the specificity of functional inhibition of SCARB1 as cause of CYS-mediated HCVpp cell entry inhibition.

Applying a bioinformatic molecular docking approach (MOE), only one potential CYS binding site within the modeled structure of SCARB1 was identified. The determined binding pocket is located at the extracellular domain of the protein, potentially important for interaction with native binding partners. CYS blocking of this site might hinder interaction of these binding partners with SCARB1, potentially explaining the inhibitory properties of CYS against HCVpp entry.[177] However, based on the docking results, multiple poses of CYS in the binding pocket appear feasible (**Figure S2.31**). Future studies will validate the mode of binding of CYS to SCARB1 in more detail and enable the opportunity for structure-guided optimization towards efficient inhibition of this host target.

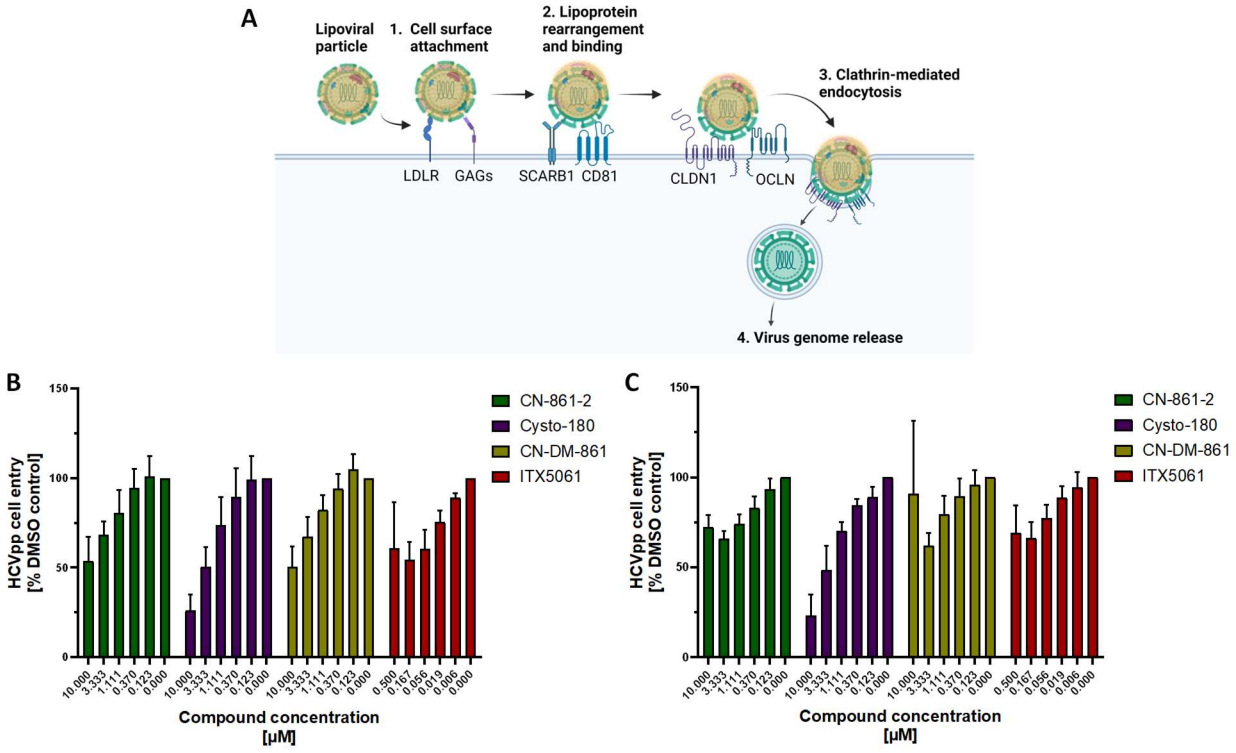

Figure 2.6. Binding of CYS to SCARB1 leads to functional inhibition of HCVpp entry into hepatocytes. (**A**) SCARB1 is known for its crucial role in binding and transfer of HCV lipoviral particles into hepatocytes (created with BioRender.com). (**B**) HCVpp entry assays with glycoprotein JFH-1 (genotype 2a). Binding of CYS to SCARB1 leads to concentration dependent inhibition of HCVpp entry into hepatocytes. ITX5061 was used as positive control. (**C**) HCVpp entry assays with glycoprotein

Con1 (genotype 1b) also showed concentration dependent entry inhibitory activity of CYS. Data are shown as mean values with standard deviation (*n* = 5).

These findings could not only broaden the potential therapeutic applications of CYS from broad-spectrum antibiotic to antiviral agent, but also extend to various non anti-infective indications. The inhibition of SCARB1 by CYS might affect its lipid- and cholesterol transporter activity *in vivo*. In previous *in vivo* mouse studies, suppression of SCARB1 by ITX5061 successfully led to increased beneficial HDL cholesterol levels and partially reduced atherosclerotic lesions.[172] In addition, inhibition of SCARB1 is currently under investigation for potential therapeutic benefits across various medical conditions, including arteriosclerosis and other cardiovascular diseases, non-alcoholic fatty liver disease, or specific cancer types associated with the upregulation of SCARB1.[170–172,178,179]

3.4 CONCLUSION

Herein, we demonstrated the safety of cystobactamids in cell culture assays and in *in vivo* zebrafish embryo models. The antibiotics showed slight uncoupling of the mitochondrial ETC, which might contribute to their ROS protective properties. This influence on the ETC does not seem to have harming effects *in vitro* or *in vivo* as assessed by cell viability as well as developmental, cardio- and hepatotoxicity in zebrafish embryos. *In vitro* DMPK studies revealed glucuronidation and amide bond hydrolysis as the main biotransformation pathways of cystobactamids. Their metabolic stability was substantially enhanced by supplementation with cobicistat, an OATP- and CYP-inhibitor, offering the opportunity to explore combination therapy as viable approach to improve PK/PD properties of cystobactamids *in vivo*. In addition, on a molecular level, cystobactamids bound to the cholesterol and lipoprotein receptor

SCARB1 as the main eukaryotic off-target proteins in the whole cell environment. By binding to SCARB1, they actively prevented the entry of hepatitis C virus into hepatocytes. Analysis of the binding mode to SCARB1 might guide further development and optimization of cystobactamids, along with related compound classes such as albicidin and coralmycin, for various possible therapeutic areas.

3.5 MATERIALS AND METHODS

3.5.1 Cell culture

All cell types were cultivated at 37 °C with 5 % CO_2. HepG2, HEK293, HCT116, CHO-K1, HeLa-CCL-2 and Huh-7.5 were purchased at ATCC. The respective cell media (Gibco) was supplemented with 10 % FBS (Gibco) before usage. Cells were used between passage #5 and #30. To obtain biological repeats, cells were split separately for at least two passages.

3.5.2 Topoisomerase IIα inhibition

Inhibition of topoisomerase activity was examined using human topoisomerase II alpha decatenation assay kit (Inspriralis) as indicated by the manufacturer. Briefly, a compound dilution series was prepared in DMSO. Water, dilution buffer, assay buffer, plasmid and enzyme were mixed with compound solution and incubated at 37°C for 30 min. A positive control (100% activity) was prepared without compound and a negative control (0% activity) was prepared without compound and enzyme. The reaction was stopped by adding gSTEB-buffer and chloroform/isoamylalcohol (24:1 v/v). The samples were vortexed and centrifuged before running gel-electrophoresis. The gel was stained with ethidium bromide and imaged using a Fusion Fx gel imager (Vilber Lourmat). Subsequent analysis was done using ImageJ and GraphPad Prism (Version 10.0.2).

3.5.3 Cytotoxicity

Cells were washed with PBS and 0.5 mL trypsin was added. Afterwards, cells were incubated for 5 min before adding 10 mL medium containing 10 % FBS. Per well, 120 µL cell suspension ($5x10^4$ cells/mL) was seeded in transparent 96 well cell bind plates and incubated for 2 h (37 °C, 5 % CO_2). Dilution series (1:3) of test compounds was prepared in respective media containing 10 % FBS and added (60 µL) to the prepared cell plate. Cells were incubated for further 72 h (37 °C, 5 % CO_2). Next, 20 µL MTT (5 mg/mL in PBS) was added to each well and incubated for 2 h (37 °C, 5 % CO_2). The wells were emptied and 100 µL isopropanol/10 N HCl (1000:4) per well was added.

The plates were analyzed by measuring the absorbance at 570 nm (plate reader Infinite® 200 Pro, Tecan). After normalization of data to the respective solvent controls, the calculated percentage of growth inhibition was plotted using GraphPad Prism software (version 10.0.2).

3.5.4 Micronucleus test

CHO-K1 cells were washed and seeded like described above with a concentration of $5x10^4$ cells/mL . Cells were treated with CYS (20 µM, 100 µM for Cysto-180) and incubated for 24 h. Mitomycin C (0.05 µM), doxorubicin (0.05 µM) and etoposide (0.25 µM) were used as positive controls. Cells were washed and stained with Hoechst (5 µg/mL) (Thermo) in F12 media for 15 min. Subsequently, cells were washed three times with PBS and imaged using Celldiscoverer 7 (Zeiss).

3.5.5 Mitochondrial toxicity

Seahorse mitotox assay was carried out according to Agilent seahorse XF mito tox assay kit user guide (kit 103595-100, Agilent). Briefly, sensor cartridge was hydrated

at 37 °C, non-CO_2, one day before the assay started in 200 µL water and 2 h in calibrant solution before usage. HepG2 cells were seeded with a density of $10x10^3$ per well in 80 µL and incubated overnight at 37 °C, 5 % CO_2. At the day of the assay, 100 mL Seahorse XF DMEM medium was prepared by addition of glucose (10 mM), pyruvate (1.0 mM) and glutamine (2.0 mM). CYS compound dilutions were prepared in assay medium as well as positive controls menadione (50 µM) and Rot/AA (1.0 µM). Cells were washed with assay medium and compounds were added, followed by 2 h incubation at 37 °C, non-CO_2. Oligomycin (1.5 µM) and FCCP (1.0 µM) were prepared and added to the respective ports in the sensor cartridge. The utility plate with sensor cartridge was inserted into the Seahorse system (Agilent) and calibrated. Afterwards the cell plate was added and measurement of the oxygen consumption rate (OCR) was started. The assay was repeated three times independently with at least 6 technical replicates per condition. Uncoupling MTI was calculated as follows:

$$\boldsymbol{Uncoupling\ MTI} = \frac{\boldsymbol{Max\ Oligo\ OCR\ (Compound) - Min\ Oligo\ OCR\ (Vehicle)}}{\boldsymbol{Max\ FCCP\ OCR\ (Vehicle) - Min\ Oligo\ OCR\ (Vehicle)}} \quad (1)$$

3.5.6 Mitochondrial superoxide formation

CYS were tested for their potential of inducing oxidative stress in U-2 OS cells. Therefore, 120 µL of a cell suspension in McCoy`s (+10 % FBS) containing 5 x 10^4 cells/mL were seeded into black 96-well imaging plate (BD Falcon). The plates were incubated for two days (37 °C, 5 % CO_2) until the cells reached approximately 70 % confluence. Subsequently, the cells were washed with HBSS buffer, prior to adding CYS (20 µM) and the ROS inducer menadione (50 µM) as positive control, along with the staining solution (HBSS, calcium, magnesium, 5 µM MitoSOX red and 10 µg/mL Hoechst (Thermo)). To check for ROS protective properties, menadione (50 µM) was added directly to the staining solution. The cells were incubated for 1-2 h at 37 °C and

5 % CO_2. Afterwards, the cells were washed twice with HBSS. The cells were imaged using an automated fluorescence microscope (Celldiscoverer 7, Zeiss) (excitation: 485 nm, emission: 535 nm) to analyze the fluorescence intensity of the superoxide tracker MitoSOX red. The experiment was carried out with six replicates per condition. Quantification was done by high-content image analysis using the ZEN software (version 3.4, blue edition, Zeiss). Data presentation was done using GraphPad Prism (version 10.0.3) with ordinary one-way ANOVA including multiple comparison to the control group for statistical analysis of sample without ROS induction via menadione in the staining solution. Multiple unpaired t-test was used to compare samples for ROS protective properties, which were incubated with menadione in the staining solution.

3.5.7 Metabolic stability in mouse liver microsomes

For the evaluation of phase I metabolic stability, the compound (1 µM) was incubated with 0.5 mg/mL pooled mouse liver microsomes (Xenotech, Kansas City, USA), 2 mM NADPH, 10 mM $MgCl_2$ at 37 °C for 120 min on a microplate shaker (Eppendorf, Hamburg, Germany). The metabolic stability of testosterone, verapamil and ketoconazole was determined in parallel to confirm the enzymatic activity of mouse liver microsomes. For combination experiments, cobicistat was added to the incubation mixture together with test compounds. The incubation was stopped after defined time points by precipitation of aliquots of enzymes with 2 volumes of cold internal standard solution (15 nM diphenhydramine in 10% methanol/acetonitrile). Samples were stored on ice until the end of the incubation and precipitated protein was removed by centrifugation (15 min, 4 °C, 4,000 g). Concentration of the remaining test compound at the different time points was analyzed by HPLC-MS/MS (Vanquish Flex coupled to a TSQ Altis Plus, Thermo Fisher, Dreieich, Germany) and used to determine half-life ($t_{1/2}$).

3.5.8 Metabolic stability in mouse hepatocytes

For the evaluation of combined phase I and phase II metabolic stability, the compound (1 µM) was incubated with 0.25 x 10^6 cells/mL of pooled mouse hepatocytes (Xenotech, Kansas City, USA). Cells were thawed in Leibovitz's L-15 medium without phenol red (ThermoFisher Scientific, Waltham, USA). Briefly, cells were transferred into 50 mL of medium, followed by centrifugation at 55 g for 6 min. Supernatant was discarded and the cell count determined after gently resuspending the cell pellet in 1 mL of medium. Hepatocytes were diluted to 0.5 x 10^6 cells/mL and incubated at 37 °C, 700 rpm for 10 min, to achieve the desired final cell count after addition of an equal volume of test compounds in medium, leading to final test concentration of 1 µM at 1% DMSO. Samples were incubated for 240 min at 37 °C, 700 rpm and the incubation was stopped after defined time points by precipitation of aliquots in 4 volumes cold internal standard solution (12.5 nM diphenhydramine in 10% methanol/acetonitrile). For the determination of metabolism in presence of cobicistat, this drug was added together with test compounds in the desired concentration range. The metabolic stability of testosterone, verapamil, ketoconazole and 7-hydroxycoumarine were determined in parallel to confirm the enzymatic activity of mouse hepatocytes. Samples were stored on ice until the end of the incubation and precipitated protein was removed by centrifugation (15 min, 4 °C, 4,000 g). Concentration of the remaining test compound at the different time points was analyzed by HPLC-MS/MS (Vanquish Flex coupled to a TSQ Altis Plus, Thermo Fisher, Dreieich, Germany) and used to determine half-life ($t_{1/2}$). Intrinsic clearance was calculated as follows:

$$\boldsymbol{CL_{int}}\ [\frac{\mu \boldsymbol{L}}{\boldsymbol{min}\times\boldsymbol{10^6}\ \boldsymbol{cells}}] = \frac{\boldsymbol{Incubation\ volume}\ [\mu \boldsymbol{L}]\times \boldsymbol{ln(2)}}{\boldsymbol{Cells\ in\ incubation\ mixture}\ [\boldsymbol{10^6}]\times \boldsymbol{t_{1/2}}} \quad (2)$$

For metabolite idenfication studies, test compounds were incubated at 10 µM final concentration and samples were analyzed using HPLC-HRMS (Ultimate 3000 coupled to a Q Exactive Focus, Thermo Fisher, Dreieich, Germany). LC conditions were as follows: column: Accucore Phenyl-Hexyl (2.6 µm, 100 x 2.1 mm; Thermo Fisher, Dreieich, Germany); temperature 40 °C; flow rate 0.500 mL/min; solvent A: water + 0.1% formic acid; solvent B: acetoni-trile + 0.1% formic acid; gradient[180]: 0–4.0 min 2–35% B, 4.0–7.0 min 35–98% B, 7.0–8.0 min 98% B, 8.0–10.0 min 2% B. MS analysis was performed using full scan mode (switching polarity, full MS resolution 35,000, scan range 200–2,000; data-dependent MS/MS ($ddMS^2$) resolution 17,500, stepped collision energy with 17.5, 35, 52.5). Blank samples using DMSO were run in parallel for background subtraction. Sample processing for metabolite identification was performed usind Compound Discoverer 3.2 (Thermo Fisher, Dreieich, Germany). Metabolites were identified based on mass shifts and feasibility of the metabolic reaction also in view of MS peak intensities over time.

3.5.9 Zebrafish handling

Handling of adult zebrafish and experiments with zebrafish embryos were performed in accordance to the EU directive 2010/63/EU and the German Animal Welfare Act (§11 Abs. 1 TierSchG). An automatic aquatic eco-system (PENTAIR, Apoka, UK) was used for zebrafish housing. Adult zebrafish were mated pairwise in our zebrafish facility after one night in the mating cages (light/dark cycle: 14 h/10 h). The eggs were collected after 2 h mating and placed in a petri dish with fish water (pH 7.36 ± 0.08, conductivity: 800 ± 50 µs). The eggs were washed with 0.3x Danieau´s medium (17 mM NaCl, 0.2 mM KCl, 0.12 mM $MgSO_4$, 0.18 mM $Ca(NO_3)_2$, 1.5 mM HEPES, pH 7.1–7.3, and 1.2 µM methylene blue). 300 eggs were placed per petri dish and stored in the incubator at 28 °C overnight. 24 h post mating, the unfertilized eggs were

discarded. The 0.3x Danieau´s media in the petri dishes was replaced every 24 h and embryos with developmental issues were euthanized using ice water. Embryo-/genotoxicity, cardiotoxicity and hepatotoxicity were tested using zebrafish embryos younger than 120 hours post-fertilization (hpf). The wild-type AB line was used for embryo-/genotoxicity and cardiotoxicity, and the transgenic line Tg(fabp10a:DsRed; elaA:EGFP) was used for hepatotoxic evaluation. Embryos were treated with phenylthiourea (PTU) starting from 1 day post fertilization (dpf) for hepato- and cardiotoxicity analysis. Previous to compound addition, embryos were dechorionated using pronase (1 mg/mL) and washed several times. The embryos were euthanized on ice after maximum 120 hpf and frozen at -20 °C.

3.5.10 Maximum tolerated concentration (MTC)

Zebrafish embryos (AB line) were dechorionated with pronase at 1 dpf. For embryo-/genotoxicity testing, 20 embryos per condition were treated with 20 µM CN-861-2, CN-DM-861 (solubility limit) and 200 µM (solubility limit), 100 µM, 50 µM and 20 µM Cysto-180 from 1 dpf till 5 dpf. DMSO (0.2 %) was used as negative control and 3,4-dichloroaniline (16 µg/mL) as positive control. For acute *in vivo* toxicity testing, embryos were treated from 4 to 5 dpf accordingly with maximal soluble concentrations of CYS and DMSO (0.2 %) and 3,4-dichloroaniline (32 and 64 µg/mL) as negative and positive controls, respectively. Kaplan-Meier curves were generated using GraphPad Prism (version 10.0.3, GraphPad, Boston, MA, USA). Dead embryos were defined when no heart beat was observable.

3.5.11 *In vivo* cardiotoxicity in zebrafish embryos

Embryos were prepared as described above. At 2 dpf, the embryos were placed in 6 well plates with 10 embryos per well. Embryos were treated with CYS (20 µM) and the

positive control terfenadin (10, 20 µM) in Danieau´s media. Danieau´s with DMSO was used as negative control. At least 20 embryos were tested per condition. Embryos were incubated at 28 °C for 24 h. Afterwards, embryos were anesthetized with tricaine added to the media (40 µg/mL, 0.004 % (*w/v*)) and videos were recorded using a stereomicroscope (1.25x magnification) (Stemi 508, Zeiss) with Media Recorder (version 4.0) und analyzed via DanioScope software (version 1.2.208, Noldus). The embryos were checked with attention to specific cardiotoxic phenotypes defined as decreased heartrate, arrhythmia and pericardial edema. Death was defined as absence of heartbeat. Data presentation was done using GraphPad Prism (version 10.0.3) with ordinary one-way ANOVA including multiple comparison to the control group and multiple unpaired t-test for statistical analysis.

3.5.12 *In vivo* hepatotoxicity in zebrafish embryos

Zebrafish embryos [Tg(fabp10a:DsRed; elaA:EGFP)] were prepared as described above. Embryos were placed in 6 well plates with 10 embryos per well. Treatment with CYS as well as the positive control valproic acid (20, 40 µg/mL) was done by soaking from 3 to 5 dpf in 0.3x Danieau´s media. Per condition, at least 15 embryos were treated. Danieau´s media with DMSO was used as negative control. The embryos were incubated at 28 °C. After 48 h treatment, the embryos were checked via a fluorescence stereomicroscope (M205 FA, Leica) with attention to liver degeneration. Fluorescence images were taken after anesthetizing the embryos with tricaine (40 µg/mL) and placing them laterally (excitation: 558 nm, emission 583 nm, 35x magnification). The specific phenotypic hepatotoxic endpoint was liver degeneration defined as liver size reduction. The liver size was calculated using ImageJ software (format: 8 bit, threshold: 40-255, binary, particle size: 10.0-infinite). The liver size of the control embryos was set to 100%. The relative liver sizes of treated embryos were

calculated accordingly and normalized to the control group. Data presentation was done using GraphPad Prism (version 10.0.3) with ordinary one-way ANOVA including multiple comparison to the control group for statistical analysis.

3.5.13 Affinity-based protein profiling (AfBPP) sample preparation

Cells were seeded in 100 mm cell-bind petri dishes with a concentration of 2.8 x 10^6 cells per sample and incubated (37 °C, 5 % CO_2) for 3 days to reach ~80 % confluence. Cells were washed with warm PBS prior to compound addition. Affinity based proteome profiling was performed by treating the respective cell line with Cysto-354 (2.5 µM) for 3 h. For competition samples, cells were treated with CN-861-2 (12.5 µM) for 1h, prior to addition of photo-probe Cysto-354 (2.5 µM) for 3 h incubation time. Control samples were treated with DMSO. Afterwards, cells were UV-irradiated for 10 minutes on ice, scraped off and transferred to Eppendorf tubes for washing with 1 mL cold PBS (centrifuge 5 min, 500xg, 4 °C). The cell pellet was stored at -80 °C until lysis. Further sample preparation was done as previously described.[132] Briefly, the cell pellet was lysed in 0.4 % SDS in PBS by sonication (Bandelin Sonoplus). After proteome adjustment (1000 µg/sample), azide-alkyne cycloaddition of labeled proteins with biotin was performed. Subsequently, the proteome was precipitated and washed with acetone and methanol, followed by avidin-bead enrichment. Afterwards, samples were digested (trypsin platinum, Promega), desalted and dried in a speedVac, before solving the samples in 1 % FA. Samples were filter (Merck Millipore, UFC30GV0S) and transferred to HPLC autosampler vials (QuanRecovery, Waters).

3.5.14 LC-MS measurement of HepG2 proteome

Peptides were measured and online-separated using an UltiMate 3000 nano HPLC system (*Dionex*) coupled to a *Bruker* timsTOF Pro mass spectrometer via a

CaptiveSpray nano-electrospray ion source and *Sonation* column oven. Peptides were first loaded on the trap column (Acclaim PepMap 100 C18, 75 µm ID x 2 cm, 3 µm particle size, *Thermo Scientific*), washed with 0.1 % formic acid in water for 7 min at 5 µL/min and subsequently transferred to the separation column (*IonOpticks* Aurora C18 column, 25 cm × 75 µm, 1.7 µm) and separated over a 60 min gradient from 5 % to 28 % B, then to 40 % B over 13 min, followed by 10 min at 95 % before re-equilibration and at a flow rate of 400 nL/min. The mobile phases A and B were 0.1 % (v/v) formic acid in water and 0.1 % (v/v) formic acid in acetonitrile, respectively. The timsTOF Pro was operated in data-dependent PASEF mode with the dual TIMS analyzer operating at equal accumulation and ramp times of 100 ms each with a set $1/K_0$ ion mobility range from 0.85 to 1.40 V × s × cm^{-2}. The capillary voltage of the CaptiveSpray source was set to 1500 V. 10 PASEF scans per topN acquisition cycle were performed, resulting in a total cycle time of 1.17 s. The mass range was set from 100 to 1700 m/z. Only Precursors reaching an intensity threshold of 1750 arbitrary units were considered for fragmentation, precursors reaching a target intensity of 14500 arbitrary units were dynamically excluded for 0.4 min. The quadrupole isolation width was set to 2 *m/z* for *m/z* < 700 and to 3 *m/z* for *m/z* > 800. The collision energy was ramped linearly as a function of the mobility from 59 eV at $1/K_0$ = 1.6 V × s × cm^{-2} to 20 eV at $1/K_0$ = 0.6 V × s × cm^{-2}. TIMS elution voltages were calibrated linearly to obtain the reduced ion mobility coefficients ($1/K_0$) using three Agilent ESI-L Tuning Mix ions (*m/z* 622, 922 and 1,222) spiked on the CaptiveSpray Source inlet filter.

MS raw data was analyzed using MaxQuant software (version 2.0.3.0) and peptides were searched against Uniprot database for Homo sapiens (taxon identifier: 9606, downloaded on 11.03.2022, canonical, reviewed). Carbamidomethylation of cysteine was set as fixed modification and oxidation of methionine and acetylation of *N*-termini

were set as variable modifications. Trypsin was set as proteolytic enzyme with a maximum of 2 missed cleavages. For main search, precursor mass tolerance was set to 4.5 ppm and fragment mass tolerance to 0.5 Da. Label free quantification (LFQ) mode was activated with a LFQ minimum ratio count of 2. Second peptide identification was enabled, and false discovery rate (FDR) determination carried out by applying a decoy database and thresholds were set to 1 % FDR at peptide-spectrum match and at protein levels and “match between runs” (0.7 min match and 20 min alignment time windows) option was enabled. Normalized LFQ intensities extracted from the MaxQuant result table proteinGroups.txt were further analyzed with Perseus software (version 2.03.1).

3.5.15 LC-MS measurement of HeLa-CCL-2 and HEK293 proteome

Sample analysis was done as previously described.[132] Samples have been analyzed using nanoElute nano flow liquid chromatography system (Bruker, Germany) coupled to a timsTOF Pro (Bruker, Germany). Loading of the samples to the trap column (Thermo Trap Cartridge 5 mm) was performed, followed by washing with 6 µL 0.1 % FA with a flow rate of 10 µL/min. Transferring of the peptide samples to the analytical column (Aurora Ultimate CSI 25 cm x 75 µm ID, 1.6 µm FSC C18, IonOpticks) was done, with subsequent separation by a gradient elution (eluent A: H2O + 0.1 % FA, B: ACN + 0.1 % FA; 0 % to 3 % in 1 min, 3 % to 17 % in 57 min, 17 % to 25 % in 21 min, 25 % to 34 % in 13 min, 34 % to 85 % in 1 min, 85 % kept for 8 min) using a flow rate of 400 nL/min. Captive Spray nanoESI source (Bruker, Germany) was applied for ionizing the peptides at 1.5 kV with 180 °C dry temperature at 3 L/min gas flow. timsTOF Pro (Bruker, Germany) was operated using default dia-PASEF long gradient mode with TIMS set to 1/K0 start at 0.6 Vs/cm^2, end at 1.6 Vs/cm^2, with a ramp and accumulation time of 100 ms each and a ramp rate of 9.43 Hz. Mass range was set

from 100.0 Da to 1700 Da with positive ion polarity. Dia-PASEF mass range was arranged to 400.0 Da to 1201.0 Da with a mobility range of 0.60 1/K0 to 1.43 1/K0 and a cycle time of 1.80 s. Collision energy for 0.60 1/K0 was fixed to 20.00 eV and ramped for 1.6 1/K0 to 59.00 eV. Tuning MIX ES-TOF (Agilent) was applied for calibration of *m/z* and mobility. Raw data were processed using DIA-NN (version 1.8.1), and proteins were identified against Uniprot Homo sapiens reference proteome (Proteome ID: UP000005640, downloaded 27/12/2023). Default settings were used, except precursor charge range was from 2 to 4. C-carbamidomethylation was set as fixed modification. To allow further data processing with Perseus Software, "--relaxed-prot-inf" was added in additional options. Further data analysis was performed in Perseus software (version 2.0.5.0), were the values were transformed to their log_2-value and the biological replicates were grouped. To allow the comparison of the whole datasets, missing values were imputed by default settings and the differential protein abundance between different treatment regimens were evaluated using two-tailed student's t-test. The cut-offs for $-log_{10}$ *P* was set to 1.3 ($P = 0.05$) and for t-test difference > 2. Proteins fitting these thresholds were seen as significantly enriched compared to the control only treated with DMSO. Significant competition was evaluated comparing CN-861-2 co-treated samples with Cysto-354-only treated samples.[132]

3.5.16 Surface plasmon resonance (SPR)

Binding analysis of CYS to SCARB1 was done by using SPR (Biacore X100, Cytiva). Therefore, biotinylated SCARB1 (Acrobiosystems) was immobilized on a SPR sensor chip SA (Cytiva) on flow cell (FC) 2. Afterwards, CYS (20 µM) were solved and centrifuged in running buffer. CYS were tested by interaction analysis over the reference FC1 and FC2, where SCARB1 has been immobilized. To conclude binding,

the subtraction of FC2-1 was analyzed. HBS-EP+ (Cytiva) with 1 % DMSO was used as running buffer.

3.5.17 HCVpp cell entry assay

Lentiviral pseudotypes were prepared by 293T transfection as described previously.[181] 293T cells were seeded in a density of $3x10^6$ cells in 10 cm plates and incubated at 37 °C and 5 % CO_2. After 24 hours, the cells were transfected with 2 µg of the lentiviral Gag-Pol expression construct pCMV-ΔR8.74[182], 2 µg of the reporter plasmid coding for a firefly luciferase (pWPI-F-Luc-BLR)[183,184] and 2 µg of either pcDNA3_CMV_dcE1E2_Con1, pcDNA3_CMV_dcE1E2_JFH[185] or pczVSV-G[186] coding for the glycoproteins of interest or 2 µg of the empty vector control (pcDNA3). For transfection, the plasmids were mixed in Opti-MEM containing a final concentration of 0.035 mg/ml polyethylenimine (PEI) and afterwards added to the cells. After overnight incubation, sodium butyrate was added at a final concentration of 10 mM. After 6 hours of incubation, a medium change was performed and after a subsequent overnight incubation, the pseudoparticle containing supernatant was harvested and cleared of cell debris by passing through 0.45 µm pore size filter and used for entry assay.

The evaluation of effect on entry by the compounds was performed on Huh-7.5 cells. Huh-7.5 cells were seeded in 96-well plates at a density of 7.2×10^3/well and incubated for 24 hours at 37 °C and 5 % CO_2. Compounds were diluted in six subsequent 3-fold dilutions with a final DMSO concentration of 1 % and freshly harvested pseudoparticles were added and transferred to the cells. After 72 hours of incubation, the cells were lysed with lysis buffer (1 % triton-X-100, 25 mM glycylglycine, 15 mM $MgSO_4$, 4 mM EGTA, 1 mM dithiothreitol) and frozen at -20°C. The luciferase activity measurements were performed by transferring 72 µL of assay buffer (25 mM

glycylglycine, 5 mM KPO_4, 50 mM $MgSO_4$, 10 mM EGTA, 2 % ATP, 1 mM dithiotreitol) to a white 96-well plate and adding 20 µL of the cell-lysis suspension with subsequent adding of 40 µL D-Luciferin and immediate measuring using the Berthold LB960 Centro XS3 plate luminometer.

3.5.18 Molecular Docking

For molecular docking, the AlphaFold structure (AF-Q8WTV0-F1) of scavenger receptor class B member 1 was downloaded as a PDB file and loaded into MOE (version 2022.02). Structural issues were corrected using the “Structure Preparation” tool and the protein was protonated using “Protonate3D” with a set pH to 7.4. The structure was energy minimized before screening for a potential binding site with “Site Finder”. Atom dummies were loaded in the potential binding site. CYS derivatives Cysto-180, CN-861-2 and CN-DM-861 were prepared (protonated, energy minimized) in MOE and loaded into a compound database as a .mdb file. This .mdb file was used for docking the compounds to the previous prepared SCARB1 structure. Dummy atoms were selected as target site with triangle matcher (score: London dG) as placement method and induced fit (score: GBVI/WSA dG) for refinement. Potential poses were browsed and optimized via protonation and energy minimization.

3.6 DATA AVAILABILITY

Datasets and further information of current and ongoing related studies are available upon request from the corresponding author. The mass spectrometry proteomics data have been deposited to the ProteomeXchange Consortium via the PRIDE partner repository with the data set identifiers PXD053711 (HepG2) and PXD052895 (HEK293, HeLa).

Reviewers access details (HepG2):

Project accession: PXD053711

Token: KfP437WEj9a6

Username: reviewer_pxd053711@ebi.ac.uk

Password: zFzWzExpYFTk

Reviewers access details (HEK293 and HeLa):

Project accession: PXD052895

Token: nyCCMJvkf4bK

Username: reviewer_pxd052895@ebi.ac.uk

Password: IrKDq3L4vxby

3.7 ACKNOWLEDGEMENTS

This study was funded by the German Federal Ministry of Education and Research (OpCyBac-project grant number: 16GW0219K). The funder played no role in study design, data collection, analysis and interpretation of data, or writing of this manuscript.

3.8 DECLARATION OF GENERATIVE AI AND AI-ASSISTED TECHNOLOGIES

During the preparation of this work, the author(s) used ChatGPT (GPT-4) in order to polish the phrasing of some passages. After using this tool, the author(s) reviewed and edited the content as needed and take(s) full responsibility for the content of the publication.

3.9 AUTHOR CONTRIBUTIONS

TR designed, performed and analyzed the majority of mentioned experiments and wrote the manuscript. DH, TS, DS, DK synthesized and provided the cystobactamid derivatives. AMK performed and analyzed the *in vitro* pharmacokinetic experiments. JHo supported the seahorse assay. JSH and DM supported proteomic sample preparation and data analysis. BH performed and analyzed the HCVpp assay and cytotoxicity testing on Huh-7.5 cells. FF supported the topoisomerase assays and helped writing the manuscript. JH, RM, MB, AK, AKK, TP and SS provided supervision and funding. TR, JH and RM designed the project. All authors were involved in reviewing and editing the manuscript and approved the final version.

3.10 COMPETING INTERESTS

All authors declare no financial or non-financial competing interests.

3.11 SUPPLEMENTARY INFORMATION CHAPTER 2

Synthesis and NMR spectra for Cysto-354 (Figures S2.7-S2.27) are not included in the SI shown here and can be found online.

3.11.1 Synthesis of CN-861-2, CN-DM-861 and Cysto-180

CN-861-2 was synthesized according to published literature.[93,94]

HRMS (ESI) calculated 842.2780 [M+H$^+$], 842.2759 found.

Purity (LC-MS): 99%.

CN-DM-861 was synthesized according to published literature.[93,94]

HRMS (ESI) calculated 812.2675 [M+H$^+$], 812.2675 found.

Purity (LC-MS): 99%.

Cysto-180 was synthesized according to published literature.[132]

HRMS (ESI) calculated 797.2930 [M+H$^+$], 797.2935 found.

Purity (LC-MS): 99%.

3.11.2 Micronucleus test

The micronucleus test was performed like described in the methods section. Pictures displayed are exemplary for all wells imaged and examined.

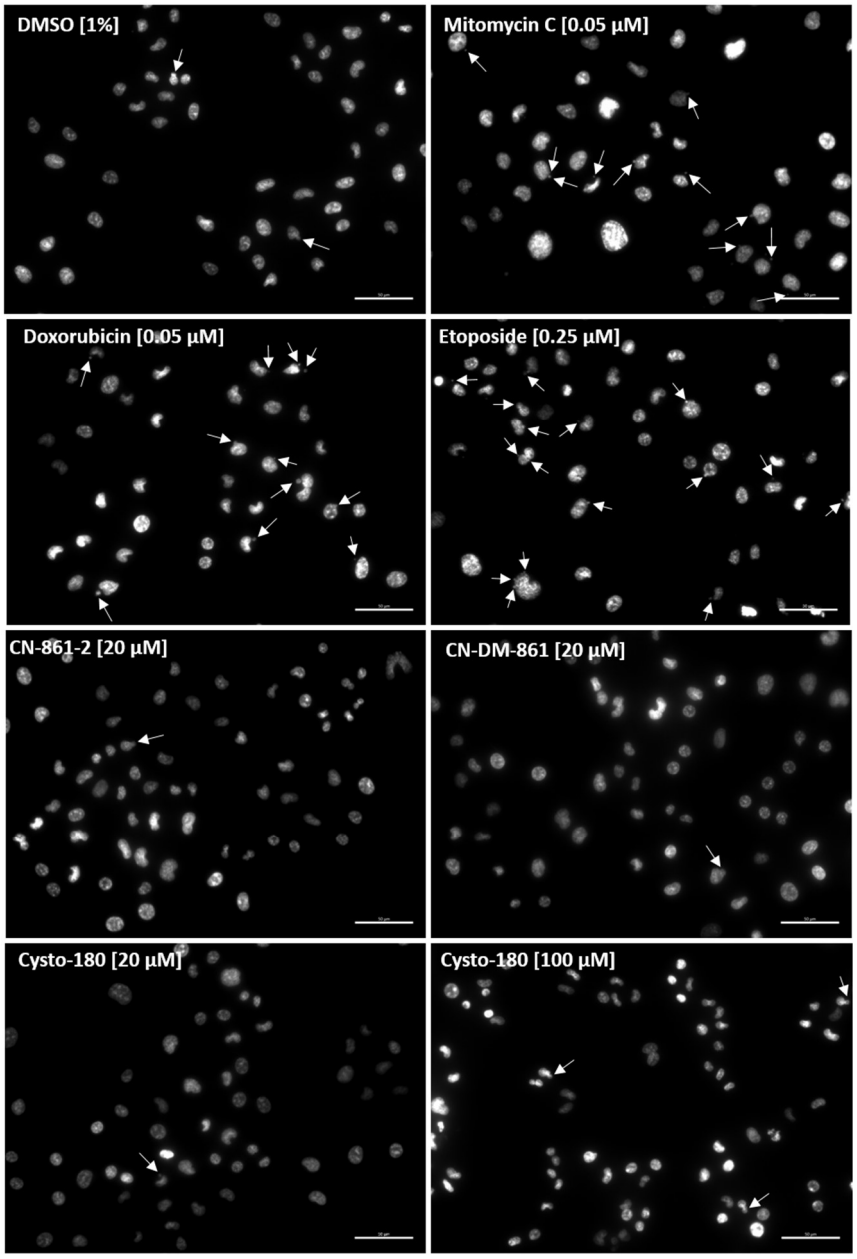

Figure S2.1 (Related to Figure 2.1). Genotoxic evaluation showed extensive micronucleus formation for the positive controls mitomycin C, doxorubicin and etoposide as clastogenic and aneugenic agents. CYS showed micronucleus formation comparable to the DMSO control. (Nuclei colored in white, white arrows indicating micronucleus formation, scale bar is set to 50 µm) (*n* = 3).

3.11.3 *In vitro* drug metabolism and pharmacokinetics (DMPK)

Table S2.1. *In vitro* metabolism studies of CYS derivatives including mouse liver microsomal (MLM), murine S9 fraction, mouse hepatocyte and plasma stability testing as well as plasma protein binding (PPB). ($n \geq 2$)

Code	MLM $t_{1/2}$ [min] / Cl_{int} [µl/mg/min] / % remaining at 2 h	Mouse Hepatocytes $t_{1/2}$ [min] / Cl_{int} [µl/mg/10^6 cells]	Mouse Plasma $t_{1/2}$ [min]	Mouse PPB [%]
CN-861-2	**>120 / <11.6 / 59 ± 11**	**>180 / <5.1**	**>240**	**99.63 ± 0.16**
CN-DM-861	**89.0 ± 1.3 / 15.6 ± 0.2**	**94 ± 15 / 10 ± 2**	**>240**	**99.85 ± 0.08**
Cysto-180	**>120 / <11.6 / 81 ± 10**	**41 ± 16 / 26 ± 12**	**>240**	**95.9 ± 2.4**

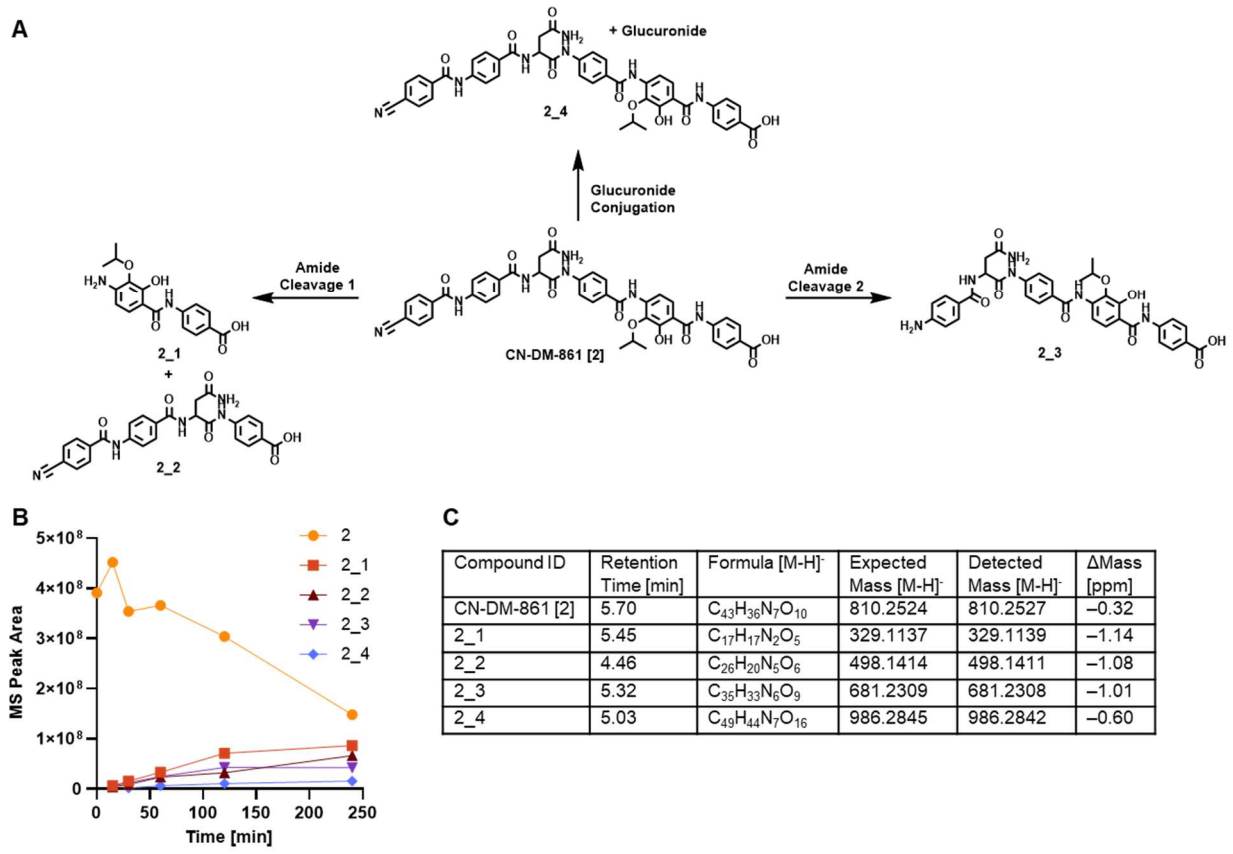

Compound ID	Retention Time [min]	Formula $[M-H]^-$	Expected Mass $[M-H]^-$	Detected Mass $[M-H]^-$	ΔMass [ppm]
CN-DM-861 [2]	5.70	$C_{43}H_{36}N_7O_{10}$	810.2524	810.2527	–0.32
2_1	5.45	$C_{17}H_{17}N_2O_5$	329.1137	329.1139	–1.14
2_2	4.46	$C_{26}H_{20}N_5O_6$	498.1414	498.1411	–1.08
2_3	5.32	$C_{35}H_{33}N_6O_9$	681.2309	681.2308	–1.01
2_4	5.03	$C_{49}H_{44}N_7O_{16}$	986.2845	986.2842	–0.60

Figure S2.2. Metabolite identification (MetID) of CN-DM-861. (**A**) MetID of CN-DM-861 showed amide bond hydrolysis and glucuronidation as main metabolic degradation pathways in mouse hepatocytes. (**B**) Time-dependent analysis of mass signals for the respective compounds showed a correlation between parent compound degradation and increase of identified metabolites, where amide cleavage between rings C and D seemed to be the most prominent path. The exact position of the glucuronidation could not be clearly identified between the hydroxy and the carboxy group. (**C**) Corresponding chromatographic and MS data of identified metabolites. (See also Figure S2.3)

2

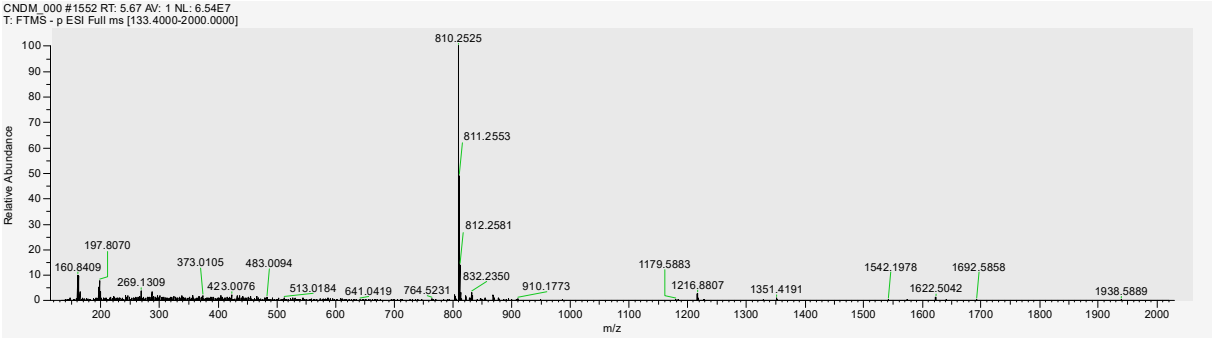
CNDM_000 #1552 RT: 5.67 AV: 1 NL: 6.54E7
T: FTMS - p ESI Full ms [133.4000-2000.0000]
Relative Abundance
m/z
810.2525
811.2553
812.2581
197.8070
160.8409
373.0105
483.0094
269.1309
423.0076
513.0184
641.0419
764.5231
832.2350
910.1773
1179.5883
1216.8807
1351.4191
1542.1978
1692.5858
1622.5042
1938.5889

2_1

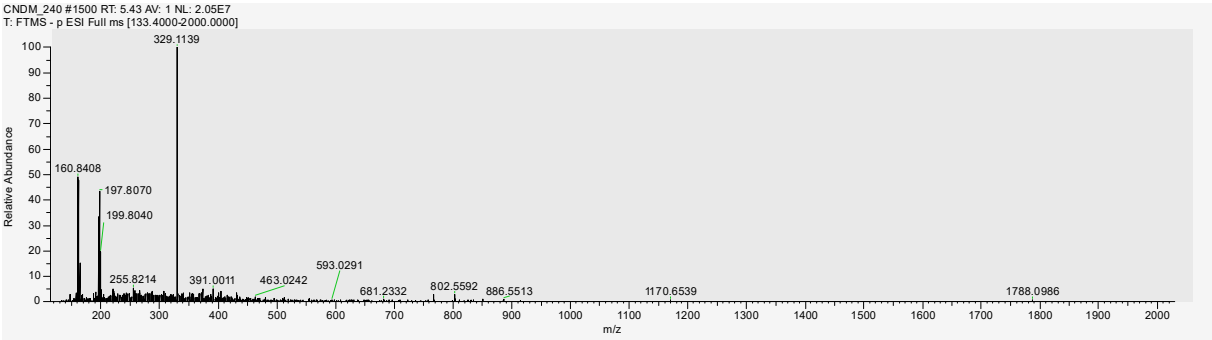
CNDM_240 #1500 RT: 5.43 AV: 1 NL: 2.05E7
T: FTMS - p ESI Full ms [133.4000-2000.0000]
Relative Abundance
m/z
329.1139
160.8408
197.8070
199.8040
255.8214
391.0011
463.0242
593.0291
681.2332
802.5592
886.5513
1170.6539
1788.0986

2_2

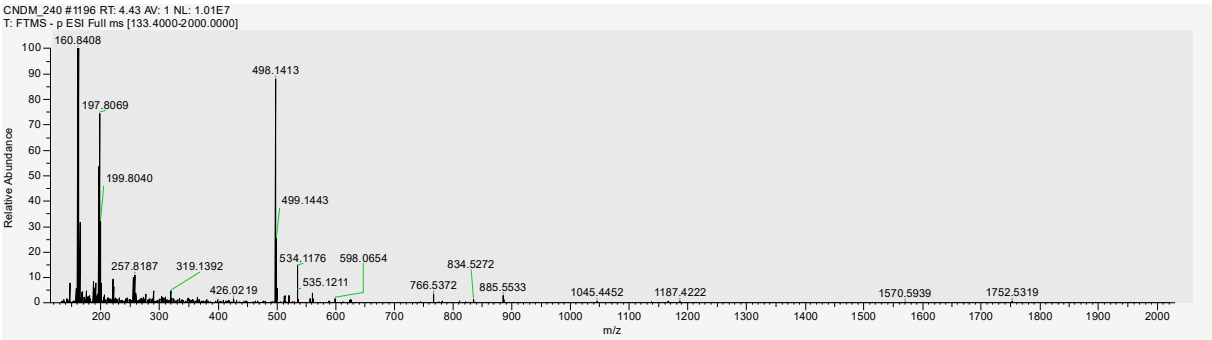
CNDM_240 #1196 RT: 4.43 AV: 1 NL: 1.01E7
T: FTMS - p ESI Full ms [133.4000-2000.0000]
Relative Abundance
m/z
160.8408
498.1413
197.8069
199.8040
499.1443
534.1176
598.0654
257.8187
319.1392
426.0219
535.1211
766.5372
834.5272
885.5533
1045.4452
1187.4222
1570.5939
1752.5319

2_3

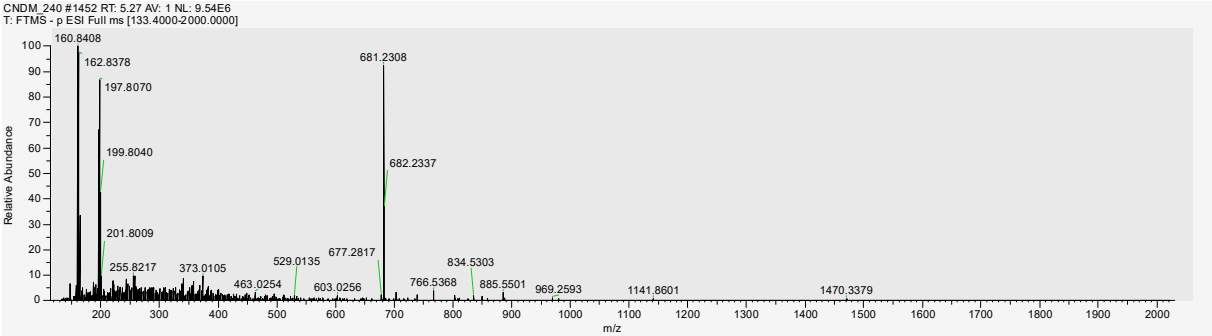

2_4

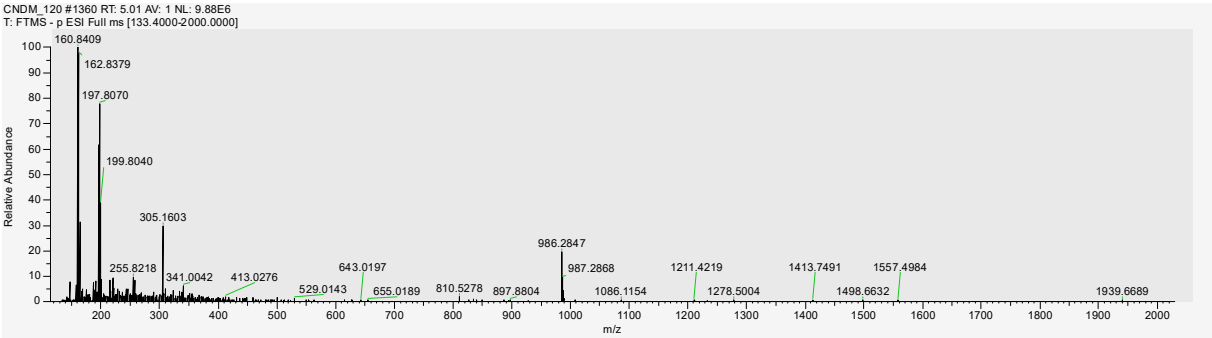

Figure S2.3. MS1 spectra of CN-DM-861 and metabolites given in Figure S2.2.

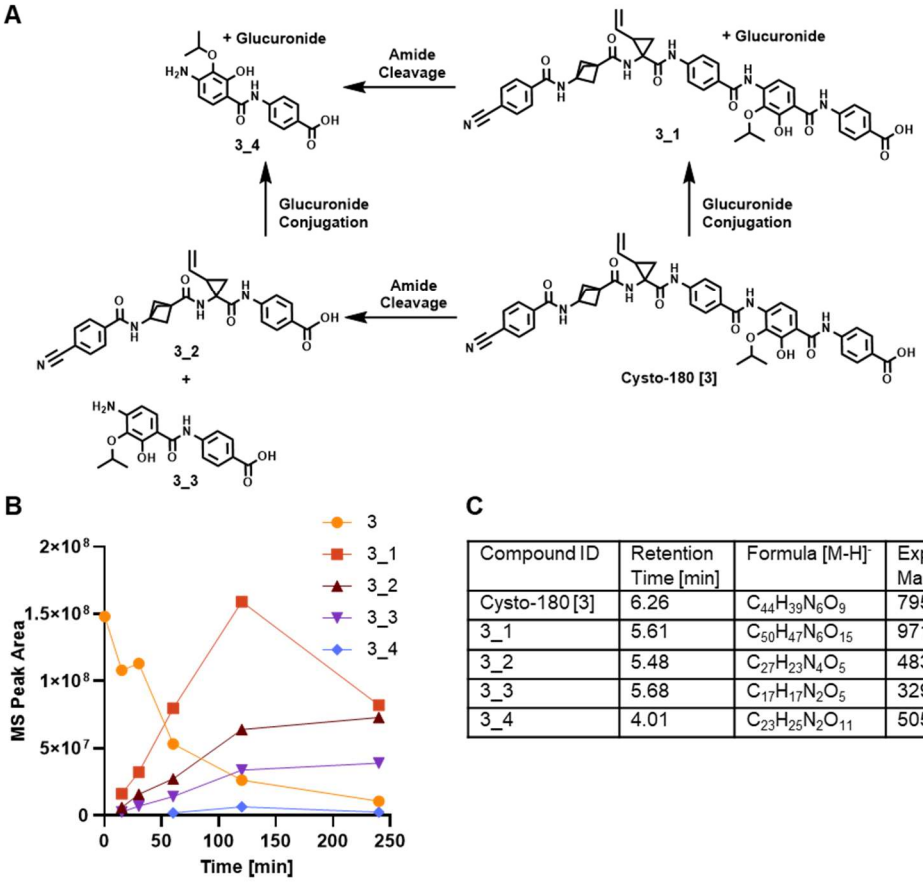

Compound ID	Retention Time [min]	Formula $[M-H]^-$	Expected Mass $[M-H]^-$	Detected Mass $[M-H]^-$	ΔMass [ppm]
Cysto-180 [3]	6.26	$C_{44}H_{39}N_6O_9$	795.2779	795.2786	0.88
3_1	5.61	$C_{50}H_{47}N_6O_{15}$	971.3099	971.3105	0.62
3_2	5.48	$C_{27}H_{23}N_4O_5$	483.1668	483.1673	1.03
3_3	5.68	$C_{17}H_{17}N_2O_5$	329.1137	329.1140	0.91
3_4	4.01	$C_{23}H_{25}N_2O_{11}$	505.1458	505.1460	0.40

Figure S2.4. MetID of Cysto-180. (**A**) MetID of Cysto-180 showed glucuronidation and amide bond hydrolysis as main metabolic degradation pathways in mouse hepatocytes. (**B**) Time-dependent analysis of mass signals for the respective compounds showed a correlation between parent compound degradation and increase of identified metabolites, where glucuronidation as well as amide cleavage between rings C and D of the parent compound seemed to be the most prominent paths. The exact position of the glucuronidation could not be clearly identified between the hydroxy and the carboxy group. (**C**) Corresponding chromatographic and MS data of identified metabolites. (See also Figure S2.5)

3

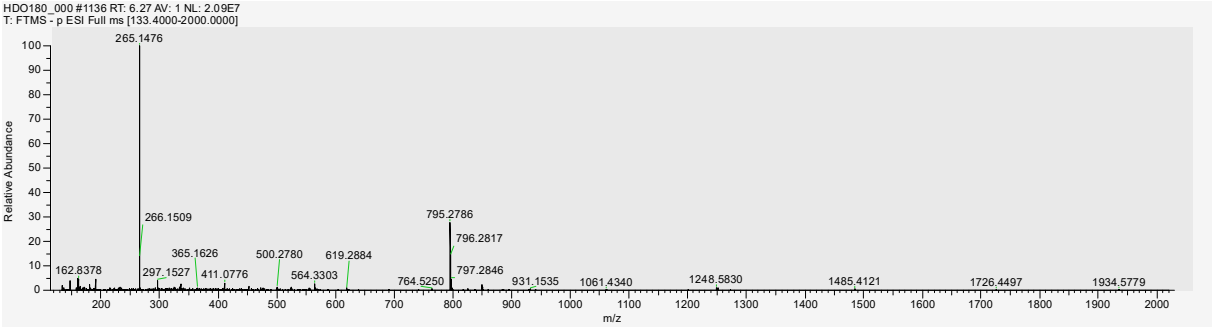
HDO180_000 #1136 RT: 6.27 AV: 1 NL: 2.09E7
T: FTMS - p ESI Full ms [133.4000-2000.0000]
Relative Abundance
m/z
265.1476
266.1509
795.2786
796.2817
797.2846
365.1626
500.2780
619.2884
162.8378
297.1527
411.0776
564.3303
764.5250
931.1535
1061.4340
1248.5830
1485.4121
1726.4497
1934.5779

3_1

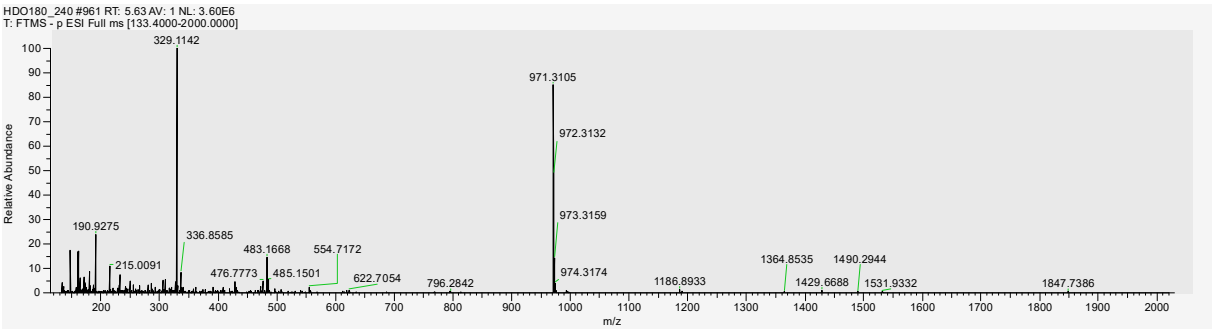
HDO180_240 #961 RT: 5.63 AV: 1 NL: 3.60E6
T: FTMS - p ESI Full ms [133.4000-2000.0000]
Relative Abundance
m/z
329.1142
971.3105
972.3132
973.3159
974.3174
190.9275
336.8585
483.1668
554.7172
215.0091
476.7773
485.1501
622.7054
796.2842
1186.8933
1364.8535
1490.2944
1429.6688
1531.9332
1847.7386

3_2

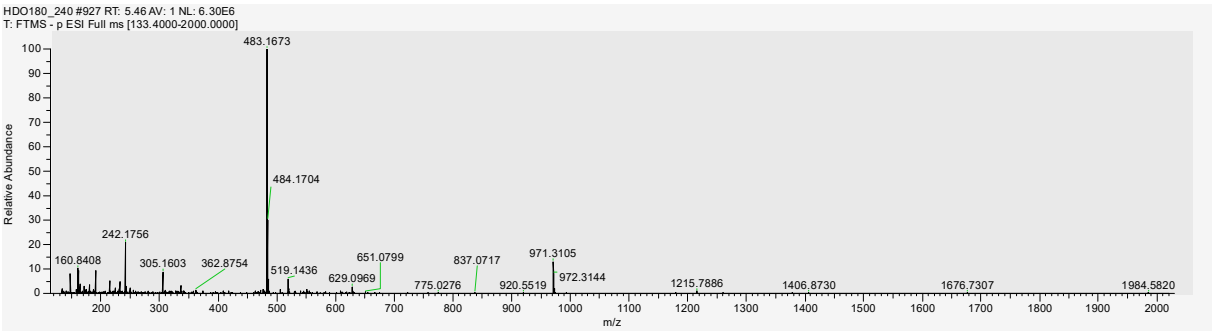
HDO180_240 #927 RT: 5.46 AV: 1 NL: 6.30E6
T: FTMS - p ESI Full ms [133.4000-2000.0000]
Relative Abundance
m/z
483.1673
484.1704
242.1756
160.8408
305.1603
362.8754
519.1436
651.0799
629.0969
837.0717
775.0276
971.3105
920.5519
972.3144
1215.7886
1406.8730
1676.7307
1984.5820

3_3

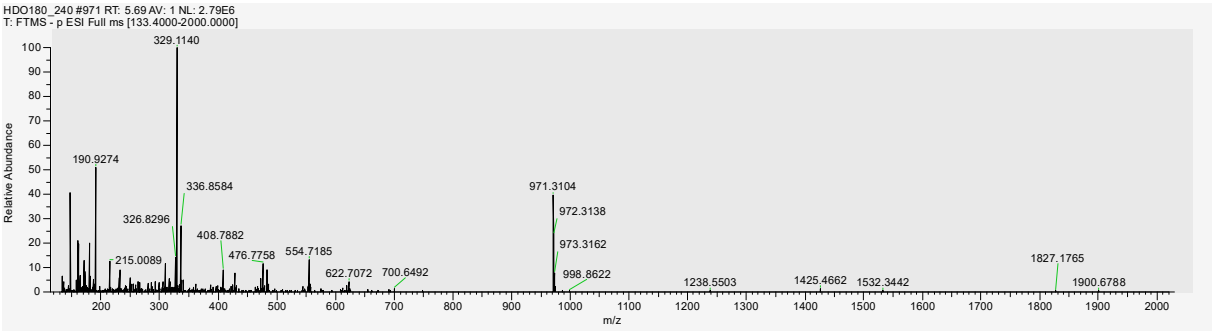
HDO180_240 #971 RT: 5.69 AV: 1 NL: 2.79E6
T: FTMS - p ESI Full ms [133.4000-2000.0000]
Relative Abundance
m/z
329.1140
190.9274
336.8584
971.3104
972.3138
326.8296
408.7882
973.3162
554.7185
476.7758
215.0089
622.7072
700.6492
998.8622
1238.5503
1425.4662
1532.3442
1827.1765
1900.6788

3_4

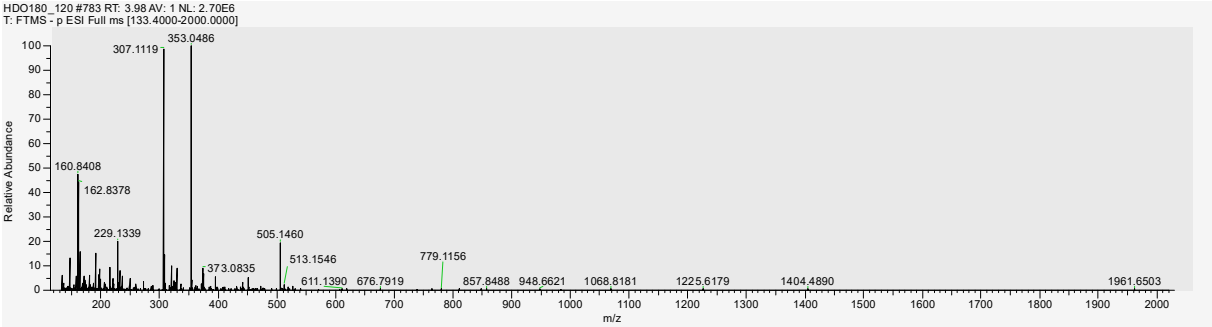

Figure S2.5. MS1 spectra of Cysto-180 and metabolites given in Figure S2.4.

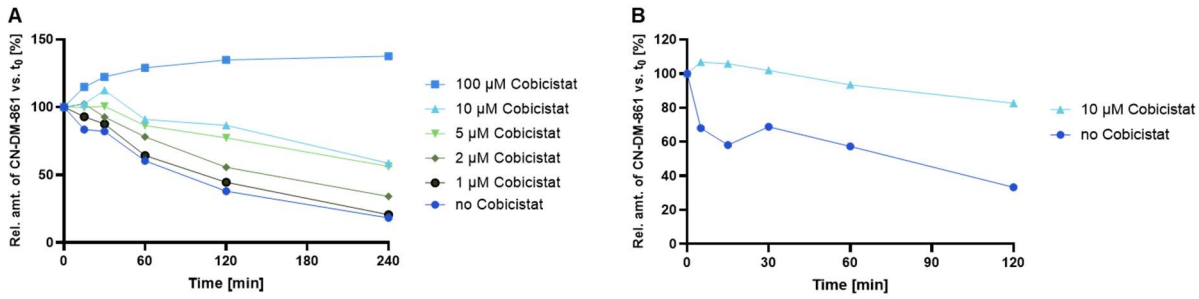

Figure S2.6. Concentration-dependent increase of metabolic stability of CN-DM-861 via cobicistat co-treatment. (**A**) CN-DM-861 incubated with mouse hepatocytes in presence of cobicistat indicates stabilization due to OATP-inhibition. (**B**) In mouse liver microsomes, cobicistat shows a similar effect, showing a possible involvement of CYP3A inhibition.

3.11.4 Cytotoxic evaluation of Cysto-354

MTT assay was performed as described in the methods section. Cysto-354 showed slightly higher cytotoxic potential on tested cell lines than non-functionalized CYS derivatives (see also Figure 2.1C).

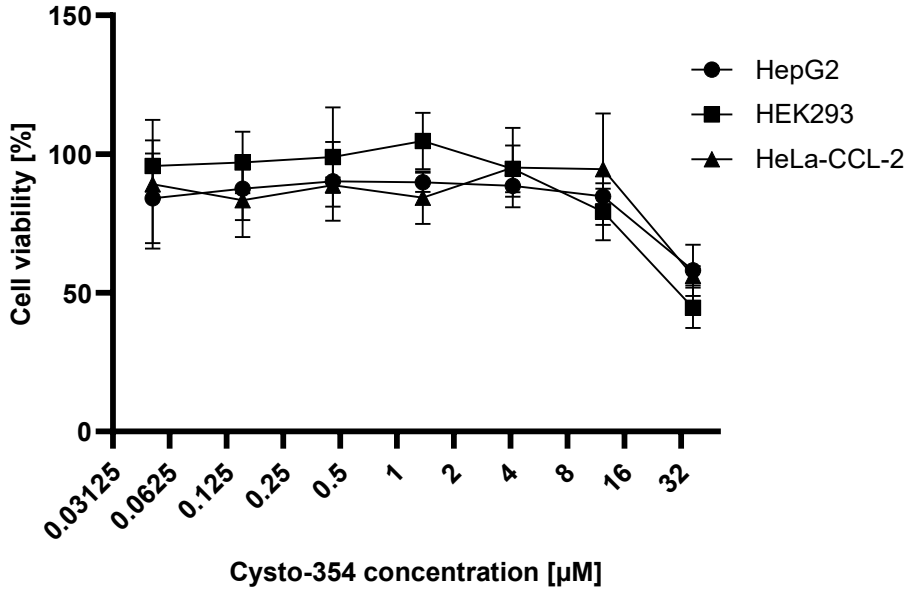

Figure S2.28. Cysto-354 showed reduction of cell viability at the highest tested concentration (37 µM). (*n* = 3)

3.11.5 No enrichment of human topoisomerases could be observed

Topoisomerase enrichment after Cysto-354 treatment was checked, since CYS inhibit bacterial type II DNA topoisomerases and human topoisomerase IIα (TOP2A) *in vitro*. No significant enrichment of TOP1, TOP2A nor TOP2B could be observed, indicating whole cell selectivity of CYS to bacterial topoisomerases.

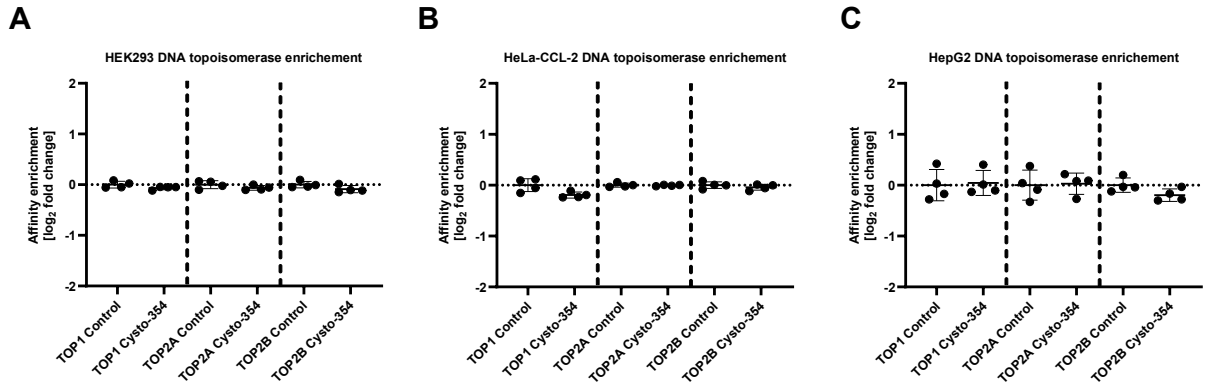

Figure S2.29 (Related to Figure 2.5). Human topoisomerase (TOP1, TOP2A and TOP2B) affinity enrichment. (**A**) AfBPP in HEK293 did not show significant enrichment of human topoisomerases. (**B**) AfBPP in HeLa-CCL-2 did not show significant enrichment of human topoisomerases. (**C**) AfBPP in HepG2 did not show significant enrichment of human topoisomerases. (*n* = 4)

3.11.6 VSVpp entry assay supported specificity of CYS for SCARB1 related HCVpp cell entry inhibition

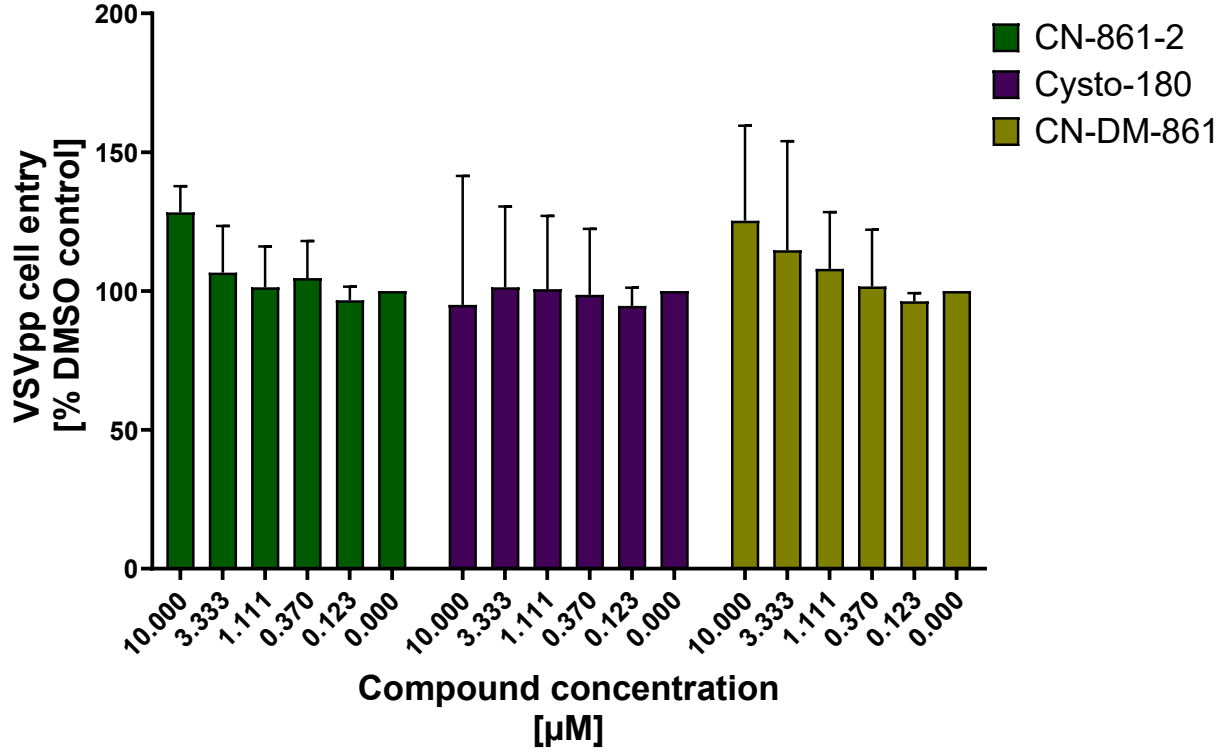

Figure S2.30 (Related to Figure 2.6). Lentivirus-pseudoparticle (pp) cell entry assay. CYS treatment did not demonstrate inhibitory activity on VSVpp cell entry. (*n* = 3)

3.11.7 Molecular docking of CYS to SCARB1

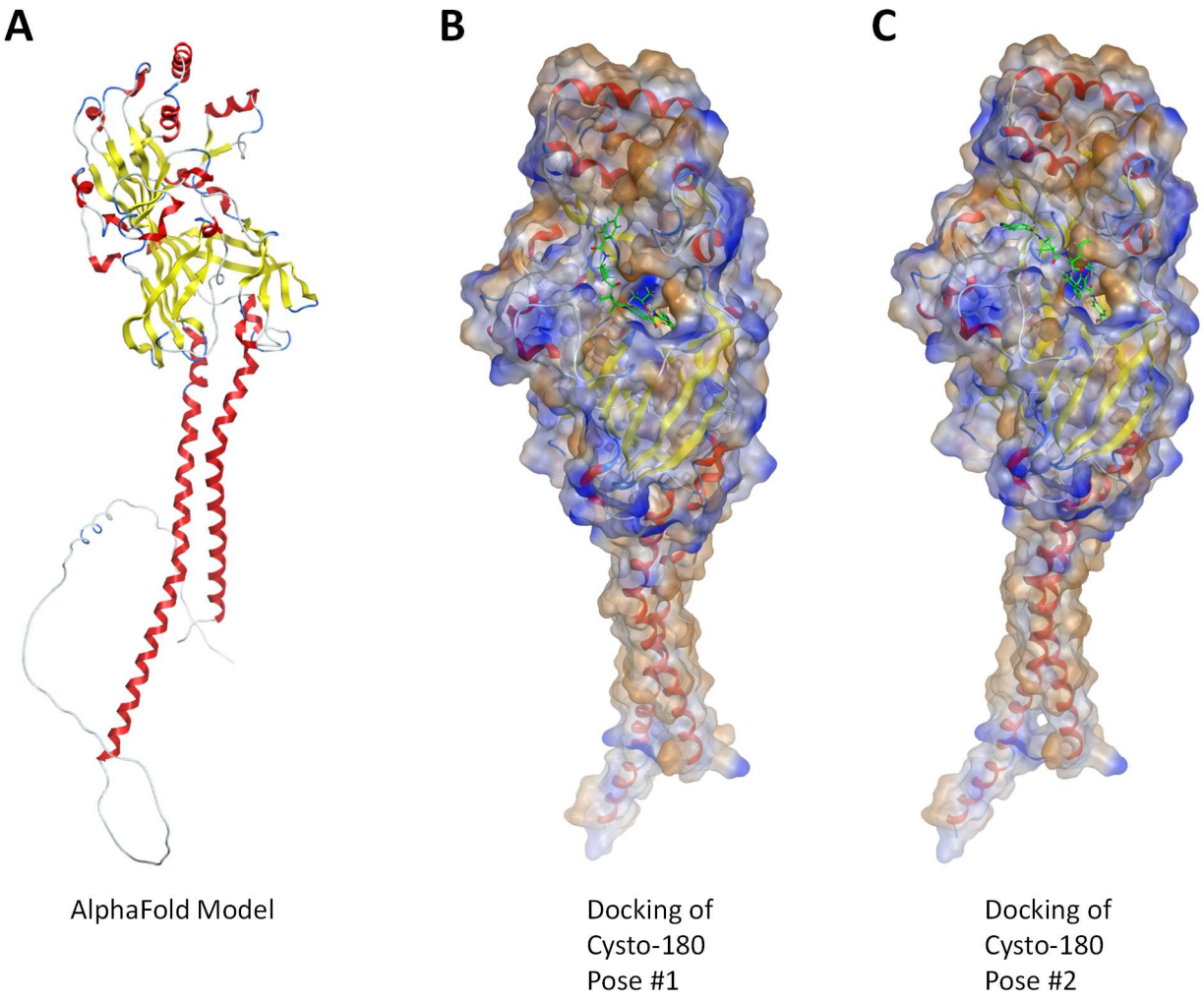

Figure S2.31. Molecular docking of CYS to the AlphaFold model of SCARB1. (**A**) AlphaFold model of SCARB1. (**B**) First pose of Cysto-180 molecular docking to SCARB1 model indicates a potential binding pocket in the head group of the protein. (**C**) Second pose of Cysto-180 shows that multiple poses of CYS inside the pocket seem to be possible.

4. General Discussion

4.1 SUMMARY OF THE RESULTS

In this study, we identified a previously uncharacterized mechanism of cystobactamid resistance in the high-priority pathogen *Escherichia coli*, which was linked to the overexpression of the YgiV protein. This overexpression was due to stable single-nucleotide mutations in the promoter region of the *ygiV* gene. Our results demonstrate that YgiV binds cystobactamids with nanomolar affinity, preventing their interaction with its antimicrobial targets, gyrase and topoisomerase IV. Furthermore, we found that YgiV itself exhibits DNA cleavage activity and directly inhibits the gyrase activity, potentially contributing to the observed resistance phenotype.

In addition, cystobactamid-resistant *E. coli* exhibited downregulation of virulence factors, fimbriae and flagellin. This effect is likely attributed to the observed mutations in the *ygiV* promoter, which also leads to the upregulation of *qseB*, a gene located in close genetic proximity to *ygiV* and known to influence the expression of fimbriae and flagella.[187] Using affinity-based protein profiling, we identified the efflux pump AcrB as a major off-target protein in bacteria. However, its overexpression resulted in only minor changes in cystobactamid antibiotic activity (**Figure GD.1**).

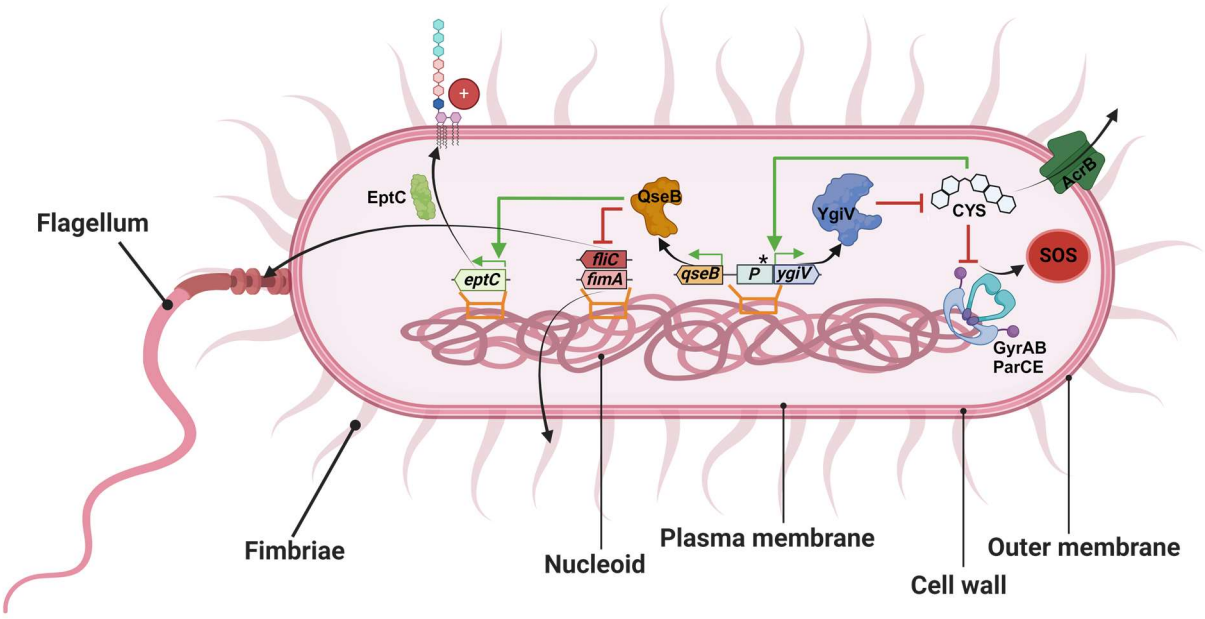

Figure GD.1. Scheme of physiological effects of *E. coli* resistance development against CYS. Briefly, promotor mutation (P*) of *ygiV* lead to induction (green arrows) of YgiV expression. YgiV inhibits (red inhibitor arrows) CYS from obstructing the topoisomerase (GyrAB/ParCE) activity, which in turn would lead to SOS response. CYS treatment amplifies the YgiV overexpression further, while CYS also undergoes efflux mediated by AcrB. Furthermore, the *ygiV* promotor mutation leads to QseB overexpression, which inhibits *fliC* (flagellum) and *fimA* (fimbriae) transcription and causes an induction of *eptC*. EptC overexpression results in addition of phosphoethanolamin to LPS, leading to a more positively charged outer membrane. (Created with BioRender.com)

In eukaryotic cells, the human lipoprotein, lipid and cholesterol receptor SCARB1 was identified as the major off-target protein of cystobactamids. This receptor is also known to facilitate the entry of hepatitis C lipoviral particles into hepatocytes. Therefore, its functional inhibition was confirmed by observed reduction of HCV particle cell entry upon cystobactamid treatment.

Toxicological investigations revealed a favorable safety profile of cystobactamids *in vitro*, with minimal to none cytotoxic, genotoxic, and mitotoxic effects, despite the observed inhibition of human topoisomerase and a slight uncoupling of the mitochondrial respiratory chain. Interestingly, this mitochondrial uncoupling might explain the discovered superoxide suppression properties of cystobactamids. Organotoxicity assessments in zebrafish embryos further supported the *in vivo* safety

of cystobactamids, demonstrating no significant developmental, cardiac, or liver toxicity.

Furthermore, we elucidated the metabolism of cystobactamids in mouse hepatocytes, involving glucuronic acid conjugation and amide bond hydrolysis. Metabolic stabilization was achieved by inhibiting OATP and CYP enzymes with cobicistat supplementation, thereby reducing the rate of metabolic degradation of cystobactamids (**Figure GD.2**).

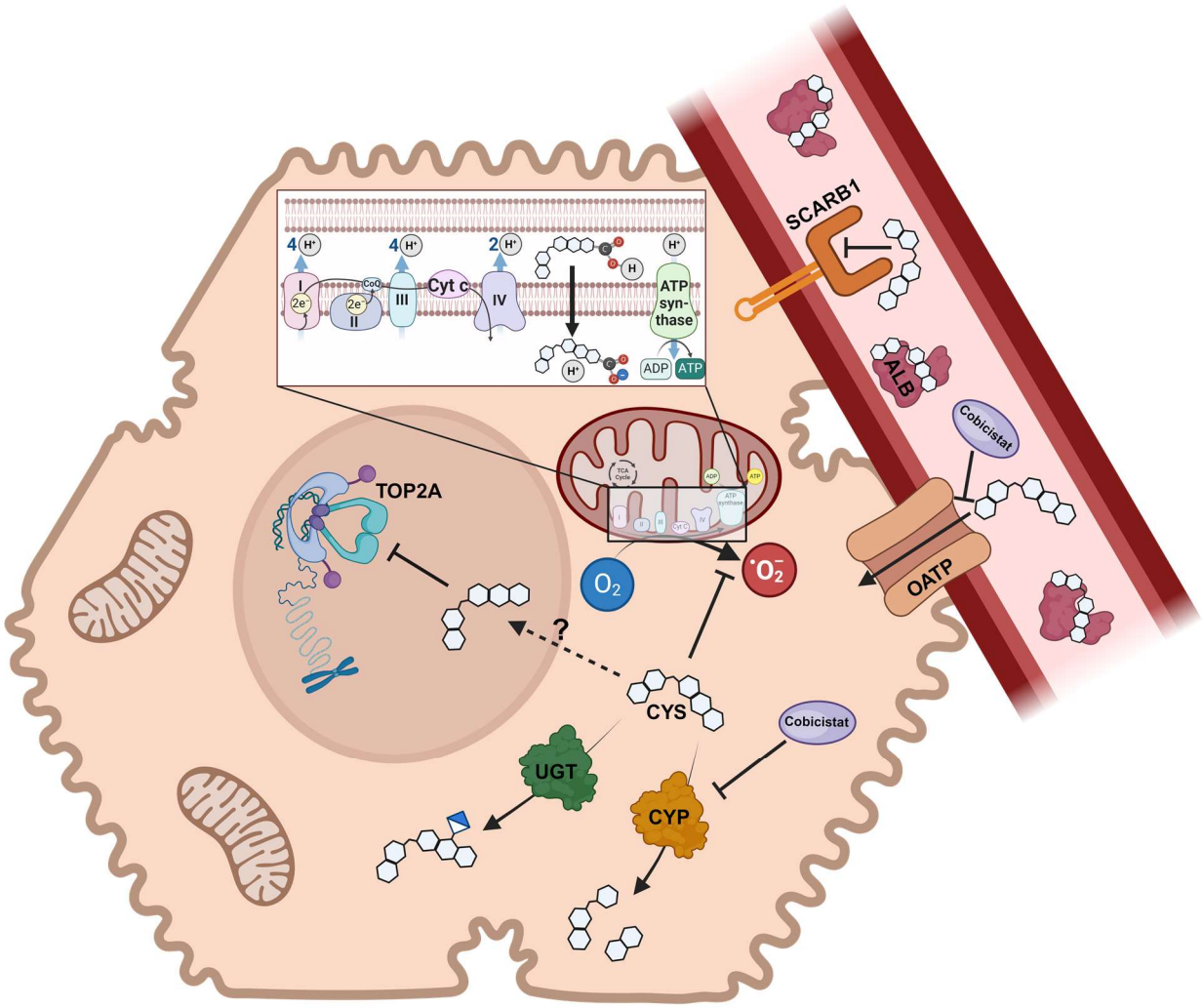

Figure GD.2. Scheme of pharmacological effects of CYS in eukaryotic cells. CYS exhibit plasma protein/albumin (ALB) binding in the bloodstream, where they inhibit SCARB1 on the extracellular receptor surface (inhibitor arrow). CYS are transported into hepatocytes via the organic anion transporter (OATP), which can be hindered by cobicistat. Within hepatocytes, CYS undergo biodegradation through glucuronic acid conjugation mediated by uridine 5'-diphospho-glucuronosyltransferase (UGT), and amid bond cleavage. Cobicistat inhibits the amide bond cleavage

of CYS by blocking cytochrome P450 (CYP) enzymes (esterase activity). CYS mildly uncouple the mitochondrial electron transfer chain and suppress oxidative cell stress ($O_2^{\cdot-}$). CYS inhibit the human topoisomerase activity (TOP2A), however, their ability to penetrate the nucleus in the cellular environment remains uncertain (dashed arrow with "?"). (Created with BioRender.com)

4.2 RESULTS IN THE CONTEXT OF ANTIMICROBIAL RESISTANCE AND THE CLINICAL APPLICATION OF ANTIBIOTICS

A recently published systematic analysis from 1990 to 2021 was looking at occurring bacterial antimicrobial resistance (AMR) with forecasts to 2050[13]. The study revealed 4.71 million estimated deaths associated or attributed to AMR in 2021. The authors suppose that these numbers will increase to estimated 10.13 million deaths in the year 2050 if no action will be taken to combat this global threat. They predict that 92.0 million deaths could be prevented between 2025 and 2050 by better access to antibiotics with 11.1 million deaths directly avertable by development of new drugs to primarily treat infections caused by often multidrug-resistant pathogens.[13] *Escherichia coli* as leading pathogen for resistance associated deaths was responsible for more than 800,000 deaths in 2019, followed by *Staphylococcus aureus*, *Klebsiella pneumoniae, Streptococcus pneumoniae*, *Acinetobacter baumannii*, and *Pseudomonas aeruginosa*.[10] *E. coli* shows a great ability to develop multi-drug resistance by accumulating resistance genes. The spectrum of mechanisms contributing to antimicrobial resistance of *E. coli* already covers all clinically used antimicrobial agents including β-lactam antibiotics (i.e. via β-lactamases and carbapenemases), aminoglycosides (i.e. via 16S rRNA methylases), fluoroquinolones (i.e. via protective pentapeptides and target mutations) and even the last-resort antimicrobial class of polymyxins (via membrane modifying transferases).[108]

The current candidates in the antibiotics pipeline are insufficient to tackle the emergence of antimicrobial resistance, primarily due to a lack of innovation, as it largely relies on continuous development of existing compound classes already in clinical use. Development of a successful (reserve) antibiotic needs to consider the WHO-defined criteria for innovative antibiotics including the absence of cross-resistance, new mechanism of actions, and new structural classes.[75]

Cystobactamids have been shown to address these criteria comprehensively. Although cystobactamids inhibit topoisomerase IV and gyrase as antimicrobial targets, their molecular mode of action differs from the ones observed for quinolone antibiotics and the so called new bacterial topoisomerase inhibitors (NBTIs) like gepotidacin.[91,188] Quinolone antibiotics exert an antimicrobial effect by obstructing the gyrase-DNA cleavage complex by symmetrically intercalating between cleaved DNA fragments, thereby preventing the religation of the double-stand breaks in the DNA.[35,189] In contrast, cystobactamids and the structurally related albicidins have been found to act via a dual mode of action during the catalytic cycle of the gyrase. These compound classes have shown to require DNA-strand passaging for gyrase interaction. They bind asymmetrically, with their *N*-terminal region intercalating into the DNA and their *C*-terminal region in the α3/α3´ binding pocket, which opens during DNA passaging and cleavage at the DNA gate (**Figure GD.3**). This binding site is unique to these natural product classes and does not overlap with the binding sites of other known gyrase inhibitors.[91]

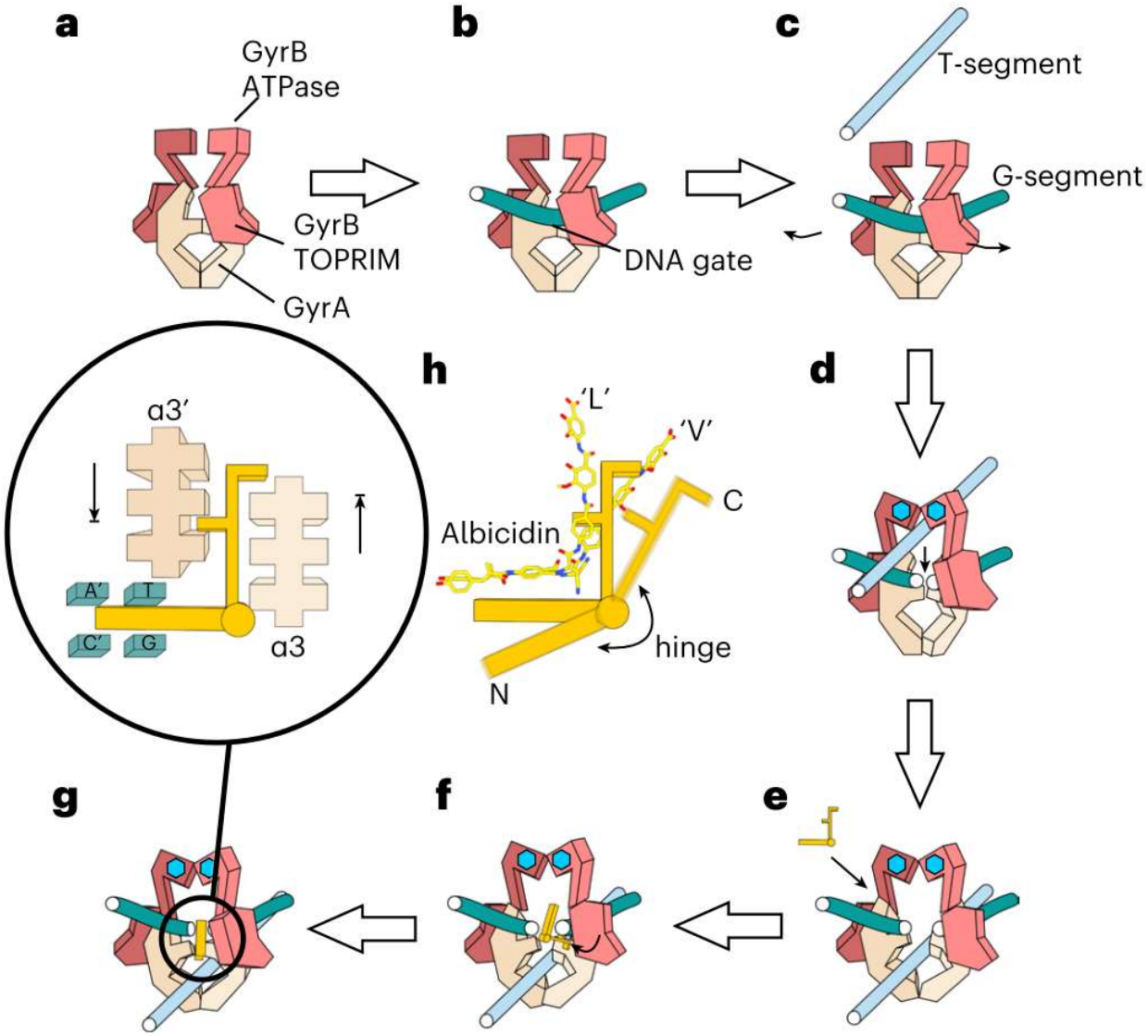

Figure GD.3 Mechanistic scheme of gyrase inhibition by albicidin (and cystobactamids). **a** Initial state, shown as apo-gyrase complex. **b** Binding of the G-segment DNA fragment. **c** Capture of the T-segment DNA by the ATPase domains of GyrB, followed by DNA cleavage. **d** ATP binding (blue hexagons) stimulates dimerization of the ATPase domains, driving the transport of the T-segment through the enzyme. **e** The T-segment is passed to the bottom chamber, where DNA religation is required to release the T-segment. Albicidin intercalates into DNA in the outer-rotated conformation (XT state). **f** Albicidin rotates and binds the pocket between two GyrA monomers. **g** Albicidin blocks the enzyme's movement, preventing progression to a productive state. **Inset** Enlarged diagram showing the albicidin–DNA–gyrase interaction in the locked state. **h** Diagram of the albicidin molecule, comprising rigid *N*- and *C*-terminal fragments connected by a flexible hinge. (Figure taken from *Michalczyk et al., Nature Catalysis, 2023)*[91]

This novel molecular mode of action and its untraditional structural composition contribute to the resistance breaking properties with no known pre-existing cross-resistances to quinolone antibiotics or other clinically used antimicrobial agents.[94]

Nevertheless, the clinical success of an antibiotic is strongly influenced by the rate of resistance development and the specific mechanism by which resistance arises. Thereby, the investigation of emerging resistances to cystobactamids is of utmost importance to conclude on the clinical potential of the class.[75] By doing so, we were able to identify and characterize a unique resistance-causing mechanism in the high priority pathogen *E. coli*, and thereby add a previously uncharacterized resistance mechanism to the repertoire of how this pathogen gains resistance to antimicrobial agents.[132] Furthermore, these results may provide insights for the potential future clinical application of cystobactamids. The overexpression of YgiV might be detectable via already applied mass-spectrometry based biotyping systems for more personalized, targeted and effective therapies.[132,190]

Our findings demonstrate that *E. coli* seems incapable of developing high-level cystobactamid resistance in the absence of YgiV.[132] These results are also in contrast with the resistance mechanism of *E. coli* to the structurally related albicidins. For albicidins, mutations in genetic sequence of the nucleoside-specific channel-forming protein Tsx have been identified as the primary cause of facilitating resistance in *E. coli*. These mutations resulted in decreased active transport of albicidins across the outer membrane but had no effect on cystobactamid activity in *E. coli*. YgiV overexpression was also found to play a secondary role in the development of resistance to albicidin in *E. coli* and *Salmonella Typhimurium*. Notably, YgiV overexpression in albicidin resistant mutants was facilitated by gene amplification events of the *ygiV* gene and its genetic neighborhood. In contrast to the stable *ygiV*

promotor mutations seen with cystobactamids, these gene amplifications were reversible upon incubation without selective pressure. This reversibility suggests a fitness costs associated with the albicidin-mediated gene amplifications, whereas no metabolic disadvantage compared to the WT was observable for *E. coli* with *ygiV* promotor mutations facilitated by cystobactamid treatment. Moreover, gene amplification events occur at much higher rates (10^{-4}-10^{-2}/cell/division) than point mutations, enabling bacteria to quickly respond to external stress and potentially rapidly develop resistance to the triggering antibiotic.[47,112,114,191] Interestingly, contrarily to quinolone antibiotics, mutations at the gyrase target site do not appear in *E. coli* for either of these related compound classes.[35]

In addition to that, this study demonstrates that *ygiV* promotor mutations associated with cystobactamid resistance appear to reduce the expression of the virulence factors fimbriae and flagella. Consequently, we propose that the development of cystobactamid resistance during the treatment of conditions such as urinary tract infection could result in a physiological disadvantage for the infectious *E. coli* by reducing its ability for epithelial attachment and motility, respectively.[132] However, this effect can only merely be estimated from *in vitro* experiments and needs to be further investigated in *in vivo* urinary tract infection models. It is important to note that the studies presented in this work were conducted *in vitro* and thereby are limited by their complexity. The resistance development *in vivo* may differ from the effects observed in the *in vitro* environment. Thus, future studies need to address *in vivo* resistance development, utilizing clinically relevant *E. coli* strains, with subsequent investigations for the evaluation of a potential virulence reduction in urinary tract infections (UTI) through the mechanisms discussed above.

Nevertheless, given its specificity and the fact that *E. coli* was not able to develop resistance independently of *ygiV*, it is highly likely that YgiV overexpression and observed downstream effects play a significant role in the *in vivo* resistance of *E. coli* to cystobactamids.

With regards to these findings, urinary tract infections further represent a promising development target for cytobactamids, as they have shown broad-spectrum activity against multiple UTI key pathogens, including not only *E. coli* as main cause of complicated urinary tract infections, but also *K. pneumoniae* and *Enterococcus sp*.[94,99] The clinical development pathway for urinary tract infection also offers a more common and feasible clinical setup as “gateway to the market” with the potential for subsequent label expansion to other indications, such as respiratory tract infections caused by the cystobactamid susceptible carbapenem-resistant *Acinetobacter baumannii*.[100]

Notably, the observed metabolic stabilization of cystobactamids through cobicistat supplementation is of particular interest in relation to the treatment of urinary tract infections by potentially enhancing their therapeutic efficacy.[192] Cobicistat, an approved metabolic stabilizer used in HIV therapy, has been shown to inhibit the biotransformation of cystobactamids *in vitro*.[155] If this effect translates to *in vivo* conditions, the hindered metabolic degradation could enhance plasma stability, prolong exposure, and increase the amounts of unmodified cystobactamids excreted renally. Thereby, cobicistat co-administration might lead to increased effective doses in the urinary tract. Furthermore, the issue of high plasma protein binding currently observed in development may become less relevant after renal filtration, allowing the compound to act unbound in treating the target pathogen. However, further development efforts should also include characterization and optimization of

properties such as tissue specific exposure levels (e.g. kidney) and anti-biofilm activity to enhance therapeutic efficacy.

Nevertheless, higher plasma concentrations and prolonged half-lives of active substances might also increase the risk of potential adverse effects. Antimicrobial chemotherapy can induce toxicity through various mechanisms, ranging from toxicity on a cellular level, such as DNA metabolism inhibition or mitochondrial dysfunction, to more complex functional (organo-) toxicity. The latter include e.g., cardiotoxicity due to hERG-channel inhibition, and hepatotoxicity caused by e.g., disruption of fatty acid exporters or oxidative stress during metabolism. For quinolone antibiotics, which are seen as the direct competitor for cystobactamid application, adverse effects such as central nervous system toxicity, tendon damage and organ toxicities have been reported.[141,193,194] These issues have led to the market withdrawal of some derivatives and multiple black box warnings by the FDA to restrict the use and thereby the risk associated with quinolone therapy, potentially opening a new market value for cystobactamid treatment.[195] Thus, the detailed understanding of the pharmacological and toxicological effects of cystobactamids is indispensable to estimate their safety profile and thereby their potential clinical success and target product profile, hence their economic value. The revealed favorable biological properties of cystobactamids with no harming effects observable on the cellular to the organismal level support the intentions to develop cystobactamids for clinical use. However, while mild uncoupling of the mitochondrial electron transfer chain, as seen for cystobactamids, is linked to beneficial health effects and likely leads to the observed suppression of cellular oxidative stress, it has been shown that potent uncouplers carry a high risk as they are prone to induce pronounced toxicities related to mitochondrial dysfunction.[144,150,151,196] In case of an 2,4-Dinitrophenol overdose, the excessive

mitochondrial uncoupling leads to rapid loss of ATP production, resulting in severe side effects with multiple organ toxicities including cardio-, kidney- and hepatotoxicity, and lethal hyperthermia.[197] These effects are unlikely to occur given the mild uncoupling effect observed for cystobactamids, however, this finding should be considered in further risk-reduction strategies. In addition to that, although it was not possible to observe topoisomerase binding or a genotoxic phenotype in the cellular or organismal context, the identified inhibitory activity on human topoisomerases should be accounted in safety efforts for this or related compound classes during development. Continuous de-risking of mitochondrial toxicity and eukaryotic topoisomerase inhibition is especially relevant in the development of cystobactamids, as these effects have been reported to contribute to the above discussed adverse effects associated with quinolone therapy.[141,142]

The discovered inhibition of SCARB1 by cystobactamids as their major off-target in eukaryotic cells is of particular interest due to its involvement in various functions and its association with multiple diseases. SCARB1 is the main receptor for binding of high density lipoprotein (HDL) particle to facilitate phospholipid and cholesterol transport into the cytosol.[167] In addition, SCARB1 has been identified as important entry receptor for hepatitis C, dengue and SARS-CoV-2 lipoviral particles.[173,179,198] Thus, inhibition of SCARB1 can be related to increased HDL levels, offering potential benefits for prevention of arteriosclerotic events, and reduction of the viral infection rate. Due to its function as lipid transporter, SCARB1 inhibition, along with mitochondrial uncoupling, is under consideration for therapeutic use in patients suffering from non-alcoholic fatty liver disease.[171] Moreover, overexpression of SCARB1 has been demonstrated in various cancer types including breast, ovarian, colorectal, and pancreatic cancer, where it contributes to cancer proliferation, progression and tumor

aggressiveness.[168] In cancers like castration-resistant prostate cancer, the inhibition of SCARB1 dependent transport of cholesterol, and thereby its intracellular availability as precursor for steroid synthesis, has been linked to the suppression of cancer cell growth and viability.[170,178]

The discovery of SCARB1 inhibition through cystobactamid treatment expands the therapeutic potential of these antimicrobial active natural products, suggesting unexpected indication areas ranging from viral infections and metabolic diseases to oncology.

5. Summary & Conclusion

The globally escalating antimicrobial resistance is a widely underestimated risk for human and animal health. The development of novel antimicrobial agents to combat this silent pandemic requires extended public, industrial and political attention.[13] However, to tackle antimicrobial resistance sustainably, the novel strategies needed must incorporate not only the reuse and derivatization of known chemical scaffolds but also the extension of the structural and mechanistic portfolio.[19] Nevertheless, a comprehensive understanding of the biological properties of these novel structural compound classes is essential not only to prevent potential harmful effects but also to fully exploit their pharmacological potential.

In this work, we examined the interactions of the novel compound class cystobactamids with eukaryotes and bacteria, aiming to gain insights into their pharmacological properties and resistance profile on a phenotypic and molecular level. We successfully identified and characterized a previously unknown YgiV-mediated antibiotic resistance mechanism, which is likely influencing the regulation of fimbriae and flagella expression. In addition, we identified the efflux pump AcrB as off-target of cystobactamids, however, without tremendously influencing their bioactivity. Consequently, the demonstrated necessity and specificity of the YgiV-mediated mechanism for acquiring resistance in *E. coli* provide valuable insights into why cystobactamids effectively bypass broader, non-specific cross-resistance to other classes of antimicrobial compounds, even when tested against multidrug-resistant clinical isolates. Thus, these results further support the development of cystobactamids as last-line antibiotic for clinical use.

However, for successful clinical application, it is essential to extensively investigate not only the efficacy but also the safety profile of a fundamentally new structural class.

Here, we provide evidence for the cellular and organismal safety of cystobactamids. Unexpectedly, we uncovered even protective properties against oxidative cell stress associated with treatment using this compound class. Moreover, by investigating the molecular off-targets in human cells, we identified a so far unknown mode of action of cystobactamids as SCARB1 inhibitors. This effect expands the possible indication areas of cystobactamids not only from antibacterial to antiviral agents by inhibiting i.e. SCARB1-dependent HCV cell entry, but also to other SCARB1 related diseases like arteriosclerosis, non-alcoholic fatty liver disease and as co-treatment for cancer types overexpressing this protein. However, targeted structure development would be necessary to aim for optimized and selective cystobactamid-derived SCARB1 inhibitors.

In addition, we identified and investigated new strategies for extending the exposure of cystobactamids through metabolic stabilization of the compound. Reduced metabolic degradation may result in higher and more sustained treatment concentrations at the site of infection when evaluated *in vivo*.

This work highlights the importance of comprehensively understanding the pharmacological properties of a novel compound class. As shown in this study, such thorough investigations may lead to unexpected scientific discoveries and potentially broadens the therapeutic opportunities of an active agent in a previous unanticipated way.

Future experiments will emphasize the significance of the findings presented in this work and elucidate how these results translate into an *in vivo* context for supporting the development of cystobactamids as treatment option against multidrug-resistant bacteria.

6. References

1. Hutchings, M., Truman, A. & Wilkinson, B. Antibiotics: past, present and future. *Curr. Opin. Microbiol.* **51**, 72–80 (2019).
2. Debus, A. G. Paracelsus and the mediacal revolution of the renaissance. *Hahnemann Univ. Libr.* (2014).
3. Gelpi, A., Gilbertson, A. & Tucker, J. D. Magic bullet: Paul Ehrlich, Salvarsan and the birth of venereology. *Sex. Transm. Infect.* **91**, 68–69 (2015).
4. Otten, H. Domagk and the development of the sulphonamides. *J. Antimicrob. Chemother.* (1986) doi:10.1136/bmj.s3-1.14.287.
5. Fleming, A. On the antibacterial action of cultures of a penicillium, with special reference to their use in the isolation of B. influenzae. *Br. J. Exp. Pathol.* (1929).
6. Nicolaou, K. C. & Rigol, S. A brief history of antibiotics and select advances in their synthesis. *J. Antibiot. (Tokyo).* **71**, 153–184 (2018).
7. Waksman, S. A., Schatz, A. & Reynolds, D. M. Production of antibiotic substances by actinomycetes. *Ann. N. Y. Acad. Sci.* **1213**, 112–124 (2010).
8. Newman, D. J. & Cragg, G. M. Natural Products as Sources of New Drugs from 1981 to 2014. *J. Nat. Prod.* **79**, 629–661 (2016).
9. Fleming, A. Penicillin. *Nobel Lect.* (1945).
10. Murray, C. J. *et al.* Global burden of bacterial antimicrobial resistance in 2019: a systematic analysis. *Lancet* **399**, 629–655 (2022).
11. Alarcon, A. & Omenaca, F. Antimicrobial Resistance in Escherichia coli Sepsis. *Pediatr. Infect. Dis. J.* **23**, 979–980 (2004).
12. Munita, J. M. & Arias, C. A. Mechanisms of antibiotic resistance. *Virulence Mech. Bact. Pathog.* 481–511 (2016) doi:10.1128/9781555819286.ch17.
13. Resistance, G. 2021 A. Global burden of bacterial antimicrobial resistance

1990–2021: a systematic analysis with forecasts to 2050. *Lancet* (2024) doi:10.1016/S0140-6736(24)01867-1.

14. Dyar, O. J., Huttner, B., Schouten, J. & Pulcini, C. What is antimicrobial stewardship? *Clin. Microbiol. Infect.* **23**, 793–798 (2017).
15. Aiesh, B. M. *et al.* Impact of an antibiotic stewardship program on antibiotic utilization, bacterial susceptibilities, and cost of antibiotics. *Sci. Rep.* **13**, 1–9 (2023).
16. Todd, M. H. *et al.* There is no market for new antibiotics: This allows an open approach to research and development. *Wellcome Open Res.* **6**, 1–14 (2021).
17. Butler, M. S., Henderson, I. R., Capon, R. J. & Blaskovich, M. A. T. Antibiotics in the clinical pipeline as of December 2022. *J. Antibiot. (Tokyo).* **76**, 431–473 (2023).
18. Mathers, C. D. & Loncar, D. Projections of global mortality and burden of disease from 2002 to 2030. *PLoS Med.* **3**, 2011–2030 (2006).
19. Miethke, M. *et al.* Towards the sustainable discovery and development of new antibiotics. *Nat. Rev. Chem.* **5**, 726–749 (2021).
20. Brad Spellberg, M.D., John G. Bartlett, M.D., and David N. Gilbert, M. D. The Future of Antibiotics and Resistance. *N. Engl. J. Med.* **368**, 297–299 (2013).
21. WHO. *2023 Antibacterial Agents in Clinical and Preclinical Development*. *World Health Organization 2021* https://www.who.int/publications/i/item/9789240021303 (2021).
22. Kong, K. F., Schneper, L. & Mathee, K. Beta-lactam antibiotics: From antibiosis to resistance and bacteriology. *APIMS* **118**, 1–36 (2010).
23. Tony Velkov, Kade D Roberts, Roger L Nation, Philip E Thompson, and J. L. Pharmacology of polymyxins: new insights into an ‘old’ class of antibiotics. *Futur.*

Microbiol. **7**, 114–137 (2013).

24. Cate, Daniel N. Wilson, J. H. D. The structure and function of the eukaryotic ribosome. *Cold Spring Harb Perspect Biol* 251–263 (2012) doi:10.1101/cshperspect.a011536.
25. Wimberly, B. T. *et al.* Structure of the 30S ribosomal subunit. *Nature* **407**, 327–339 (2000).
26. Wilson, D. N. Ribosome-targeting antibiotics and mechanisms of bacterial resistance. *Nat. Rev. Microbiol.* **12**, 35–48 (2014).
27. Bermingham, A. & Derrick, J. P. The folic acid biosynthesis pathway in bacteria: Evaluation of potential for antibacterial drug discovery. *BioEssays* **24**, 637–648 (2002).
28. Ovung, A. & Bhattacharyya, J. Sulfonamide drugs: structure, antibacterial property, toxicity, and biophysical interactions. *Biophys. Rev.* **13**, 259–272 (2021).
29. Klotz, I. M. The Mode of Action of Sulfonamides. *J. Am. Chem. Soc.* (1944).
30. Quinlivan, E. P., McPartlin, J., Weir, D. G. & Scott, J. Mechanism of the antimicrobial drug trimethoprim revisited. *FASEB J.* **14**, 2519–2524 (2000).
31. Lee, J. & Borukhov, S. Bacterial RNA polymerase-DNA interaction-The driving force of gene expression and the target for drug action. *Front. Mol. Biosci.* **3**, (2016).
32. Campbell, E. A. *et al.* Structural mechanism for rifampicin inhibition of bacterial RNA polymerase. *Cell* **104**, 901–912 (2001).
33. Floss, H. G. & Yu, T. W. Rifamycin - Mode of action, resistance, and biosynthesis. *Chem. Rev.* **105**, 621–632 (2005).
34. Clara Calvori, Laura Frontali, Louisa Leoni, G. T. Effect of Rifamycin on Protein

Synthesis. *Nature* (1965).

35. Aldred, K. J., Kerns, R. J. & Osheroff, N. Mechanism of quinolone action and resistance. *Biochemistry* **53**, 1565–1574 (2014).
36. Gore, J. *et al.* Mechanochemical analysis of DNA gyrase using rotor bead tracking. *Nature* **439**, 100–104 (2006).
37. Reece, R. J., Maxwell, A. & Wang, J. C. DNA gyrase: Structure and function. *Crit. Rev. Biochem. Mol. Biol.* **26**, 335–375 (1991).
38. Levine, C., Hiasa, H. & Marians, K. J. DNA gyrase and topoisomerase IV: Biochemical activities, physiological roles during chromosome replication, and drug sensitivities. *Biochim. Biophys. Acta - Gene Struct. Expr.* **1400**, 29–43 (1998).
39. Brusselaers, N., Vogelaers, D. & Blot, S. The rising problem of antimicrobial resistance in the intensive care unit. *Ann. Intensive Care* **1**, 47 (2011).
40. Rotondo, C. M. & Wright, G. D. Inhibitors of metallo-β-lactamases. *Curr. Opin. Microbiol.* **39**, 96–105 (2017).
41. Queenan, A. M. & Bush, K. Carbapenemases: The versatile β-lactamases. *Clin. Microbiol. Rev.* **20**, 440–458 (2007).
42. Gigante, V. *et al.* Multi-year analysis of the global preclinical antibacterial pipeline : trends and gaps. *Antimicrob. Agents Chemother.* **68**, (2024).
43. Guckes, K. R. *et al.* Strong cross-system interactions drive the activation of the QseB response regulator in the absence of its cognate sensor. *Proc. Natl. Acad. Sci. U. S. A.* **110**, 16592–16597 (2013).
44. Dortet, L. *et al.* Rapid detection of colistin resistance in Acinetobacter baumannii using MALDI-TOF-based lipidomics on intact bacteria. *Sci. Rep.* **8**, 1–5 (2018).
45. Herrera, C. M., Hankins, J. V. & Trent, M. S. Activation of PmrA inhibits LpxT-

dependent phosphorylation of lipid A promoting resistance to antimicrobial peptides. *Mol. Microbiol.* **76**, 1444–1460 (2010).

46. Fernández, L. & Hancock, R. E. W. Adaptive and mutational resistance: Role of porins and efflux pumps in drug resistance. *Clin. Microbiol. Rev.* **25**, 661–681 (2012).

47. Robert G. Brich, John M. Pemberton, W. V. S. B. Stable albicidin resistance in Escherichia coli involves an altered outer-membrane nucleoside uptake system. *J. Gen. Microbiol.* 51–58 (1990) doi:10.1099/00221287-136-1-51.

48. Nikaido, H. & Pagès, J. M. Broad-specificity efflux pumps and their role in multidrug resistance of Gram-negative bacteria. *FEMS Microbiol. Rev.* **36**, 340–363 (2012).

49. Swick, M. C., Morgan-Linnell, S. K., Carlson, K. M. & Zechiedrich, L. Expression of multidrug efflux pump genes acrAB-tolC, mdfA, and norE in Escherichia coli clinical isolates as a function of fluoroquinolone and multidrug resistance. *Antimicrob. Agents Chemother.* **55**, 921–924 (2011).

50. Du, D. *et al.* Structure of the AcrAB-TolC multidrug efflux pump. *Nature* **509**, 512–515 (2014).

51. Lin, J., Zhou, D., Steitz, T. A., Polikanov, Y. S. & Gagnon, M. G. Ribosome-Targeting Antibiotics: Modes of Action, Mechanisms of Resistance, and Implications for Drug Design. *Annu. Rev. Biochem.* **87**, 451–478 (2018).

52. Lambert, P. A. Bacterial resistance to antibiotics: Modified target sites. *Adv. Drug Deliv. Rev.* **57**, 1471–1485 (2005).

53. Schwartz, L., de Dios Ruiz-Rosado, J., Stonebrook, E., Becknell, B. & Spencer, J. D. Uropathogen and host responses in pyelonephritis. *Nat. Rev. Nephrol.* **19**, 658–671 (2023).

54. Tamimi, N. A. M. & Ellis, P. Drug development: From concept to marketing! *Nephron - Clin. Pract.* **113**, 125–131 (2009).

55. Hefti, F. F. Requirements for a lead compound to become a clinical candidate. *BMC Neurosci.* **9**, 1–7 (2008).

56. Hillisch, A., Heinrich, N. & Wild, H. Computational Chemistry in the Pharmaceutical Industry: From Childhood to Adolescence. *ChemMedChem* **10**, 1958–1962 (2015).

57. Jayatunga, M. K. P., Xie, W., Ruder, L., Schulze, U. & Meier, C. AI in small-molecule drug discovery: a coming wave? *Nat. Rev. Drug Discov.* **21**, 175–176 (2022).

58. Hoffmann, S. & Hartung, T. Toward an evidence-based toxicology. 497–513 (2006).

59. Hughes, J. P., Rees, S. S., Kalindjian, S. B. & Philpott, K. L. Principles of early drug discovery. *Br. J. Pharmacol.* **162**, 1239–1249 (2011).

60. Adrio, J. L. & Demain, A. L. Genetic improvementof processes yielding microbial products. *FEMS Microbiol. Rev.* **30**, 187–214 (2006).

61. Lipsky, M. S. & Sharp, L. K. From idea to market: The drug approval process. *J. Am. Board Fam. Pract.* **14**, 362–367 (2001).

62. European Medicines Agency (EMA). *Guideline for Good Clinical Practice E6(R2)*. https://www.ema.europa.eu/en/documents/scientific-guideline/ich-e-6-r2-guideline-good-clinical-practice-step-5_en.pdf (2018).

63. Harrison, R. K. Phase II and phase III failures: 2013-2015. *Nat. Rev. Drug Discov.* **15**, 817–818 (2016).

64. ICH. *INTEGRATED ADDENDUM TO ICH E6(R1): GUIDELINE FOR GOOD CLINICAL PRACTICE E6(R2)*. (2016).

65. WHO. *Guidance for best practices for clinical trials*. (2024).

66. Singh, N. *et al.* Drug discovery and development: introduction to the general public and patient groups. *Front. Drug Discov.* **3**, 1–11 (2023).

67. EMA. *Pharmacovigilance Risk Assessment Committee*. (2021).

68. EMA, P. Fluoroquinolone and quinolone antibiotics : PRAC recommends restrictions on use New restrictions follow review of disabling and potentially long-lasting side. *European Medicines Agency Science Medicines Health,* 1–2 (2018).

69. Dathe, K. & Schaefer, C. Drug safety in pregnancy: the German Embryotox institute. *Eur. J. Clin. Pharmacol.* **74**, 171–179 (2018).

70. Begley, C. G. *et al.* Drug repurposing: Misconceptions, challenges, and opportunities for academic researchers. *Sci. Transl. Med.* **13**, 1–13 (2021).

71. Zhang, H. W. *et al.* Application of omics- and multi-omics-based techniques for natural product target discovery. *Biomed. Pharmacother.* **141**, 111833 (2021).

72. Paananen, J. & Fortino, V. An omics perspective on drug target discovery platforms. *Brief. Bioinform.* **21**, 1937–1953 (2020).

73. Gleissner, C. M. L. *et al.* Neocarzilin A Is a Potent Inhibitor of Cancer Cell Motility Targeting VAT-1 Controlled Pathways. *ACS Cent. Sci.* **5**, 1170–1178 (2019).

74. Wright, M. H., Fetzer, C. & Sieber, S. A. Chemical Probes Unravel an Antimicrobial Defense Response Triggered by Binding of the Human Opioid Dynorphin to a Bacterial Sensor Kinase. *J. Am. Chem. Soc.* **139**, 6152–6159 (2017).

75. Melchiorri, D., Rocke, T., Alm, R. A., Cameron, A. M. & Gigante, V. Review Addressing urgent priorities in antibiotic development : insights from WHO 2023 antibacterial clinical pipeline analyses. *Lancet Microbe* (2024)

doi:10.1016/j.lanmic.2024.100992.

76. Kowalska-Krochmal, B. & Dudek-Wicher, R. The minimum inhibitory concentration of antibiotics: Methods, interpretation, clinical relevance. *Pathogens* **10**, 1–21 (2021).

77. Cushnie, T. P. T. *et al.* Bioprospecting for Antibacterial Drugs: a Multidisciplinary Perspective on Natural Product Source Material, Bioassay Selection and Avoidable Pitfalls. *Pharm. Res.* **37**, (2020).

78. Bagla, V. P., McGaw, L. J., Elgorashi, E. E. & Eloff, J. N. Antimicrobial activity, toxicity and selectivity index of two biflavonoids and a flavone isolated from Podocarpus henkelii (Podocarpaceae) leaves. *BMC Complement. Altern. Med.* **14**, 2–7 (2014).

79. Ahluwalia, K. *et al.* The Future of CMC Regulatory Submissions: Streamlining Activities Using Structured Content and Data Management. *J. Pharm. Sci.* **111**, 1232–1244 (2021).

80. International Conference on Harmonisation. *ICH Q7 - Good Manufacturing Practice for Active Pharmaceutical Ingredients*. *ICH Quality Guidelines* https://www.ema.europa.eu/en/documents/scientific-guideline/ich-q-7-good-manufacturing-practice-active-pharmaceutical-ingredients-step-5_en.pdf (2000).

81. Baumann, S. *et al.* Cystobactamids: Myxobacterial topoisomerase inhibitors exhibiting potent antibacterial activity. *Angew. Chemie - Int. Ed.* **53**, 14605–14609 (2014).

82. Kaimer, C., Weltzer, M. L. & Wall, D. Two reasons to kill: predation and kin discrimination in myxobacteria. *Microbiology* **169**, 1–11 (2023).

83. Schneiker, S. *et al.* Complete genome sequence of the myxobacterium

Sorangium cellulosum. *Nat. Biotechnol.* **25**, 1281–1289 (2007).

84. Blattner, F. R. *et al.* The complete genome sequence of Escherichia coli K-12. *Science (80-.).* **277**, 1453–1462 (1997).
85. Medema, M. H. *et al.* Minimum Information about a Biosynthetic Gene cluster. *Nat. Chem. Biol.* **11**, 625–631 (2015).
86. Reichenbach, H. Myxobacteria, producers of novel bioactive substances. *J. Ind. Microbiol. Biotechnol.* **27**, 149–156 (2001).
87. Groß, S., Schnell, B., Haack, P. A., Auerbach, D. & Müller, R. In vivo and in vitro reconstitution of unique key steps in cystobactamid antibiotic biosynthesis. *Nat. Commun.* **12**, 1–15 (2021).
88. Kim, Y. J. *et al.* Isolation of Coralmycins A and B, Potent Anti-Gram Negative Compounds from the Myxobacteria Corallococcus coralloides M23. *J. Nat. Prod.* **79**, 2223–2228 (2016).
89. Hashimi, S. M. Albicidin, a potent DNA gyrase inhibitor with clinical potential. *J. Antibiot. (Tokyo).* **72**, 785–792 (2019).
90. Hegde, S. S. *et al.* A fluoroquinolone resistance protein from Mycobacterium tuberculosis that mimics DNA. *Science (80-.).* **308**, 1480–1483 (2005).
91. Michalczyk, E. *et al.* Molecular mechanism of topoisomerase poisoning by the peptide antibiotic albicidin. *Nat. Catal.* **6**, 52–67 (2023).
92. Miller, W. R. & Arias, C. A. ESKAPE pathogens: antimicrobial resistance, epidemiology, clinical impact and therapeutics. *Nat. Rev. Microbiol.* **22**, 598–616 (2024).
93. Hüttel, S. *et al.* Discovery and Total Synthesis of Natural Cystobactamid Derivatives with Superior Activity against Gram-Negative Pathogens. *Angew. Chemie - Int. Ed.* **56**, 12760–12764 (2017).

94. Testolin, G. *et al.* Synthetic studies of cystobactamids as antibiotics and bacterial imaging carriers lead to compounds with high: In vivo efficacy. *Chem. Sci.* **11**, 1316–1334 (2020).

95. Kohnhäuser, D. *et al.* Optimization of the Central α-Amino Acid in Cystobactamids to the Broad-Spectrum, Resistance-Breaking Antibiotic CN-CC-861. *J. Med. Chem.* (2024) doi:10.1021/acs.jmedchem.4c00927.

96. Elgaher, W. A. M. *et al.* Cystobactamid 507: Concise Synthesis, Mode of Action, and Optimization toward More Potent Antibiotics. *Chem. - A Eur. J.* **26**, 7219–7225 (2020).

97. Cheng, B., Müller, R. & Trauner, D. Total Syntheses of Cystobactamids and Structural Confirmation of Cystobactamid 919-2. *Angew. Chemie - Int. Ed.* **56**, 12755–12759 (2017).

98. Moeller, M. *et al.* Scalable Syntheses of Methoxyaspartate and Preparation of the Antibiotic Cystobactamid 861-2 and Highly Potent Derivatives. *Org. Lett.* **21**, 8369–8372 (2019).

99. Seedorf, T., Kirschning, A. & Solga, D. Natural and Synthetic Oligoarylamides: Privileged Structures for Medical Applications. *Chem. - A Eur. J.* **27**, 7321–7339 (2021).

100. Stappert, M. *et al.* Synthetic studies on the tetrasubstituted D-ring of cystobactamids lead to potent terephthalic acid antibiotics. *Commun. Chem.* 1–15 (2024) doi:10.1038/s42004-024-01337-6.

101. Testolin, G. *et al.* Synthetic studies of cystobactamids as antibiotics and bacterial imaging carriers lead to compounds with high In vivo efficacy. *Chem. Sci.* **11**, 1316–1334 (2020).

102. Planke, T. *et al.* Cystobactamids 920-1 and 920-2: Assignment of the

Constitution and Relative Configuration by Total Synthesis. *Organic Letters* vol. 21 1359–1363 (2019).

103. Seedorf, T. Synthesis of an antibacterial oligopeptide library. (2023).
104. Kohnhäuser, D. Synthetic optimization of cystobactamid analogs as antibiotics. (2021). doi:https://doi.org/10.15488/11137.
105. Arias, C. A. & Murray, B. E. Antibiotic-Resistant Bugs in the 21st Century — A Clinical Super-Challenge. *N. Engl. J. Med.* **360**, 439–443 (2009).
106. O´Neill, J. Tackling drug-resistant infections globally: Final Report and Recommendations. *Rev. Antimicrob. Resist.* **7**, 110 (2016).
107. Wu, D., Ding, Y., Yao, K., Gao, W. & Wang, Y. Antimicrobial Resistance Analysis of Clinical Escherichia coli Isolates in Neonatal Ward. *Front. Pediatr.* **9**, 1–7 (2021).
108. Laurent Poirel, Jean-Yves Madec, Agnese Lupo, Anne-Kathrin Schink, Nicolas Kieffer, Patrice Nordmann, S. S. Antimicrobial Resistance in Escherichia coli. *Microbiol. Spectr.* **6**, (2018).
109. Zhang, X. S., García-Contreras, R. & Wood, T. K. Escherichia coli transcription factor YncC (McbR) regulates colanic acid and biofilm formation by repressing expression of periplasmic protein YbiM (McbA). *ISME J.* **2**, 615–631 (2008).
110. Isalan, M. *et al.* Evolvability and hierarchy in rewired bacterial gene networks. *Nature* **452**, 840–845 (2008).
111. Yuan, H. *et al.* GyrI-like proteins catalyze cyclopropanoid hydrolysis to confer cellular protection. *Nat. Commun.* **8**, (2017).
112. Saathoff, M. *et al.* Gene amplifications cause high-level resistance against albicidin in gram-negative bacteria. *PLoS Biol.* 2022.09.15.507240 (2023) doi:10.1371/journal.pbio.3002186.

113. Baba, T. *et al.* Construction of Escherichia coli K-12 in-frame, single-gene knockout mutants: The Keio collection. *Mol. Syst. Biol.* **2**, (2006).

114. Andersson, D. I. & Hughes, D. Gene amplification and adaptive evolution in bacteria. *Annu. Rev. Genet.* **43**, 167–195 (2009).

115. Hadjifrangiskou, M. *et al.* A central metabolic circuit controlled by QseC in pathogenic Escherichia coli. *Mol. Microbiol.* **80**, 1516–1529 (2011).

116. Darwin, A. J. The phage-shock-protein response. *Mol. Microbiol.* **57**, 621–628 (2005).

117. Lloyd, L. J. *et al.* Identification of a new member of the phage shock protein response in Escherichia coli, the phage shock protein G (PspG). *J. Biol. Chem.* **279**, 55707–55714 (2004).

118. Melanie N. Hurst1, Connor J. Beebout, Alexis Hollingsworth, Kirsten R. Guckes,#, Alexandria Purcell, Tomas A. Bermudez, Diamond Williams2, Seth A. Reasoner, M. S. T. and M. H. The QseB response regulator imparts tolerance to positively charged antibiotics 2 by controlling metabolism and minor changes to LPS. *bioRxiv* 1–40 (2023).

119. Casella, L. G. Modifications to Lipid A in *Acinetobacter baumannii*: Potential biomarkers for rapid diagnosis of Colistin resistance. *ProQuest Diss. Theses* 66 (2013) doi:10.1128/AAC.02501-1.

120. Zhao, Y. *et al.* Structural and mechanistic insights into polymyxin resistance mediated by EptC originating from Escherichia coli. *FEBS J.* **286**, 750–764 (2019).

121. Mancini, S. *et al.* Population-based inference of aminoglycoside resistance mechanisms in Escherichia coli. *EBioMedicine* **46**, 184–192 (2019).

122. Klemm, P. Fimbrial adhesins of escherichia coli. *Rev. Infect. Dis.* **7**, 321–340

(1985).

123. Wang, X. *et al.* QseBC controls flagellar motility, fimbrial hemagglutination and intracellular virulence in fish pathogen Edwardsiella tarda. *Fish Shellfish Immunol.* **30**, 944–953 (2011).

124. Zhou, Y. *et al.* Urinary Tract Infections Caused by Uropathogenic Escherichia coli: Mechanisms of Infection and Treatment Options. *Int. J. Mol. Sci.* **24**, (2023).

125. Baquero, M. R., Bouzon, M., Varea, J. & Moreno, F. sbmC, a stationary-phase induced SOS Escherichia coli gene, whose product protects cells from the DNA replication inhibitor microcin B17. *Molecular Microbiology* vol. 18 301–311 (1995).

126. Maslowska, K. H., Makiela-Dzbenska, K. & Fijalkowska, I. J. The SOS system: A complex and tightly regulated response to DNA damage. *Environ. Mol. Mutagen.* **60**, 368–384 (2019).

127. Keeney, D., Ruzin, A., Mcaleese, F., Murphy, E. & Bradford, P. A. MarA-mediated overexpression of the AcrAB efflux pump results in decreased susceptibility to tigecycline in Escherichia coli. *J. Antimicrob. Chemother.* **61**, 46–53 (2008).

128. *WHO Bacterial Priority Pathogens List , 2024*. (2024).

129. Nathan, C. & Cars, O. Antibiotic Resistance - Problems, Progress, and Prospects. *New Engll. J. Med.* **371**, 1761–1763 (2014).

130. Rossolini, G. M. & Mantengoli, E. Antimicrobial resistance in Europe and its potential impact on empirical therapy. *Clin. Microbiol. Infect.* **14**, 2–8 (2008).

131. European Medicines Agency. The European Medicines Agency Road map to 2015 : The Agency ' s contribution to Science , Medicines , Health. **44**, (2015).

132. Risch, T., Kolling, D., Mostert, D., Herrmann, J. & Müller, R. Point mutations in

the ygiV promoter region lead to cystobactamid resistance and reduced virulence in. *ResearchSquare* (2024) doi:https://doi.org/10.21203/rs.3.rs-3751821/v1 License:

133. Arrowsmith, J. & Miller, P. Trial Watch: Phase II and Phase III attrition rates 2011-2012. *Nat. Rev. Drug Discov.* **12**, 569 (2013).
134. Muller, P. Y. & Milton, M. N. The determination and interpretation of the therapeutic index in drug development. *Nat. Rev. Drug Discov.* **11**, 751–761 (2012).
135. Kalyaanamoorthy, S. & Barakat, K. H. Development of Safe Drugs: The hERG Challenge. *Med. Res. Rev.* **38**, 525–555 (2018).
136. Redfern, W. S. *et al.* Relationships between preclinical cardiac electrophysiology, clinical QT interval prolongation and torsade de pointes for a broad range of drugs: Evidence for a provisional safety margin in drug development. *Cardiovasc. Res.* **58**, 32–45 (2003).
137. Information, S. Cystobactamid 507: Concise Synthesis, Mode of Action, and Optimization toward More Potent Antibiotics.
138. Fotakis, G. & Timbrell, J. A. In vitro cytotoxicity assays: Comparison of LDH, neutral red, MTT and protein assay in hepatoma cell lines following exposure to cadmium chloride. *Toxicol. Lett.* **160**, 171–177 (2006).
139. Minotti, G., Menna, P., Salvatorelli, E., Cairo, G. & Gianni, L. Anthracyclines: Molecular advances and pharmacologie developments in antitumor activity and cardiotoxicity. *Pharmacol. Rev.* **56**, 185–229 (2004).
140. Tomasz, M. Mitomycin C: small, fast and deadly (but very selective). *Chem. Biol.* **2**, 575–579 (1995).
141. Kalghatgi, S. *et al.* Bactericidal antibiotics induce mitochondrial dysfunction and

oxidative damage in mammalian cells. *Sci. Transl. Med.* **5**, (2013).

142. Hangas, A. *et al.* Ciprofloxacin impairs mitochondrial DNA replication initiation through inhibition of Topoisomerase 2. *Nucleic Acids Res.* **46**, 9625–9636 (2018).
143. Tilmant, K. *et al.* In vitro screening of cell bioenergetics to assess mitochondrial dysfunction in drug development. *Toxicol. Vitr.* **52**, 374–383 (2018).
144. Shrestha, R., Johnson, E. & Byrne, F. L. Exploring the therapeutic potential of mitochondrial uncouplers in cancer. *Mol. Metab.* **51**, 101222 (2021).
145. Herb, M., Gluschko, A. & Schramm, M. Reactive Oxygen Species: Not Omnipresent but Important in Many Locations. *Front. Cell Dev. Biol.* **9**, 1–12 (2021).
146. Chang, T. K. H. & Abbott, F. S. Oxidative stress as a mechanism of valproic acid-associated hepatotoxicity. *Drug Metab. Rev.* **38**, 627–639 (2006).
147. Maillet, A. *et al.* Modeling Doxorubicin-Induced Cardiotoxicity in Human Pluripotent Stem Cell Derived-Cardiomyocytes. *Sci. Rep.* **6**, 1–13 (2016).
148. Carrasco, R., Castillo, R. L., Gormaz, J. G., Carrillo, M. & Thavendiranathan, P. Role of Oxidative Stress in the Mechanisms of Anthracycline-Induced Cardiotoxicity: Effects of Preventive Strategies. *Oxid. Med. Cell. Longev.* **2021**, (2021).
149. Monteiro, J. P. *et al.* A biophysical approach to menadione membrane interactions: Relevance for menadione-induced mitochondria dysfunction and related deleterious/therapeutic effects. *Biochim. Biophys. Acta - Biomembr.* **1828**, 1899–1908 (2013).
150. Cadenas, S. Mitochondrial uncoupling, ROS generation and cardioprotection. *Biochim. Biophys. Acta - Bioenerg.* **1859**, 940–950 (2018).

151. Zhao, R. Z., Jiang, S., Zhang, L. & Yu, Z. Bin. Mitochondrial electron transport chain, ROS generation and uncoupling (Review). *Int. J. Mol. Med.* **44**, 3–15 (2019).

152. Haider, K., Haider, M. R., Neha, K. & Yar, M. S. Free radical scavengers: An overview on heterocyclic advances and medicinal prospects. *Eur. J. Med. Chem.* **204**, (2020).

153. Guengerich, F. P., Liebler, D. C. & Reed, D. L. *Enzymatic activation of chemicals to toxic metabolites*. *Critical Reviews in Toxicology* vol. 14 (1985).

154. Baillie, T. A. Metabolism and toxicity of drugs. Two decades of progress in industrial drug metabolism. *Chem. Res. Toxicol.* **21**, 129–137 (2008).

155. Xu, L. *et al.* Cobicistat (GS-9350): A potent and selective inhibitor of human CYP3A as a novel pharmacoenhancer. *ACS Med. Chem. Lett.* **1**, 209–213 (2010).

156. Custodio, J. M. *et al.* Pharmacokinetics of cobicistat boosted-elvitegravir administered in combination with rosuvastatin. *J. Clin. Pharmacol.* **54**, 649–656 (2014).

157. Peng, H. M., Raner, G. M., Vaz, A. D. N. & Coon, M. J. Oxidative cleavage of esters and amides to carbonyl products by cytochrome P450. *Archives of Biochemistry and Biophysics* vol. 318 333–339 (1995).

158. Parng, C., Seng, W. L., Semino, C. & McGrath, P. Zebrafish: a preclinical model for drug screening. *Assay Drug Dev. Technol.* **1**, 41–48 (2002).

159. Zhu, J. J. *et al.* Human cardiotoxic drugs delivered by soaking and microinjection induce cardiovascular toxicity in zebrafish. *Journal of Applied Toxicology* vol. 34 139–148 (2014).

160. He, J. H. *et al.* A zebrafish phenotypic assay for assessing drug-induced

hepatotoxicity. *J. Pharmacol. Toxicol. Methods* **67**, 25–32 (2013).

161. Strähle, U. *et al.* Zebrafish embryos as an alternative to animal experiments-A commentary on the definition of the onset of protected life stages in animal welfare regulations. *Reprod. Toxicol.* **33**, 128–132 (2012).
162. Vargesson, N. Thalidomide-Induced Teratogenesis: History and Mechanisms. *Birth Defects Res. (Part C)* 140–156 (2015) doi:10.1002/bdrc.21096.
163. Nagel, R. *et al.* Effect of 3,4-dichloroaniline on the early life stages of the zebrafish (Brachydanio retio): Results of a comparative laboratory study. *Ecotoxicol. Environ. Saf.* **21**, 157–164 (1991).
164. Zakaria, Z. Z. *et al.* Using Zebrafish for Investigating the Molecular Mechanisms of Drug-Induced Cardiotoxicity. *Biomed Res. Int.* **2018**, (2018).
165. Walker, D. K. The use of pharmacokinetic and pharmacodynamic data in the assessment of drug safety in early drug development. *Br. J. Clin. Pharmacol.* **58**, 601–608 (2004).
166. Perez-Dominguez, F. *et al.* Role of pirin, an oxidative stress sensor protein, in epithelial carcinogenesis. *Biology (Basel).* **10**, 1–13 (2021).
167. Xu, S. *et al.* Apolipoproteins of HDL can directly mediate binding to the scavenger receptor SR-BI, an HDL receptor that mediates selective lipid uptake. *J. Lipid Res.* **38**, 1289–1298 (1997).
168. Wen-Jun Shen, Salman Azhar, and F. B. K. SR-B1: A Unique Multifunctional Receptor for Cholesterol Influx and Efflux. *Annu Rev Physiol.* **176**, 139–148 (2018).
169. Ji, Y. *et al.* Scavenger receptor BI promotes high density lipoprotein-mediated cellular cholesterol efflux. *J. Biol. Chem.* **272**, 20982–20985 (1997).
170. Mooberry, L. K., Sabnis, N. A., Panchoo, M., Nagarajan, B. & Lacko, A. G.

Targeting the SR-B1 receptor as a gateway for cancer therapy and imaging. *Front. Pharmacol.* **7**, 1–11 (2016).

171. Qiu, Y. *et al.* Upregulation of caveolin-1 and SR-B1 in mice with non-alcoholic fatty liver disease. *Hepatobiliary Pancreat. Dis. Int.* **12**, 630–636 (2013).
172. Masson, D. *et al.* Increased HDL cholesterol and ApoA-I in humans and mice treated with a novel SR-BI inhibitor. *Arterioscler. Thromb. Vasc. Biol.* **29**, 2054–2060 (2009).
173. Zeisel, M. B. *et al.* Scavenger receptor class B type I is a key host factor for hepatitis C virus infection required for an entry step closely linked to CD81. *Hepatology* **46**, 1722–1731 (2007).
174. Scarselli, E. *et al.* The human scavenger receptor class B type I is a novel candidate receptor for the hepatitis C virus. *EMBO J.* **21**, 5017–5025 (2002).
175. Global HIV Hepatitis and Sexually Transmitted Infections Programmes. *Global progress report on HIV, viral hepatitis and sexually transmitted infections, 2021*. *WHO* https://www.who.int/publications/i/item/9789240027077 (2021).
176. Lindenbach, B. D. & Rice, C. M. The ins and outs of hepatitis C virus entry and assembly. *Nat. Rev. Microbiol.* **11**, 688–700 (2013).
177. Powers, H. R. & Sahoo, D. SR-B1's Next Top Model: Structural Perspectives on the Functions of the HDL Receptor. *Curr. Atheroscler. Rep.* **24**, 277–288 (2022).
178. Gordon, J. A. *et al.* Upregulation of scavenger receptor B1 is required for steroidogenic and nonsteroidogenic cholesterol metabolism in prostate cancer. *Cancer Res.* **79**, 3320–3331 (2019).
179. Wei, C. *et al.* HDL-scavenger receptor B type 1 facilitates SARS-CoV-2 entry. *Nat. Metab.* **2**, 1391–1400 (2020).
180. A. Kenneth MacLeoda, Kevin- Sebastien Coquelinb, Leticia Huertasc, Frederick

R. C. Simeonsa, Jennifer Rileya, Patricia Casadoc, Laura Guijarroc, Ruth Casanuevac, Laura Framea, Erika G. Pintoa , Liam Fergusona, Christina Duncana , Nicole Muttera, Yoko Shis, 1. Acceleration of infectious disease drug discovery and development using a humanized model of drug metabolism. *Proc. Natl. Acad. Sci.* **121**, (2024).

181. Haid, S., Grethe, C., Bankwitz, D., Grunwald, T. & Pietschmann, T. Identification of a Human Respiratory Syncytial Virus Cell Entry Inhibitor by Using a Novel Lentiviral Pseudotype System. *J. Virol.* **90**, 3065–3073 (2016).
182. Dull, T. *et al.* A Third-Generation Lentivirus Vector with a Conditional Packaging System. *J. Virol.* **72**, 8463–8471 (1998).
183. Vieyres, G. *et al.* ABHD5/CGI-58, the Chanarin-Dorfman Syndrome Protein, Mobilises Lipid Stores for Hepatitis C Virus Production. *PLoS Pathog.* **12**, (2016).
184. Pham, H. M., Argañaraz, E. R., Groschel, B., Trono, D. & Lama, J. Lentiviral Vectors Interfering with Virus-Induced CD4 Down-Modulation Potently Block Human Immunodeficiency Virus Type 1 Replication in Primary Lymphocytes. *J. Virol.* **78**, 13072–13081 (2004).
185. Haid, S. *et al.* Isolate-dependent use of claudins for cell entry by hepatitis C virus. *Hepatology* **59**, 24–34 (2014).
186. Kalajzic, I. *et al.* Use of VSV-G pseudotyped retroviral vectors to target murine osteoprogenitor cells. *Virology* **284**, 37–45 (2001).
187. Kostakioti, M., Hadjifrangiskou, M., Pinkner, J. S. & Hultgren, S. J. QseC-mediated dephosphorylation of QseB is required for expression of genes associated with virulence in uropathogenic Escherichia coli. *Mol. Microbiol.* **73**, 1020–1031 (2009).

188. Collins, J. A. & Osheroff, N. Gyrase and Topoisomerase IV: Recycling Old Targets for New Antibacterials to Combat Fluoroquinolone Resistance. *ACS Infect. Dis.* **10**, 1097–1115 (2024).

189. Bush, N. G., Diez-Santos, I., Abbott, L. R. & Maxwell, A. Quinolones: Mechanism, Lethality and Their Contributions to Antibiotic Resistance. *Molecules* **25**, 5662 (2020).

190. Furniss, C. R. D. *et al.* Fast and robust detection of colistin resistance in Escherichia coli using the MALDI Biotyper Sirius mass spectrometry system. *bioRxiv* **57**, 1–7 (2019).

191. Reams, A. B., Kofoid, E., Savageau, M. & Roth, J. R. Duplication frequency in a population of Salmonella enterica rapidly approaches steady state with or without recombination. *Genetics* **184**, 1077–1094 (2010).

192. Risch, T., Hellwinkel, B., Mostert, D. & Kany, A. M. Cystobactamid off-target profiling reveals favorable safety , superoxide reduction, and SCARB1 inhibition in eukaryotes. *bioRxiv* (2024) doi:10.1101/2024.10.10.617689.

193. Adikwu, E. & Brambaifa, N. Ciprofloxacin_Cardiotoxicity_and_Hepatotoxicity_in.pdf. *Pharmacol. Pharm.* **3**, 207–213 (2012).

194. Stahlmann, R. & Lode, H. Toxicity of quinolones. *Drugs* **58**, 37–42 (1999).

195. Sankar, A. *et al.* Association of Fluoroquinolone Prescribing Rates with Black Box Warnings from the US Food and Drug Administration. *JAMA Netw. Open* **4**, 1–12 (2021).

196. Mookerjee, S. A., Divakaruni, A. S., Jastroch, M. & Brand, M. D. Mitochondrial uncoupling and lifespan. *Mech. Ageing Dev.* **131**, 463–472 (2010).

197. Grundlingh, J., Dargan, P. I., El-Zanfaly, M. & Wood, D. M. 2,4-Dinitrophenol

(DNP): A Weight Loss Agent with Significant Acute Toxicity and Risk of Death. *J. Med. Toxicol.* **7**, 205–212 (2011).

198. Li, Y., Kakinami, C., Li, Q., Yang, B. & Li, H. Human Apolipoprotein A-I Is Associated with Dengue Virus and Enhances Virus Infection through SR-BI. *PLoS One* **8**, (2013).

7. Declaration of AI-assisted technologies

During the preparation of this work, the author used ChatGPT (GPT-4) in order to polish the phrasing of some passages. After using this tool, the author reviewed and edited the content as needed and takes full responsibility for the content of the thesis.

8. Acknowledgements

First, I want to thank my doctor father Prof. Dr. Rolf Müller for his support, trust and the opportunity to set up the proteomics platform and work on these complex but rewarding projects. I would like to express my deepest gratitude to him for paving the way for so many scientists to access such an outstanding scientific infrastructure, independent of specific funding, which can rarely be found elsewhere.

I also would like to extend my greatest appreciation to Dr. Jennifer Herrmann who always had an open ear for new ideas and issues, which I faced. Her scientific advice, outstanding network and remarkable writing skills were of immeasurable value. Thank you!

Further, I would like to thank Dr. Dietrich Mostert and Prof. Dr. Stephan A. Sieber for the warm welcome at the Technical University Munich and the invaluable support in teaching and helping me establish the proteomics workflow, equipment and methods to realize the experiments I had in mind.

I especially want to thank my co-workers Felix Deschner, Franziska Fries, Anna-Lisa Jäckel, Sari Rasheed, Alexander Volz, Philipp Donate, Carsten Seifert and Selina Deckarm who helped me with unnamable support, scientifically and as colleagues and friends.

Now, I want to thank the people who make me who I am. First, my partner in crime, adventure buddy and love of my live Nina, who always keeps me on the ground. My live would literally not be the same without you.

My hard working parents, who gave me and my brothers Jan and Dennis every opportunity in live. You taught us principles, which make us who we are. You maybe did not understand but supported every decision I made.

Although they will never be able to read this, I deeply want to thank my grandparents Heinrich and Gerlinde Hindenberger, Hugo and Marliese Risch. You are inspiring me every day to make the best out of me and the opportunities I have in life. Without you, I would not be.

“If I have seen further it is by standing on the shoulders of giants”

-Isaac Newton (1675)

Mail: timo-risch@gmx.de Mobile: +4915224205796 Hangweg 36
66583 Spiesen, Deutschland

Timo Risch - Curriculum Vitae

Persönliche Daten

Geburtstag:	26.05.1995
Geburtsort:	Homburg, Saarland, Deutschland
Status:	ledig

Ausbildung

02/2021-heute **Promotion im Fach Pharmazie• Helmholtz-Institut für Pharmazeutische Forschung**
Universität des Saalandes, Pharmazeutische Biotechnologie
Supervisor: Prof. Dr. Rolf Müller

02/2021 - heute **Fachapotheker für Pharmazeutische Analytik und Technologie**
Apothekerkammer des Saarlandes, ABDA
Supervisor: Prof. Dr. Rolf Müller

07/2020 - 12/2020 **M. Sc. Pharmazie • Helmholtz-Institut für Pharmazeutische Forschung**
Universität des Saarlandes
„Drug Metabolism and Toxicological Investigations of Cystobactamids“
Supervisors: Prof. Dr. Rolf Müller, Dr. Jennifer Herrmann
Note: sehr gut (1.0)

04/2015 - 05/2020 **Approbation zum Apotheker • Pharmazeutische Prüfung**
Universität des Saarlandes, Apothekerkammer des Saarlandes
Note: sehr gut (1.42)

Arbeitserfahrung

02/2021 - heute **Wissenschaftlicher Mitarbeiter • Helmholtz-Institut für Pharmazeutische Forschung**
Prof. Dr. Rolf Müller, Dr. Jennifer Herrmann

04/2019 - 10/2019 **Pharmazeut im Praktikum • Boehringer Ingelheim Pharma GmbH**
Biologicals Development Germany - Pharm. Dev. Biologicals
Dr. Joschka Bauer, Dr. Anne Karow-Zwick

12/2017 - 11/2018 **Studentische Hilfskraft • Universität des Saarlandes**
Institut für Biopharmazie and Pharmazeutische Technologie
Prof. Dr. Marc Schneider

03/2017 - 06/2017 **Erasmus+ Trainee • University of East Anglia (England)**
School of Pharmacy - Research Group of Tissue Engineering
Prof. Dr. Aram Saeed

Publikationen

11/2024 **YgiV promoter mutations cause resistance to cystobactamids and reduced virulence factor expression in *Escherichia coli***
npj Antimicrobials and Resistance, DOI: 10.1038/s44259-024-00050-7

Saarbrücken, 11.2024

Mail: timo-risch@gmx.de Mobile: +4915224205796 Hangweg 36
66583 Spiesen, Deutschland

10/2024 **Chemical proteomics reveal human off-targets of fluoroquinolone induced mitochondrial toxicity**
chemRxiv, DOI: 10.26434/chemrxiv-2024-sgtgf-v2

10/2024 **Cystobactamid off-target profiling reveals favorable safety, superoxide reduction, and SCARB1 inhibition in eukaryotes**
bioRxiv, DOI: 10.1101/2024.10.10.617689

06/2024 **The RNA binding protein IGF2BP2/IMP2 alters the cargo of cancer cell-derived extracellular vesicles supporting tumor-associated macrophages**
Cell Communication and Signaling, DOI: 10.1186/s12964-024-01701-y

04/2024 **The Peptide Antibiotic Corramycin Adopts a β-Hairpin-like Structure and Is Inactivated by the Kinase ComG**
Journal of the American Chemical Society, DOI: 10.1021/jacs.3c13208

12/2023 **Nitroxoline resistance is associated with significant fitness loss and diminishes in vivo virulence of Escherichia coli**
Microbiology Spectrum, DOI: 10.1128/spectrum.03079-23

05/2023 **Evaluation of extraction methods for untargeted metabolomic studies for future applications in zebrafish larvae infection models**
Scientific Reports, DOI: 10.1038/s41598-023-34593-y

Stipendium

03/2017 - 06/2017 **Erasmus + Internship**
Universität des Saarlandes, University of East Anglia

Preise und Auszeichnungen

27.04.22 **Saarländischer Forschungspreis: Ersatz von Tierversuchen**
Saarländisches Ministerium für Umwelt- und Verbraucherschutz, für die Arbeiten zum Ersatz von Tierversuchen

15.10.21 **LifeMat-at-a-Glance short video contest, Second Prize**
GradSchool of Living Therapeutic Material , for acknowledging vision and creativity

14.06.19 **Auszeichnung**
Universität des Saarlandes und Deutsche Pharmazeutische Gesellschaft (DPhG)
Für sehr gute Leistungen in den Staatsexamen

24.10.16 **BeStE-Preis**
für das Mentorenprogramm der UniSaar, für besonderes studentisches Engagement

28.06.14 **Abiturpreis des Landkreises Neunkirchen**
Für hervorragende Leistungen im Abitur

26.06.14 **BARMER GEK Preis**
für hervorragende Leistungen im Fach Biologie

Saarbrücken, 11.2024

Mail: timo-risch@gmx.de Mobile: +4915224205796 Hangweg 36
66583 Spiesen, Deutschland

Ehrenamtliche Arbeiten

10/2016 - 09/2017	**Mentor** Saarland University
10/2015 - 03/2016	**Tutor für allgemeine und anorganische Chemie** Arbeitskreis für Bioorganische Chemie - Universität des Saarlandes Prof. Dr. Claus Jacob
2008 - 2013	**Trainer für Selbstverteidigung** Die Waldritter Manfred Leibfried

Zusätzliche Fähigkeiten

Fremdsprachen	**Englisch** - Schrift (C1) und Sprache (C1) (2020)
Software	LIMS, Spotfire, MOE, GraphPad, ChemDraw, DataAnalysis, DiaNN, Perseus, MaxQuant
Andere	FELASA (IZMC) Course (Functions A, C, D) Rescue Diver (PADI), Sport Piloten Lizenz (SPL), BZF1
Sport	Crossfit

Saarbrücken, 11.2024